Acid Catalysed Synthesis of Mesoporous Silica and Its Applications as Adsorbents, Catalyst Support and Micromotors

by

KUBİLAY ŞAHİN

A Dissertation Submitted to the
Graduate School of Sciences and Engineering
in Partial Fulfillment of the Requirements for

the Degree of

Master of Science

in

Materials Science and Engineering

KOÇ
ÜNİVERSİTESİ

July, 2021

Acid Catalysed Synthesis of Mesoporous Silica and Its Applications as Adsorbents, Catalyst Support and Micromotors

Koç University

Graduate School of Sciences and Engineering

This is to certify that I have examined this copy of a master's thesis by

KUBİLAY ŞAHİN

and have found that it is complete and satisfactory in all respects, and that any and all revisions required by the final examining committee have been made.

Committee Members:

Prof. A. LEVENT DEMİREL [Advisor]

Dr. ANNAMARIA MIKÓ [Co-Advisor]

Assist. Prof. UMUT AYDEMIR

Assoc. Prof. HATİCE DURAN DURMUŞ

Date: July, 2021

This thesis work is dedicated to my parents, Mustafa and Tamam,
who have been a constant source of support and encouragement during the challenges of graduate school and life.
I am truly thankful for having you in my life.
This work is also dedicated to my siblings, Dilek and Merdan,
who have always supported me in this adventure and have believed in their little brother to realize his dreams

ABSTRACT

Acid Catalysed Synthesis of Mesoporous Silica and Its Applications as Adsorbents, Catalyst Support and Micromotors

Kubilay Şahin

Master of Science in Materials Science and Engineering

July 2021

Micron-sized mesoporous silica particles have been used in various applications such as adsorption, separation, catalysis, and drug delivery due to their high specific surface area, pore size, high thermal/chemical stability. However, controlling the properties of mesoporous silica particles is difficult because of the need for different chemicals and additional steps required in the synthesis method. In this thesis, the properties of mesoporous silica particles have been investigated and tuned by controlling the process parameters of sol-gel synthesis method carried out by mixing Pluronic F127 surfactant and tetra ethyl orthosilicate (TEOS) in highly acidic solution at room temperature. Ternary phase diagram of mesoporous silica morphologies was determined by adjusting the compositions of three reactants in the synthesis solutions. The ternary phase diagram was an important development for the investigation of all possible morphologies that can be obtained with a simple and low-cost synthesis method. After analysis of over 150 silica samples, regions with different morphologies (sphere, monolith and polyhedron) and variable surface areas were determined. Mesoporous spherical silica particles (MSPs) with average particle sizes ranging from approximately 1.00 µm to 5.00 µm and pore sizes from 3 nm up to 15 nm were successfully synthesized. Furthermore, hydrothermal treatment process was used to improve the specific surface area (up to 1000 m^2/g) and pore size (up to 15 nm) of MSPs. With hydrothermal treatment, the surface area of MSPs was increased by up to a factor of 1.76. The synthesized mesoporous silica structures were used in the purification of wastewater from textile dyes, photocatalysis and self-propelled micromotor applications and their performances were studied.

The changes in the morphology and pore structures of the particles were successfully identified by using different acids (nitric acid (HNO_3) and sulfuric acid (H_2SO_4)) compared to the hydrochloric acid (HCl) in the investigation of ternary phase diagram. Pore size of the particles was increased from 3 nm to 14 nm by using sulfuric acid without changing the morphology of MSPs. Wastewater treatment performance of mesoporous silica particles synthesized with different acids was tested with Rhodamine 6G as a model molecule and the performances were compared. The maximum absorption capacity of about 20 mg/g was reached by silica particles synthesized with sulfuric acid. The capacity of the particles for removal of dye molecules from water was investigated by changing the process parameters (pH, temperature, time and initial concentrations). Adsorption processes were analyzed with linearized Langmuir and Freundlich isotherms, to estimate the mechanism of adhesion of dye molecules to particles. In addition, the suitability of the adsorption processes to the pseudo-first-order and pseudo-second-order kinetic models was also investigated by varying the contact time. In addition, the changes in thermodynamic parameters ($\Delta G°$, $\Delta H°$, and $\Delta S°$) of the adsorption processes were calculated with the experimental results obtained as a function of temperature at which adsorption took place. The results showed that mesoporous silica particles synthesized

with a simple and cost-effective process can satisfy the requirements for adsorbents in wastewater treatment applications.

The synthesis of metal (iron and copper) loaded porous silica particles as catalysis material has been successfully completed. The catalytic activity of the metal loaded particles was investigated by degradation of Methylene Blue (MB) textile dye selected as the model pollutant. The degradation efficiency observed by Fenton and photo-Fenton reactions was compared depending on the type of metals in the particles and the amount of loading. It was also observed that the iron-loaded mesoporous silica particles cleaned the MB solution at 100 mg/L concentration by 99% in 20 minutes under UV light. The experimental results showed that the use of catalyst particles produced by a simple synthesis method in advanced oxidation processes will provide high efficiency.

Self-propelled mesoporous silica particles have been successfully synthesized by $CaCO_3$ loading into the structure. The loading process was carried out by the formation reaction of the $CaCO_3$ structure by the reaction of $CaCl_2$ and $NaCO_3$ and proved by EDX and SEM analyses. Optimization of the $CaCO_3$ loading process has been completed and the synthesis parameters required for the highest loading yield have been determined. The ability of the loaded mesoporous silica particles to move in acidic aqueous solution (acetic acid) by bubble propulsion was observed under optical microscope. In addition, the velocities of silica particles with different particle size, surface area and pore size were compared. It has been observed that similar size particles having smaller pore diameters move faster. Moreover, it has been understood that pore size is as effective as particle size and surface area. The highest velocity was observed as 1.6 μm/s in particles with a diameter of about 1.5 μm and a surface area of 789 m^2/g. Self-propelled mesoporous silica particles have the potential to be converted to Janus particles and used in biological applications as micromotors.

ÖZETÇE

Mezogözenekli Silikanın Asit Katalizli Sentezi ve Adsorban, Katalizör Desteği ve Mikromotor Olarak Uygulamaları

Kubilay Şahin

Malzeme Bilimi ve Mühendisliği, Yüksek Lisans

Temmuz 2021

Mikron boyutlu mezogözenekli silika parçacıklar, yüksek spesifik yüzey alanı, gözenek boyutu, yüksek termal/kimyasal stabiliteleri nedeniyle adsorpsiyon, ayırma, kataliz ve ilaç taşınımı gibi çeşitli uygulamalarda kullanılmıştır. Ancak, sentez yönteminde gerekli olan farklı kimyasallara ve ek adımlara ihtiyaç duyulması nedeniyle mezogözenekli silika parçacıklarının özelliklerini kontrol etmek zordur. Bu tez çalışmasında, Pluronic F127 yüzey aktif madde ile tetra etil ortosilikatın (TEOS) oda sıcaklığında yüksek asidik çözelti içinde karıştırılmasıyla gerçekleştirilen sol-jel sentez yönteminin proses parametreleri kontrol edilerek mezogözenekli silika parçacıklarının özellikleri araştırılmış ve ayarlanmıştır. Mezogözenekli silika morfolojilerinin üçlü faz diyagramı, sentez solüsyonlarındaki üç reaktantın bileşimlerinin ayarlanmasıyla belirlendi. Üçlü faz diyagramı, basit ve düşük maliyetli bir sentez yöntemiyle elde edilebilecek tüm olası morfolojilerin araştırılması için önemli bir gelişmeydi. Yaklaşık 150 örneğin sentez ve karakterizasyon çalışmaları sonucunda farklı morfolojilere (küresel, monolit ve çokyüzlü) ve değişken yüzey alanlarına sahip bölgeler belirlenmiştir. Ortalama parçacık boyutları yaklaşık 1.00 μm ile 5.00 μm arasında değişen ve gözenek boyutları 3 nm ile 15 nm arasında değişen mezogözenekli silika küresel parçacıklar başarıyla sentezlendi. Ayrıca, MSP'lerin spesifik yüzey alanını (1000 m^2/g'ye kadar) ve gözenek boyutunu (15 nm ‘ye kadar) iyileştirmek için hidrotermal arıtma işlemi kullanıldı. Hidrotermal işlem ile küresel silika parçacıklarının yüzey alanı 1,76 faktörüne kadar arttırılmıştır. Sentezlenen mezogözenekli silika yapılar tekstil boyalarından atık suyun arıtılmasında, fotokataliz ve kendinden tahrikli mikromotor uygulamalarında kullanılmış ve performansları incelenmiştir.

Üçlü faz diyagramının incelenmesinde kullanılan hidroklorik asit (HCl) yerine farklı asitler (nitrik asit (HNO_3) ve sülfürik asit (H_2SO_4)) kullanılmasının parçacıklardaki morfoloji ve gözenek yapılarına etkisi başarılı bir şekilde tespit edilmiştir. Parçacıkların gözenek boyutu, MSP'lerin morfolojisini değiştirmeden sülfürik asit kullanılarak 3 nm'den 14 nm'ye çıkarıldı. Farklı asitlerle sentezlenen mezogözenekli silika parçacıklarının atık su arıtma performansı model molekül olarak Rhodamine 6G ile test edilmiş ve performansları karşılaştırılmıştır. Yaklaşık 20 mg/g'lık maksimum adsorpsiyon kapasitesine, sülfürik asit ile sentezlenen silika parçacıkları ile ulaşıldı. Parçacıkların boya moleküllerini sudan uzaklaştırma kapasitesi, proses parametreleri (pH, sıcaklık, zaman ve başlangıç konsantrasyonları) değiştirilerek araştırıldı. Adsorpsiyon prosesleri, lineerleştirilmiş Langmuir ve Freundlich izotermleri ile analiz edildi ve boya moleküllerinin parçacıklara yapışma mekanizması, boyanın başlangıç konsantrasyonunun değiştirilmesiyle belirlendi. Ayrıca temas süresi değiştirilerek adsorpsiyon işlemlerinin yalancı birinci dereceden ve yalancı ikinci dereceden kinetik modellere uygunluğu da araştırılmıştır. Ayrıca adsorpsiyonun gerçekleştiği sıcaklığın bir fonksiyonu olarak elde edilen deneysel sonuçlar ile adsorpsiyon proseslerinin

termodinamik parametrelerindeki (ΔG°, ΔH° ve ΔS°) değişimler hesaplanmıştır. Sonuçlar, basit ve uygun maliyetli bir işlemle sentezlenen mezogözenekli silika parçacıklarının atık su arıtma uygulamalarında adsorban ihtiyacını karşılayabileceğini göstermiştir.

Kataliz malzemesi olarak kullanılan metal (demir ve bakır) yüklü gözenekli silika parçacıklarının sentezi başarıyla tamamlanmıştır. Metal yüklü parçacıkların katalitik aktivitesi, model kirletici olarak seçilen Metilen Mavisi (MB) tekstil boyasının bozunmasıyla araştırıldı. Fenton ve foto-Fenton reaksiyonları ile gözlemlenen bozunma verimliliği, parçacıklardaki metallerin tipine ve yükleme miktarına bağlı olarak karşılaştırılmıştır. Demir yüklü mezogözenekli silika parçacıklarının 100 mg/L konsantrasyonundaki MB solüsyonunu UV ışığı altında 20 dakikada %99 oranında temizlediği gözlendi. Deneysel sonuçlar, basit bir sentez yöntemiyle üretilen katalizör parçacıklarının ileri oksidasyon işlemlerinde kullanılmasının yüksek verim sağlayacağını göstermiştir.

Kendinden hareket eden mezogözenekli silika parçacıklar, yapıya $CaCO_3$ yüklenerek başarılı bir şekilde sentezlenmiştir. Yükleme işlemi, $CaCl_2$ ve $NaCO_3$ ile $CaCO_3$ yapısının oluşum reaksiyonu ile gerçekleştirilmiş ve EDX ve SEM analizleri ile ispatlanmıştır. $CaCO_3$ yükleme işleminin optimizasyonu tamamlanmış ve en yüksek yükleme verimi için gerekli sentez parametreleri belirlenmiştir. Yüklenen mezogözenekli silika parçacıklarının asidik sulu çözelti (asetik asit) içinde kabarcık tahriki ile hareket etme yeteneği optik mikroskop altında gözlemlendi. Ayrıca farklı partikül boyutuna, yüzey alanına ve gözenek boyutuna sahip silika parçacıklarının hızları karşılaştırılmıştır. Daha küçük gözenek çaplarına sahip benzer boyuttaki parçacıkların daha hızlı hareket ettiği gözlemlenmiştir. Ayrıca gözenek boyutunun da partikül boyutu ve yüzey alanı kadar etkili olduğu anlaşılmıştır. En yüksek hız yaklaşık 1,5 μm çapında ve 789 m2/g yüzey alanına sahip parçacıklarda 1,6 μm/s olarak gözlenmiştir. Kendinden tahrikli mezogözenekli silika parçacıkları, Janus parçacıklarına dönüştürülme ve biyolojik uygulamalarda mikromotorlar olarak kullanılma potansiyeline sahiptir.

AKNOWLEDGEMENTS

I would like to express my gratitude to the people who helped me complete this master thesis, which is one of the biggest outputs of my life.

I would like to thank my dear advisor Prof. A. Levent Demirel sincerely for his vision and everything he taught me. He helped me to develop myself for science. Despite his busy agenda, he always spared me time to answer my questions. He has always showed his trust on me, and this encouraged me to give out my best. He gave me freedom to work in laboratory and created the opportunity to try everything I was curious about.

I am intensely grateful to my dear co-advisor, Dr. Annamaria Miko for her great support and interest. Without her, I would not have been able to finish this graduate study so successfully. I can't give her enough credit here for all the knowledge she taught me and all her help. She always made me feel that I can achieve my goals in academic life. Whenever I needed help, she was there for me. She helped me indefatigably to complete every task of my study. I will always be grateful to her. She is more like my elder sister to me than an advisor.

I would like to thank specially to Dr. Aatif Ijaz for sharing his valuable knowledge. He has been one of my best friends. He never let me feel that he was above me in the hierarchy as a post-doc. He shared me his knowledge about laboratory works, research plan, design of experiments. Without him it would take months to get used to work in lab. I would like to thank Ghazaleh Azizi Saadatlou for her support to my studies. Whenever I felt requirement of additional arms, she helped me without hesitate. She has been a good friend to me, and I have never felt alone in this laboratory group. We have always discussed about new ideas and they trusted my knowledge even though I was the most inexperienced. This also motivated me to work hard.

Dr. Uğur Ünal, Barış Yağcı, and Dr. Amir Motallebzadeh helped me in characterization part of my thesis. Dear Dr. Uğur Ünal allowed me to use their lab and UV lamp for my photocatalyst experiments.

I am grateful to my jury members Dr. Hatice Duran and Dr. Umut Aydemir for evaluating my thesis. I would like to thank Dr. Hatice Duran for everything she thought me in

bachelor's degree. Also, I would like to thank Dr. Umut Aydemir for his great lectures of graduate school.

I would like to thank my friends Burkay Tuğluca, Asım Önal and particularly Bengisu Yılmaz for her great help and support through last two years. She was the one who helped me during the pandemic. Even when I had Covid-19, she opened her house to me and tried to heal me. Nothing will be enough to describe her credit.

I would like to thank my friends Samet Yanık, Selin Alıca, Seyit Cengiz and Yakup Özüpek who have been with me for years, for supporting me since the first day of our friendship. I would like to thank my friend Ali Kerem Güran, who started this adventure together with me, for his support in hard times of my life.

Finally, I would like to express heartiest gratitude to my parents and siblings for their great support and unconditional love. Their credit cannot be described by words. I can say that I would not be here if they were not in my life. Mustafa Şahin, Tamam Şahin, Dilek Tatlı and Merdan Şahin, I would like to thank all of them individually. I would like to thank my nieces Başak Tatlı, Irmak Şahin, Yaprak Şahin and Arya Tatlı for their love and support. I hope all of these young girls will achieve their goals in life, like their uncle.

The financial support of TÜBİTAK (Project #: 118M624) for the work described in Chapter 2 (Synthesis of Mesoporous Silica Particles and Investigation of The Ternary Phase Diagram of HCl/Pluronic F127/TEOS System) and Chapter 5 (Investigation of Self-Propelled Mesoporous Silica Janus Particles) is acknowledged.

TABLE OF CONTENTS

LIST OF TABLES

LIST OF FIGURES

Chapter 1:
INTRODUCTION

Mesoporous silica particles (MSPs) have attracted great interest for studies in materials science since the first discovery in 1992 by researchers from Mobil Oil Corporation. Because of their superior properties such as low toxicity, high surface area, ease to utilize by surface functionalization, tunable morphology, and adjustable pore structures, MSPs have been used in applications of sensors, catalysts, drug delivery, and environmental pollution control [1]–[4]. These unique properties of MSPs can be tuned by modifying the synthesis methods depending on the reactants, concentrations, or experimental conditions. Various synthesis methods such as microemulsion, flame spray pyrolysis, and sol-gel, etc. can be used to synthesize MSPs. Sol-gel approach has been the most preferred synthesis method among all these techniques due to its advantages such as low cost, simplicity and capability of tuning the particle properties [5]. Sol-gel stands for the name of the process which starts as a stable solution of colloidal particles (sol) and ends as a unified three-dimensional "gel". The synthesis of MSPs having different properties have been achieved by modifying the sol-gel process by varying the types of surfactants (template directing agents), silica precursors, reaction conditions, and drying methods. Various types of ionic (e.g., hexadecyltrimethylammonium bromide or chloride (CTAB or CTAC) and non-ionic surfactants (e.g., amphiphilic triblock copolymers) have been employed to synthesize MSPs with different properties depending on pore structure, shape, and particle sizes [6]. In addition, different silica precursors such as inorganic precursors (e.g., sodium silicate) or alkoxide precursors (e.g., tetra alkoxysilane) have been used to synthesize porous silica structures. Most of the studies to synthesize MSPs have been carried out by alkaline solutions. There was not any systematic investigation of synthesis of MSPs by combination of non-ionic block copolymer surfactants with tetra orthosilicate (TEOS) precursor in highly acidic region until our recent study [7]. The synthesis of mesoporous silica structures by mixing amphiphilic ethylene oxide-based block copolymers with TEOS in highly acidic aqueous solutions provides the advantage as enhancing the solubility of surfactant with the presence of polyethylene oxide block. Because of water soluble part of these types of surfactants, addition of co-solvent is not required to increase the solubility or pore size. In addition, high concentration of protons

(H^+) from acid catalyst (HCl) influences the required time for completion of particle formation by enhancing the reaction kinetics. On the other hand, MSPs with high surface area can be produced under ambient conditions without any requirements of additional processes such as aging, stirring, or post treatments. Because of reduced number of reactants and process steps, that method is considered as cost-friendly and simple approach to produce mesoporous silica structures.

The effect of acid catalyst concentration on the particle properties, such as morphological characteristics, pore structure and surface area, was studied within the previous work[7]. Monolith and spherical particles were produced, and specific surface area was obtained in a range between 200 – 500 m^2/g. In this thesis, all possible particle properties that can be obtained by mixing TEOS and Pluronic F127 in HCl aqueous solution were investigated by further experimental studies. In Chapter 2, we showed the control of particle properties by changing the concentration of all reactants particularly (TEOS/Pluronic F127/HCl), applying stirring and hydrothermal treatment. The morphology dependent ternary phase diagram was established for the first time in the literature. Regions of the morphologies as spherical, monolith and polyhedron were identified in the phase diagram. The synthesized mesoporous silica particles were utilized as adsorbent, catalytic and micromotors in the following chapters.

Following the second chapter on mesoporous silica synthesis, this thesis contains three more chapters on three different applications (adsorption, catalyst, and Janus particles) of MSPs. In Chapter 3, the synthesis of mesoporous silica articles with the combination of Pluronic F127 and TEOS in acidic solutions that were prepared by three different types of acids as hydrochloric acid (HCl), nitric acid (HNO_3), and sulfuric acid (H_2SO_4). Detailed analysis to understand the effect of the type of acid catalyst on particle properties (morphology and pore structure) was presented in this chapter. Additionally, ability of synthesized silica samples to remove Rhodamine 6G textile dye from aqueous solutions were investigated by adsorption studies.

The discharge of wastewater from the textile industry into natural clean water sources is a serious threat to the sustainable ecosystem [8]. Due to the harmful effects of textile dyes such as infiltration the incoming sun light and increasing the Chemical Oxygen Demand (COD), aquatic life is seriously affected [9]. Various techniques to overcome these threats

have been studied and reported as coagulation, flocculation, chemical oxidation, decolorization, ozonation, filtration by membranes, and adsorption [10]–[15]. Adsorption is one of the most common traditional methods for wastewater treatment of the industries because it has been considered as simple, and cost-effective method [16]. Several organic and inorganic adsorbents have been employed to remediate wastewater consisting of textile dyes before discharging them into pure water sources. Alumina (Al_2O_3), silica (SiO_2), magnetic nanoparticles (for instance Fe_3O_4), carbon nanotubes, graphene oxide, and activated carbon are the most used inorganic (or synthetic) materials as adsorbents [17]–[22].

Textile dyes have been classified when only their general structure and charges are considered as ionic (cationic and anionic) and nonionic [23], [24]. It is claimed that nonionic textile dyes can be discharged into clean water sources because nonionic dyes are not toxic in aqueous solutions [10]. However, ionic dyes are required special interest because of their toxic and reactive groups formed in water. The complex structure of these dyes based on aromatic groups are not biodegradable [10], [25], [26]. Adsorption processes help cleaning of water by taking those dyes from aqueous phase onto solid particles which can later be separated. Moreover, these structural and charge differences of dye molecules require different surface chemistries on adsorbent surfaces for adsorption to happen. In this point, utilizing the MSPs as selective adsorbents is possible with functionalizing their surfaces by different chemical groups such as amine, carboxyl, etc. onto the surface of the particles including the pore walls. This functionalization of the surfaces makes the particles selective and increases their capacities for adsorbing textile dyes [27]–[32]. On the other hand, it has been reported that MSPs can adsorb positively charged dye molecules in water due to their highly negative surface charge above the isoelectric point (pH>2).

In Chapter 3, the ability of silica particles synthesized with acid catalyzed method introduced in the first chapter to adsorb Rhodamine 6G (R6G) dye molecules was investigated. In Chapter 2 presented the successful synthesis of high surface area MSPs by HCl. Within Chapter 3, different type of acids as HNO_3 and H_2SO_4 were used as catalyst of the synthesis reaction. Detailed analysis of obtained properties such as morphology, pore size, pore volume, and surface charge of the samples are given in this chapter. The adsorption capacity of the synthesized particles was determined by

systematically designed experiments under different conditions such as different pH, temperature, contact time, amount of adsorbent, and initial concentration of the dye. The mechanism of the adsorption process of each sample was modeled by using the linearized Langmuir and the Freundlich isotherms. The results showed that pore size is the main parameter to decide adsorption capacity of porous silica particles. Si/H_2SO_4 particles with 14 nm pore diameter showed higher removal of the dye under every condition (pH, temperature etc.) when they are compared with Si/HCl (d_p= 3 nm) an Si/HNO_3 (d_p= 2-3 nm). Additionally, the kinetic parameters of the adsorption processes were studied by Pseudo-First Order and Pseudo-Second Order models. High kinetic rates of the adsorption processes by our silica particles showed that synthesized particles are promising as adsorbents for textile industry. Moreover, the energy changes during adsorption were calculated from temperature dependent measurements of adsorption of R6G by MSPs. The highest Gibb's free energy change was observed from the particles synthesized under H_2SO_4 catalyzed reactions.

After realizing that the use of MSPs (synthesized by the method in Chapter 2) as adsorbent in wastewater treatment processes shows promise, host material use for catalytic applications were investigated in Chapter 4. Utilization of MSPs as catalytic materials to be used in Advanced Oxidation Processes (AOPs) for higher efficiency in wastewater treatment is studied. Advanced Oxidation Processes (AOPs) have been demonstrated as higher efficiency technique for water remediation applications [33]. Because of the efficiency and secondary pollution problems of adsorption processes, AOPs have been developed for removing the toxic dye molecules [34]–[37]. These processes typically consist of Fenton, photo-Fenton catalytic reactions, and H_2O_2/UV processes (photocatalysis) to produce OH· radicals for oxidizing the pollutants and remove them from the water [38], [39]. Mostly Titanium Oxide (TiO_2) semiconductor material have been used as the catalyst of those approaches due to its large energy band gap providing UV light adsorption. Although the energy source of the processes is sunlight, Fenton reactions require process controls such as pH adjustment which is expensive [40]. However, the wastewater treatment processes are needed to be simple, effective, and cost-friendly to be applied in the industrial levels. So, different types of catalysts have been studied to overcome high-cost problem of the technique.

Efforts to reduce costs of AOPs have led research to shift towards composite catalysts materials which are generally metal loaded inorganic matrixes [41]. The unique properties of MSPs described in the beginning have made them a great choice to be supporting host matrix for catalyst applications [42]. Loading different metals, metal oxides, or metal sulfides on MSPs increased the heterogeneous catalyst efficiency as the composite materials [43]. The larger and more oriented pore structure of MSPs have been considered as better host materials for in liquid applications when they were compared with zeolites and metal organic frameworks.

In Chapter 4, it is reported that the utilization of MSPs as catalyst composites for degradation of Methylene Blue (MB) by loading metal ions on them. Metal ions were selected as Fe^{2+} and Cu^{2+} because of comparative study of Fenton and Fenton-like reactions. Different concentrations of metals were loaded to MSPs to enhance the efficiency for dye removal in water. Also, UV light exposed experiments were studied to understand the photocatalytic activity of synthesized particles. The results showed that catalytic and photocatalytic degradation of MB was achieved with very high efficiency by synthesized metal loaded silica composites as catalyst material.

The ability of MSPs to be a micromotor after utilizing them by $CaCO_3$ loading onto the structure is reported in Chapter 5. The superior properties of MSPs such as tunable morphology, size, pore structure, high surface area and high stability have made them considerable materials to be utilized as micromotors. The locomotion of micro/nanomotors use bubble formation as the fuel in aqueous medium. Self-driven locomotion has been classified into three main groups which are i) self-diffusiophoresis, ii) self-electrophoresis and ii) bubble propulsion [44], [45]. Each type of the motion uses different mechanism as fuel. While self-diffusiophoresis is based on concentration gradient [46], [47], self-electrophoresis uses electric field formed by decomposition of H_2O_2 and the formation of water molecules [48], [49]. On the other hand, bubble propulsion is a more facile system as the formation of CO_2, O_2, etc. bubbles by reactions in an aqueous environment to push the colloids [45]. In our study, we loaded the MSPs with $CaCO_3$ to have CO_2 bubbles in acidic solutions. Detailed study to have optimizations over the synthesis of self-propelled mesoporous silica micromotors is reported. $CaCO_3$ loaded silica particles were studied for the first time. Their locomotion ability and high velocities have shown promise for the future investigations.

In the conclusion chapter, this thesis work is comprehensively concluded by emphasizing the novelty of the obtained results and their importance for the future research and applications of the mesoporous silica particles.

Chapter 2:

SYNTHESIS OF MESOPOROUS SILICA PARTICLES AND INVESTIGATION OF THE TERNARY PHASE DIAGRAM OF HCL/PLURONIC F127/TEOS SYSTEM

2.1 Motivation

In the last decades, mesoporous silica particles (MSPs) have been in great demand for critical applications such as catalysis [1], adsorption [2], separation [3], and sensors [4]. Their unique structures have very attractive properties which are their tunable morphology, specific surface area, pore size and volume, chemical stability, and simple surface functionalization. Because of these properties, MSPs are employed by the researchers to obtain functional materials for controlling environmental pollutions by removal of heavy metals [1], [50]–[52] and chemicals with low degradation such as textile dyes [53]–[55]. Also, MSPs are used as micro/nano carriers by their large pore sizes and high surface areas for targeted drug delivery applications. The structure and active surfaces which provides excellent ability to deliver numerous drug molecules, biocompatibility, and highly controlled release to ensure targeted delivery [56]. Moreover, MSPs are considered as great option when they are compared with other metal oxides such as iron oxide or titanium oxide because of their higher biocompatibility and lower toxicity [57]. Their tunable porous structure and significantly active surfaces make MSPs a considerable option to be host materials of the applications above.

Researchers continuously studied the synthesis of MSPs due to those attractive features. After the first invention of mesoporous silicates [6], different techniques such as the sol-gel approach, template-assisted techniques, microwave-assisted techniques, and chemical etching processes have been used to synthesize mesoporous silica structures [5]. Each process has its drawbacks such as high cost, low reproducibility, and complexity. However, the sol-gel mechanism which is a wet-chemical technique became the most popular approach for the synthesis of MSPs [5]. Sol-gel stands for the name of the process which starts as a stable colloidal mixture (sol) prepared by the growth of networks of reactants and continues by gelation step of the sol to form unified three-dimensional network gel in a liquid phase. The method consists of two main reactions named by

hydrolysis and condensation. Hydrolysis reactions is the step of sol-gel methods produce colloidal particles in sol. Briefly, hydrolysis is a substitution reaction in between water molecules and metal alkoxides as shown below. Condensation reaction is the following step after hydrolysis by combination of two small molecules to form a large complex molecule and ROH side products like water or alcohol. Then calcination of obtained gel creates the powder of particles. Calcination of formed gels after hydrolysis and condensation reactions produces the metal oxides.

Hydrolysis: $Si\text{-}(OR)_4 + H_2O \rightleftarrows Si\text{-}(OR)_3(OH) + ROH$

Condensation: $(OR)_3\text{-}Si\text{-}OH + HO\text{-}Si\text{-}(OR)3 \rightarrow (OR)_3Si\text{-}O\text{-}S\dot{I}(OR)_3 + H\text{-}O\text{-}H$

Although MSPs can be synthesized with the sol-gel approach by using amphiphilic block copolymers as template directing agents and inorganic precursors (e.g. sodium silicate) or alkoxide precursors (e.g. tetra alkoxysilane) either in basic [6], [58] or acidic[59] solutions, different mechanisms occur in both routes [60]. Tetraethyl orthosilicate (TEOS) and tetramethyl orthosilicate (TMOS) are commonly used silica alkoxide precursors for the synthesis [61]. When these precursors form highly branched clusters in basic aqueous solutions due to relatively low condensation and high hydrolysis rates, weekly crosslinked linear polymers are formed in acidic aqueous solutions[62], [63]. That difference in cluster formation occurs because the solubility of silicon oxide is higher in basic solutions than in acidic solutions [60]. So, more inter-linking silica clusters are favorable in the basic mediums. The dependence of the relative rates of Si(OR)4 hydrolysis and condensation reactions on different pH is shown in Fig. 2.1. In acidic medium (1st region) hydrolysis reactions are faster than condensation.

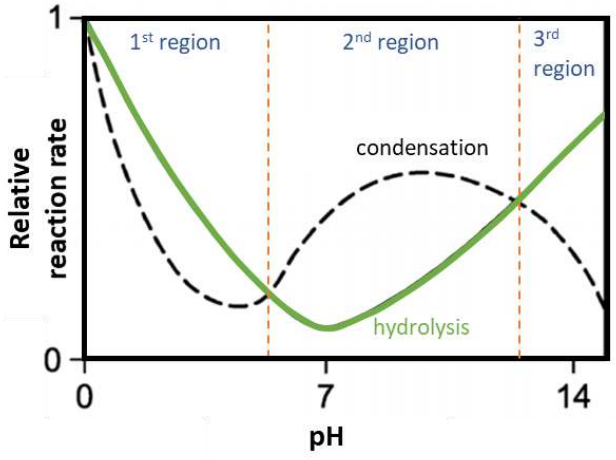

Figure 2.1 Dependence of the relative rates hydrolysis and condensation reactions of $Si(OR)_4$ on different pH [19].

Hydrolysis of all -OR groups from Si-$(OR)_4$ is not straightforward. Instead of the condensation reaction shown above, the reaction may start in between either $(-OH)_2$ or Si-OH and alkoxyl groups to form oxygen in the bridge and water or alcohol. When the condensation reaction between two Si-OH groups forms ≡Si-O-Si≡ and water, the condensation reaction between Si-OH and Si-OR forms ≡Si-O-Si≡ and alcohol. In highly acidic mediums (pH<2), the reaction rate of both hydrolysis and condensation reactions is very high. In the sol-gel approach, these two reactions are followed by growth and agglomeration. When the number of Si-O-Si groups reaches adequate numbers, nucleation of primary groups starts. Then, these formed primary clusters grow and agglomerates to form secondary colloids in the sol. Colloidal particles joint and form the three-dimensional network of the gel.

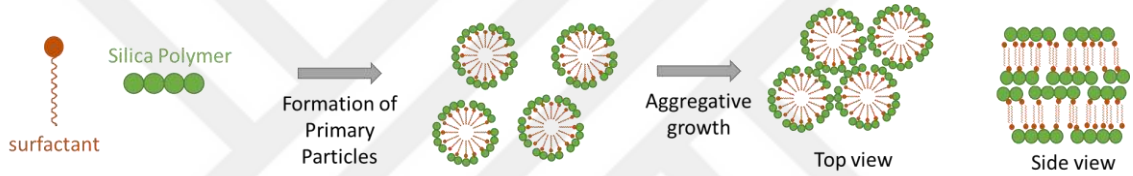

Figure 2.2 Scheme of the proposed mechanisms for the formation of ordered mesoporous silica nanoparticles [64].

Amphiphilic molecules take place as template directing agents while the growth step of sol-gel processes continuing. Hydrophobic and hydrophilic parts of the molecules form the micelles by their microphase separation in water to build the porous structure of silica. Silica clusters interact with amphiphilic molecules by hydrogen bonds to form silica micelles. When the pH<2 silica molecules carry positive charges, also the amphiphilic block copolymers. Therefore, the interaction between template directing agents and silica molecules occurs by double-layer H-bonding [60], [64]. As it is shown in Fig. 2.2, primary particles assembly around amphiphilic surfactants and agglomerate. After calcination at a high temperature to remove surfactant, MSPs are obtained.

Due to attractive properties such as high surface area, narrow pore size distribution, thermal/chemical stability, and large active sites of the surface for easy functionalization, MSPs have great potential for various applications. However, controlling the properties of MSPs is crucial to use these particles. [57], [60], [65]–[67]. As is described above sol-gel processing with template directing agents is the most popular approach to synthesize MSPs due to the simple control of the reaction mechanism [6]. Researchers have focused

modifications on the process to control the particle properties of silica particles by reaction kinetics, using different templates such as ionic or non-ionic surfactants, polymers, and electrolytes [60], [68]. Especially, the interaction between silica and surfactants has been investigated and it is reported as the type and size of the surfactant have an important impact on the pores of MSPs [69].

Different types of ionic and non-ionic surfactants can be used as template directing agents [6]. These amphiphilic molecules self-assemble into ordered micelle and interact with silica in aqueous solutions via non-covalent interactions such as electrostatic interactions or H-bonding. Since the silica molecules are positively charged in a highly acidic medium (pH<2), cetyltrimethylammonium bromide or chloride (CTAB and CTAC) are mostly used for templating due to their B^- and Cl^- counterions to be bridge in electrostatic interaction [70]. It is reported that pore volume and pore size are in correlation with the concentration of CTAB in an acidic medium [71]. In the same study, Boonamnuayvitaya et al. reported that 14.4 nm pore diameter could be synthesized by using Brij-56 non-ionic surfactant. Zhang et al. also reported that hexagonal-shaped porous structure is achieved with an average pore size up to 3.3 nm via using CTAB as template directing agents [72]. However, studies showed that using ionic surfactants as template directing agents has big limitations such as thin silica walls and smaller pore sizes.

Nonionic surfactants generally are block copolymers consisting of water-soluble and oil-soluble polymer chains. Generally, poly(ethyleneoxide) (PEO) chains are part of nonionic surfactants as water-soluble moieties to form micelles for templating. Due to their properties such as biodegradability, low-cost, low-toxicity, and ordered microdomain morphologies attracted the industry and studies in the synthesis of MSPs [73]–[76].

For the first time in 1995, Pinnavaia et al. used nonionic surfactants as template directing agents in the synthesis of mesoporous silica [74], [75]. In this work, they studied organic amines, nonionic oligomeric surfactants, and triblock copolymers as template directing agents and used TEOS as silica precursor under neutral conditions and proposed the H-bonding interactions between surfactant and silica precursor. They synthesized MSPs with worm-like shapes and narrow pore size distribution in a range of 2.4 – 5.8 nm diameters. Their MSPs were disordered but thermal stability was significantly high. After that, Attard et al. reported that ordered MSPs could be successfully synthesized with pore

sizes up to 3.0 nm by using $C_{12}EO_{18}$ and $C_{16}EO_8$ non-ionic surfactants as structure-directing agents [76].

Wiesner and his collaborators reported their approach which consists of poly(isoprene)-block-poly(ethylene oxide) (PI-b-PEO) block copolymers as template directing agents in acidic and non-aqueous mediums to form large pore sized MSPs [77]. They have proved that using high molecular weight copolymers instead of conventional non-ionic surfactants helps control the process to form large pores. After this study, many different block copolymers were used in the synthesis of MSPs. To select the best copolymer as structure-directing agents, the properties of the copolymer such as hydrophilic/hydrophobic ratio, critical micelle concentration (CMC), hydrophile–lipophile balance (HLB), critical micelle temperature (CMT), and cloud-point (CP) considered as important parameters for controlling the pore size and texture of MSPs [78].

Poloxamers or Pluronic have been widely used as template directing agents due to easy solubility in water and optimal balance between the hydrophobic and the hydrophilic portions of non-ionic di/triblock copolymers of Poly(ethylene oxide) (PEO) and Poly(propylene oxide) (PPO) [78], [79]. These properties of PEO/PPO or PEO/PPO/PEO make them one of the best solutions to create self-assembled micelles for the pore formation of MSPs [73]. Fan et al. successfully synthesized MSPs in an acidic medium by using Pluronic F127 as templating agents [80]. Their final products had a cubic ordered structure of pores, but they used potassium chloride and 1,3,5-trimethyl benzene (TMB) as additives to control the pore sizes in a range of 4-9 nm diameters.

Pluronic F127 is successfully used in MSPs synthesis by Chen et al. to produce highly ordered large pore-sized particles with different geometries [81]. Even though they obtained silica particles having order of the pores as face-centered cubic, body-centered, 2-D hexagonal, and cubic bicentered textures, they used anionic co-templating agents and additives to control morphology and pore sizes. To increase pore sizes from a range of 5-12 nm to 16 nm, swelling agents are used as an additive in a co-solvent-induced Pluronic system.

Pluronic F127 is employed by Kleitz et al. in a low acid concentration system of synthesizing MSPs to control the properties of particles simply [82] They used Pluronic

F127 as template directing agent and started synthesis in low acid concentration (~0.5 M HCl). Maximum pore size was reached to 9.3 nm by post-treatment that is hydrothermal treatment in 130 ^{o}C. Also, Wang et al. used a hydrothermal treatment approach to enhance the pore sizes of MSPs. [83] They successfully synthesized ultra-thick-walled SBA-16 particles and suggested that pore size and specific surface area of the particles can be controlled by controlling the synthesis and calcination temperatures.

The control over the final shape of the silica particles is found as important as the pore structure of the particles. Yu et al. synthesized nearly 100% rhombic dodecahedron shaped single crystal mesoporous silica particles by using nonionic block copolymer surfactants as templating agents and inorganic salts to control crystal structure [84]. Also, their pore size was obtained as 7.4 nm diameter.

Ballem and co-workers studied the size-effect of temperature during the synthesis of MSPs. [85] The size of the particles could be tuned in a range between 0.5 – 8 μm by changing the temperature of the reaction. Also, they obtained larger pore sizes by increasing the temperature in the Pluronic F127 system in an acidic medium. They concluded these investigations by the change in the reaction kinetic rates of hydrolysis and condensation of the silica precursor. Besides, Cao et al. studied the effect of synthesis temperature and inorganic salts on the morphology of porous SBA-16 particles to use them in dibenzothiophene hydrodesulfurization [86]. MSPs which were synthesized with Pluronic F127 as templating agents in a low acidic medium were obtained spherical shaped at room temperature. However, their shapes changed from spherical to decahedral and dodecahedral, then prism with increasing the temperature. They commented on the results by correlating them to the condensation reaction. They proposed that condensation reaction was controlled thermodynamically at room temperature, but in higher temperature kinetics took control over the reaction.

Different factors in synthesis, such as temperature [85], [87], stirring rate [88], [89], additives [60], [81], [90] and aging [87], [88], have been reported to affect the structure and the shape of meso-silica particles. On the other hand, the concentration of the catalyst of the systems is very important in the synthesis of mesoporous silica particles [91]. Fig. 2.1. shows that condensation and hydrolysis reactions are slower in the basic medium. The formation of silica clusters is significantly affected by this reaction kinetics. Highly

branched clusters in basic aqueous solutions are obtained due to relatively low condensation and high hydrolysis rates, and weekly crosslinked linear polymers are formed in acidic aqueous solutions. Therefore, the last morphologies of the MSPs are influenced.

Boonamnuayvitaya et al. reported the synthesis of MSPs catalyzed with both acid and base by using different template directing agents as Brij56, sodium dodecyl sulfate (SDS), and CTAB [71]. They could synthesize MSPs with 14.4 nm pore size as maximum in a basic medium by using a high amount of CTAB. They concluded that the pH of the mixture solution influenced the surface area of the particles by affecting pore size and pore volume. Also, the higher concentration of templating agents the larger pore size and volume is reported by the study. However, aging the mixture solution for 5-7 days at 90 ^{o}C was needed to get a mesoporous structure. The reason for aging requirement was that the sol molecules were crosslinking without aggregating to form clusters in acidic condition. So, with elevated temperature they could obtain gelation.

Boissière et al. synthesized spherical MSPs with 3-8 μm diameter and large pore sizes as 910 m^2g^{-1} and 2.4 nm pore sizes [92]. Micrometric MSPs were obtained by the novel synthesis approach which had separation of condensation and aggregation steps of the sol-gel method. They used sodium fluoride to initiate the hydrolysis reaction in a medium with a 2-4 pH. Moreover, the pore size and surface area of the particles could be controlled by mol% NaF/TEOS in the reaction mixture.

Mesa et al. synthesized spherical MSPs with a minimum diameter of 3 μm and 5-10 nm pore sizes by using TEOS as silica source, Pluronic P123 as the surfactant, and cetyltrimethylammonium bromide (CTMABr) as co-surfactant [93]. Morphology and porous structures were studied by controlling the reaction parameters such as time, temperature, acidity, and dilution. The comparison was made by changing the reaction route by i) one heating cycle and ii) two heating cycles. Weakening the interaction between silica and surfactant by high dilution, high temperature, and low acidity resulted in spherical silica particles in one heating cycle. Spherical MSPs had polyhedron and spherical shapes with various pore sizes (4-9 nm) and pore volumes (0.51 - 1.21 cm^3 g^{-1}).

Kosuge et al. controlled the morphologies of MSPs as rodlike and fiberlike SBA-15 by the synthesis with Pluronic P123 as surfactant, sodium silicate as silica precursor, and different acids (HCl, HNO_3, HBr, and H_2SO_4) as catalyst [94]. Morphologies of the MSPs were tuned by controlling the acid source, reaction time and temperature, initial concentrations of reactants, and shearing flow of the solutions, in addition to stirring. Fiberlike MSPs were synthesized with 10 μm thickness and several lengths (130-225 μm) while the rodlike particles were 0.5 μm wide and 1-2 μm long. It was reported that stirring helped to synthesize silica particles with fiberlike morphology.

Baute et al. studied the effect of interrelation between the concentrations of acids and salts as additives [95]. The addition of $NaNO_3$ changed the SBA-15 particles from hexagonal to cubic structure, in the synthesis system with Pluronic P123 as template directing agents. The formation and change in the morphology were attributed to the effect of salt ions on the dehydration of ethylene oxide groups of the surfactant. They suggested that salts decreased the solubility of ethylene oxide groups and micellar assembly of Pluronic which was resulted in cubic structure as final morphology.

As a summary, the morphology of MSPs has been tuned by controlling reaction parameters such as reactant types, concentrations, temperature, etc. However, the successful synthesis of the porous particles has been completed by strict control over various parameters as additives, temperature, aging, and stirring. Ultimately, Ijaz et al. reported a room temperature synthesis route for MSPs to control the morphology and pore structure of the particles. Pluronic F127 was used as a surfactant when TEOS and HCl were used as silica precursor and catalyst in the synthesis [7]. They reported a cost-effective and easy control over the morphology of MSPs. The morphology of MSPs was changed from spherical to monoliths by tuning the concentration of HCl acid catalysts. In highly acidic solutions (above 3M HCl), spherical mesoporous particles were synthesized without control over reaction temperature, stirring, aging or additives. MSPs were synthesized with Pluronic F127/TEOS/HCl system at room temperature. Their results were important to understand the effect of acid concentration on the morphology of MSPs. The size of spherical MSPs could be controlled in the range of 1-4 μm diameters and specific surface areas were obtained in the range of ~200–500 m^2/g. In lower acid concentrations (>3.00 M), MSPs were synthesized with micron-sized monolithic morphologies.

In this study, we investigated the effects of reaction parameters such as concentration ratios of the reactants, post-treatments, stirring on the final morphology of micron-sized mesoporous silica particles. Pluronic F127/TEOS/HCl system which was investigated by Ijaz et al. were used in the synthesis of the particles. The ternary phase diagram was determined, and phases of different morphologies were identified and investigated for the first time. Unlike the previous study [7], polyhedron-shaped silica particles were obtained in addition to spherical and monolithic particles. Larger surface areas (up to ~1000 m^2/g) were successfully formed by hydrothermal treatment on the particles. Spherical particles were synthesized with larger diameters by the effect of stirring rate and time. Micron-sized MSPs which are highly promising materials for the applications such as chromatography, catalyst, and adsorption were successfully synthesized and characterized. Highly reproducible and cost-effective control over the MSPs were reported for next research about such applications. The particles synthesized in this chapter were also used in the next chapters to investigate the application details.

2.2 Materials And Methods

2.2.1 Materials

Silica samples were synthesized at room temperature by using Pluronic F127 as the surfactant, TEOS as silica precursor, and HCl as acid catalyst. The amphiphilic triblock copolymer, Pluronic F127 (poly (ethylene oxide)$_{106}$–poly(propylene oxide)$_{70}$–poly(ethylene oxide)$_{106}$ ($PEO_{106}PPO_{70}$-PEO_{106}) from Sigma Aldrich was used as a structure directing agent due to its biodegradability, high solubility in acidic aqueous medium and ability to self-assemble micelle formation with hydrophilic and hydrophobic groups. The molecular weight of Pluronic F127 is 12600 g/mol. Tetraethyl orthosilicate (TEOS) with 208.33 g/mol molecular weight was purchased from MERCK and used in the synthesis due to its easier control of reaction kinetics in the acidic conditions. HCl (37 wt.%.) from Sigma Aldrich was used as catalyst of the synthesis.

2.2.2 Characterization Techniques

Scanning Electron Microscope (SEM)

To analyze the properties such as size, morphology, and surface quality of the synthesized MSPs, we used scanning electron microscopes both Field Emission SEM (FE-SEM) (ZEISS Ultra Plus SEM) and Environmental SEM. Secondary electron beam detectors of SEMs were used to produce images for analysis. In addition to particle size measurement in the software of ZEISS, ImageJ processing was applied to measure mean particle diameters. Different magnifications such as 5.0K, 10.0K, 20.0K, etc. were applied to take the images of silica particles.

Scanning Transmission Electron Microscope (STEM)

A scanning transmission electron microscope (JEOL JEM ARM200-CF) was used to analyze the porous structure of the MSPs. The order and shape of the pores were characterized by a transmission scanning electron microscope. The mesoporous structures of silica particles were investigated by annular dark field (ADF) imaging operated at 25.00 kV, using an ADF detector collection.

Specific Surface Area (SSA) Measurements

Surface areas of the synthesized silica structures were calculated from nitrogen adsorption/desorption isotherms by using Micromeritics ASAP 2020 physisorption instrument and Brunauer, Emmett and Teller (BET) theory. As it is represented in Fig. 2.3., IUPAC classified the physisorption isotherms into six different types [96].

The first isotherm (Type I) is assigned to microporous solid materials such as activated carbons and zeolites which do not have large external surfaces. Within the Type I isotherm, the adsorbed amount reaches the saturation point by a small increase in relative pressure. The accessible micropore volume of the materials is effective to obtain that saturation point of the adsorption. The slope of the trend is very low relative pressures is resulted due to very narrow pore sizes in molecular dimensions. Type I(a) and Type I(b) show the difference between two different ranges of micropores. Type I(a) isotherm belongs to the porous materials which have micropores with around <1 nm width when

Type I(b) isotherm belongs to wider micropores and possibly mesopores around <2.5 nm width.

In the case of a Type II isotherm, nonporous or macroporous adsorbents interact with gas molecules by monolayer-multilayer adsorption. This adsorption isotherm shows three different behaviors with increasing relative pressure. Concave shape in low p/p^0 turns linear in middle relative pressures and ends with convex in high pressures. Point B is the beginning of the linear part indicates the finalization of monolayer coverage.

Type III isotherm does not spot any information about the finalization of monolayer adsorption. It shows a convex increase with increasing pressure. Although the adsorbents which give isotherm Type III are nonporous or macroporous like the adsorbents in isotherm Type II, they have hot strong interactions with the adsorbed gas molecules.

Mesoporous materials such as metal oxide gels (MSPs) and mesoporous sieves give Type IV isotherm. These adsorbents show similar behavior with Type II isotherm at low pressures but at medium and high relative pressures limiting values change due to capillary condensation. Type IV(a) shows a hysteresis when the pore sizes are wider than 4 nm which means certain critical width is exceeded. Hysteresis curve belongs to adsorption and desorption of the gasses. That type of isotherm is more common than Type IV(b) isotherm. Type IV(b) isotherm is observed with mesoporous structures which have closed pores at the end.

Type V isotherm has a similar shape to Type III isotherm in lower pressures. So, the adsorbent materials have weak interactions with adsorbate molecules in that range. This type of isotherms is rarely observed by macroporous particles and water adsorption on hydrophobic micro/mesoporous particles.

In the case of Type VI isotherm, nonporous solid particles adsorb the adsorbates on their smooth surfaces layer-by-layer. As it is shown in the Figure 2.3., there are multi-steps on the curve and the height of each step represents the adsorption capacity of each layer.

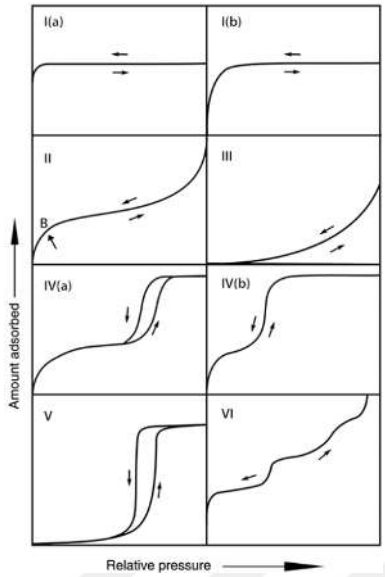

Figure 2.3 IUPAC classification of physisorption isotherms [97].

The physisorption isotherms represented adsorption behaviors of the solid particles but various new particular types of isotherms have been discovered in the last years. However, we use both physisorption isotherms and hysteresis cycles which is also classified by IUPAC in 1985 [97]. Hysteresis loops fill the blank part of isotherms which is the desorption of adsorbates. IUPAC classified the hysteresis loops into six types (Fig 2.4.).

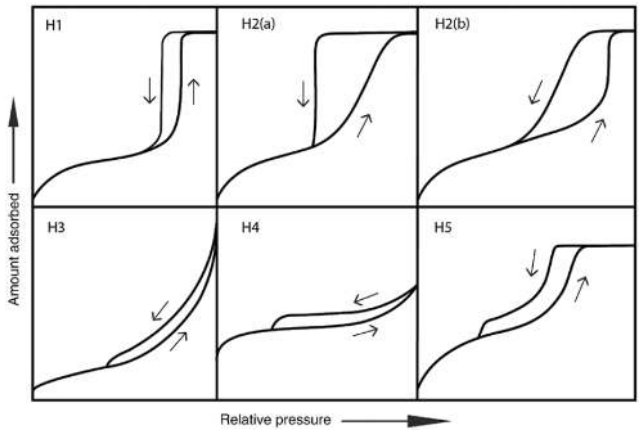

Figure 2.4 Classification of hysteresis loops by IUPAC in 1985 [97]

Mesoporous particles with uniform pores for example templated MSPs (MCM-41, SBA-15) or mesoporous carbons show the Type H1 loop. The adsorption and desorption curves are observed parallel, and a narrow hysteresis loop is observed due to the low network of the pores.

Type H2 loops are observed when the adsorbents have more complex and interconnected porous structures. Pore blockings because of narrow pore necks have a strong effect on the shape of Type H2 hysteresis loops. The adsorbents with Type H2(b) loops have larger necks than Type H2(a) adsorbents and it has resulted that a less steep desorption branch.

Loops of Type H3 are observed by plate-like particles like certain clays. The adsorption part of the loop is similar to Type II physisorption isotherm, and the desorption limits are very low. Type H4 loop is also similar to Type H3, and it is the mixture of Types I and II isotherms. This type of loop has been observed by adsorbents that have micro/mesoporous structures such as mesoporous zeolites, and micro/mesoporous carbons.

The Type H5 loop is the least common of the hysteresis loops. Porous materials which have both open and partially blocked pores show that type of loop.

The adsorption and desorption curves are obtained by the narrow range of relative pressures (~0.4 – 0.5) and in the temperature of 77 K for nitrogen [97]. Then Braunauer-Emmett-Teller method is used to determine the specific surface area of the materials [98].

2.3 Results And Discussion

2.3.1 Establishment of the Ternary Phase Diagram of HCl/Pluronic F127/TEOS System

The aim of this work was to explore the HCl/Pluronic F127/TEOS system to synthesize mesoporous silica structures over a wide range of compositions. This ternary phase diagram will help to synthesize silica structures having desired properties such as size, morphology and surface area using fast, simple, cost effective and room temperature synthesis method. In this thesis work, we investigated the ternary phase diagram on the morphology dependence of this new mesoporous silica synthesis approach with the TEOS/Pluronic F127/HCl system. The combination of the effects of concentrations of each reactant is important to see all possible morphologies of MSPs synthesized with a three-component reaction system. Because the complexity of influences of reactants' concentration (shown in next sections) makes it difficult to predict the end product by the method. The phase diagram is obtained by analysis of MSPs which are synthesized with a wide range of concentrations of TEOS, Pluronic F127, and HCl. The phase diagram is obtained by analysis of over a hundred mesoporous silica samples with designed

compositions shown in Table 2.1. The particles were synthesized under the same conditions that are given in the previous sections of the chapter. Moreover, the sample matrix was designed by taking into several important factors such as solubility limits of the surfactant in different concentrations of hydrochloric acid aqueous solutions. The experiments showed us that Pluronic F127 would not be dissolved above 50 wt% so that the part of the phase diagram which has higher than 50 wt% of Pluronic is excluded from the study. From samples #1 to #15, reactions were carried out with 20 mL of total solutions and TEOS concentration was kept constant as 200 µL/mL to get the compositions. However, our calculations showed that sample #16 - #21 requires HCl acid concentrations of 12.79- 51.18 M which were not possible to reach with the concentrated (12.178 M) HCl solution. Therefore, these samples were synthesized by ten times dilution of all the concentrations of HCl/Pluronic F127/TEOS.

Table 2.1 The designed matrix for compositions of HCl/Pluronic F127/TEOS to investigate the ternary phase diagram of MSPs.

Sample No:	Pluronic F127 (wt.%)	TEOS (wt.%)	HCl (wt.%)	Sample No:	Pluronic F127 (wt.%)	TEOS (wt.%)	HCl (wt.%)
PD01	25.00	25.00	50.00	**PD14**	6.50	87.00	6.50
PD02	37.50	25.00	37.50	**PD15**	6.50	50.00	43.50
PD03	50.00	25.00	25.00	**PD16**	6.50	8.50	85.00
PD04	12.50	37.50	50.00	**PD17**	12.50	12.50	75.00
PD05	25.50	37.25	37.25	**PD18**	25.00	12.50	62.50
PD06	37.50	37.50	25.00	**PD19**	37.50	12.50	50.00
PD07	50.00	37.50	12.50	**PD20**	50.00	12.50	37.50
PD08	12.50	50.00	37.50	**PD21**	12.50	25.00	62.50
PD09	25.00	50.00	25.00	**PD22**	14.00	43.00	43.00
PD10	37.50	50.00	12.50	**PD23**	17.00	33.00	50.00
PD11	12.50	62.50	25.00	**PD24**	20.00	20.00	60.00
PD12	25.00	62.50	12.50	**PD25**	20.00	40.00	40.00
PD13	12.50	75.00	12.50	**PD26**	29.00	57.00	14.00
				PD27	30.00	60.00	10.00

The synthesized MSPs were analyzed with SEM images to investigate the morphologies. As it is represented in Figure 2.5. three main morphologies which were spherical, monolithic, and polyhedron shaped were obtained from HCl/Pluronic F127/TEOS system. Figure 2.5 (a) represents a monolithic silica sample that was synthesized at concentrations of 12.5 wt% HCl, 50.0 wt% Pluronic F127, and 37.5 wt% TEOS. Figure 2.5. (b) and (c), represent spherical and polyhedron-shaped silica particles, respectively. Spherical silica samples represented were synthesized at concentrations of 25.0 wt% HCl, 25.0 wt% Pluronic F127, and 50.0 wt% TEOS and polyhedron-shaped silica particles,

were synthesized at concentrations of 62.5 wt% HCl, 12.5 wt% Pluronic F127, and 25.0 wt% TEOS.

Although spherical and monolith particles were already detected in this acid catalyzed system, polyhedron particles were also obtained for the first time in this synthesis method. The formation of the polyhedron morphology was found similar to the spherical morphology. Like the spherical particles, polyhedron-shaped particles were formed by the agglomeration of hexagonal primary particles. As it was observed in previous sections monolith particles were formed by agglomeration of secondary spherical particles. However, this was not the case to form polyhedrons, which could be understood from SEM images. Also, the regions of the phase diagram showed that polyhedron morphology is a transition stage from spherical to the monolith. Polyhedron shape is one of the most energetically favorable shape like spheres. So, the formation of that shape can be attributed to particle surface energy depending on size and shape of silica structures. In addition, the pH, ionic strength and temperature of the reaction mixtures are affecting the morphology of silica structures.

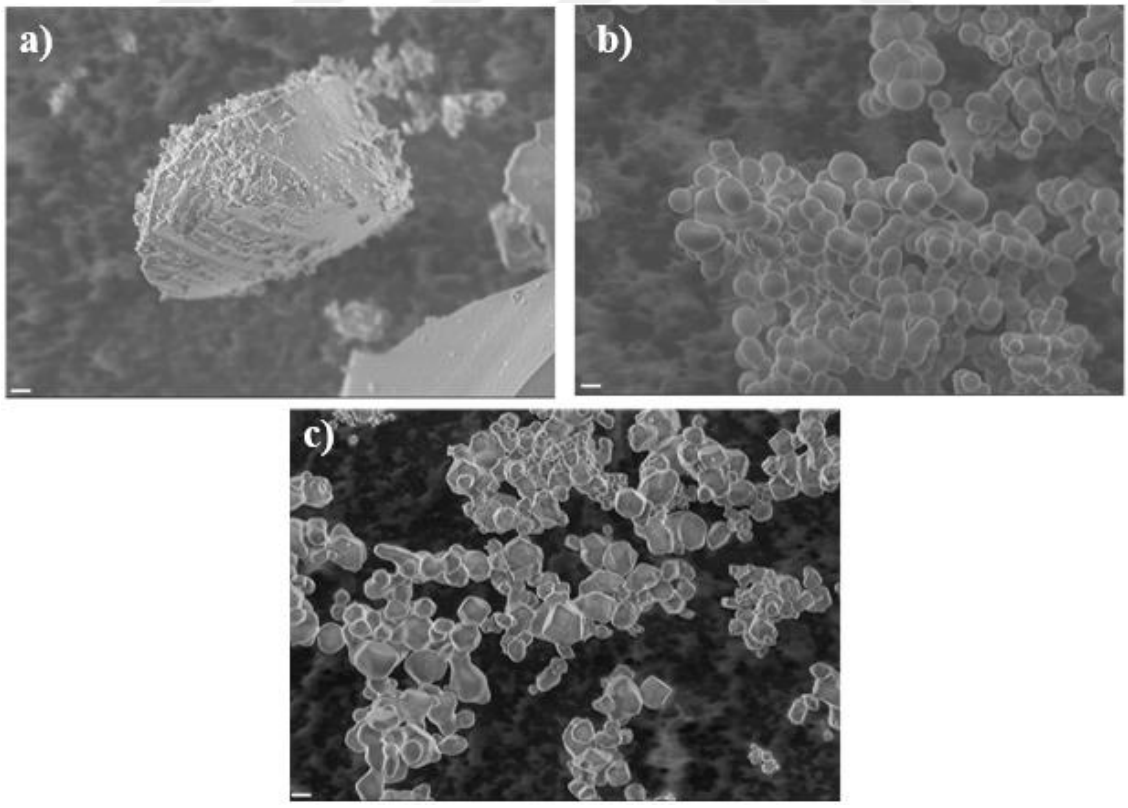

Figure 2.5 SEM images of silica particles to represent main morphologies (a) Monotoliths, b) Sphericals, c) Polyhedrons) obtained from the phase diagram of the system. The scale bars on images are 2 μm.

Figure 2.6. represents the ternary phase diagram of morphologies obtained from HCl/Pluronic F127/TEOS compositions with the constant amount of TEOS. After analyzing over hundred samples by SEM images, the domination of certain morphologies could be identified. Especially in high ratios of Pluronic F127 particles tend to fuse more and create monolith morphology. This can be attributed not only to the effect of a high amount of Pluronic F127 but also to lowering the acid concentration. Synthesizing the particles with given compositions in the matrix resulted in the combination of concentration effect of reactants. Moreover, the orange dashed line represents the estimation of the border of the transition stage from spherical morphology to the monolithic structure. Also, polyhedron-shaped silica particles were obtained on this estimated border of transition. High reproducibility of the morphologies demonstrated that a simple method could result in morphological control over silica particles just by controlling the composition of the compounds in the system. However, the region which has more than 50 wt% of the surfactant is still on the dark side of the synthesis method because of that the particles in those compositions could not be synthesized due to solubility limits of Pluronic F127 in acidic solutions. This phase diagram of morphology of silica structures was obtained without the use of any additional co-solvent or changing reaction parameters such as temperature, stirring and aging was not applied to get over that problem. Because the phase diagram of the method was designed to be as simple as the synthesis method itself.

It was observed that spherical particles varied in particle size from 1 μm to 4.5 μm with different compositions. However, spherical particles in all compositions were fused. The particles synthesized with this method tend to fuse more than the particles synthesized under basic conditions. This cannot be attributed just to the pH of reaction mixtures. As it was described above the reaction system was influenced by multiple factors such as the exact concentration of reactants and total volume of reaction mixture etc. However, it can be concluded that higher rates of hydrolysis and condensation reactions are dominant effects to have fused particles.

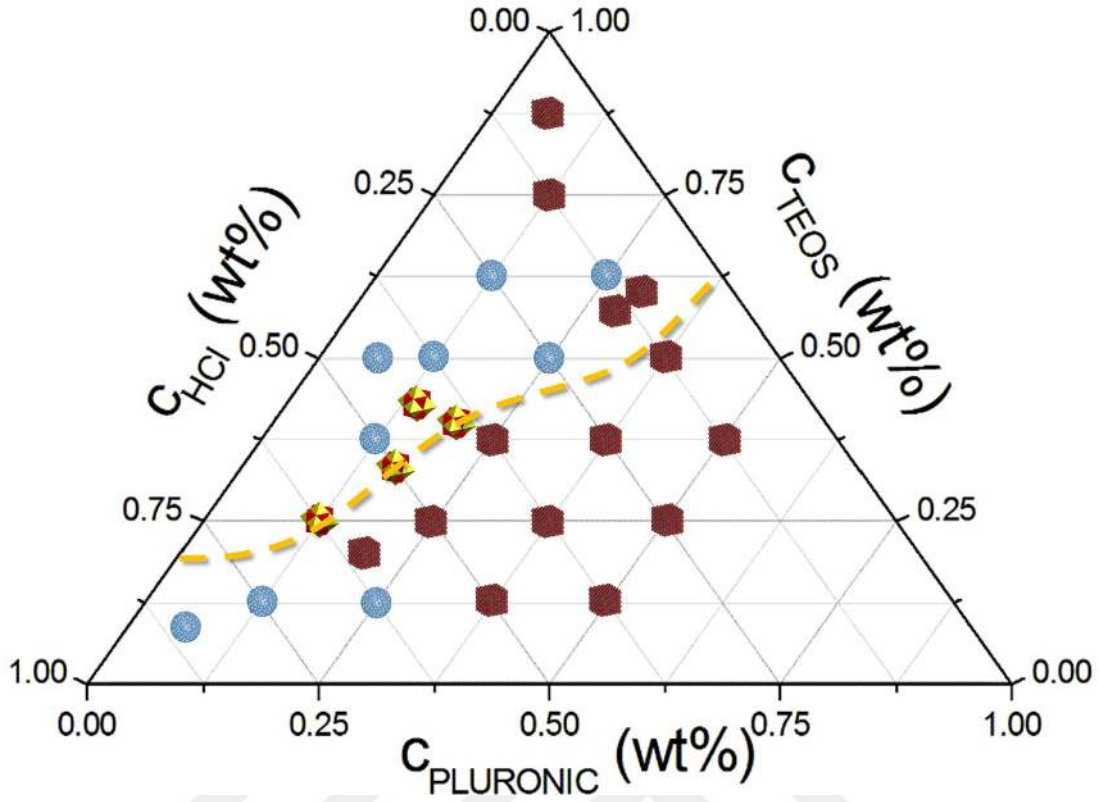

Figure 2.6 The ternary phase diagram of the morphology of MSPs synthesized by variation of concentration in HCl/Pluronic F127/TEOS system with constant TEOS concentration as 200 µL/mL. Each symbol represents defined morphologies (spheres, cubes (monoliths), and polyhedron)

The surface area of the samples was further studied by nitrogen adsorption measurements. The Brunauer–Emmett–Teller (BET) model while fitting the nitrogen adsorption isotherms was used to determine the specific surface area (SSA) of the samples. As it is summarized in Figure 2.7., we observed that specific surface areas of the most silica samples obtained in phase diagram are higher than 600 m^2/g. In most of the particles, SSA increased by increasing the amount of Pluronic F127 in the composition. However, when the weight percentage of TEOS was larger than 50 wt%, the dramatic decrease in SSA of the particles obtained. The effect of acid concentration on SSA of different silica morphologies was explained in the previous study. In lower acid concentrations (10^{-1} – 10^{-4} M), reactions were relatively slower, and resulted in monolith morphology. It created more ordered pores which result in larger hysteresis between nitrogen adsorption/desorption curves and higher SSA values. However, increase in HCl concentration in a range between 1.00 – 8.00 M resulted in higher SSA. This increase attributed to the decrease in size of spherical particles [7]. The results represented in Fig 2.7. showed that results of SSA measurements were in line with previous study. The

increase in weight percent of HCl acid resulted in increase in SSA for example 459 m^2/g to 740 m^2/g for spherical particles. In addition, monolith structures showed increase in SSA values by decreasing the acid concentration and the change obtained in a range between 589 m^2/g and 710 m^2/g. On the other hand, combined effects of concentration of reactants showed different SSA values.

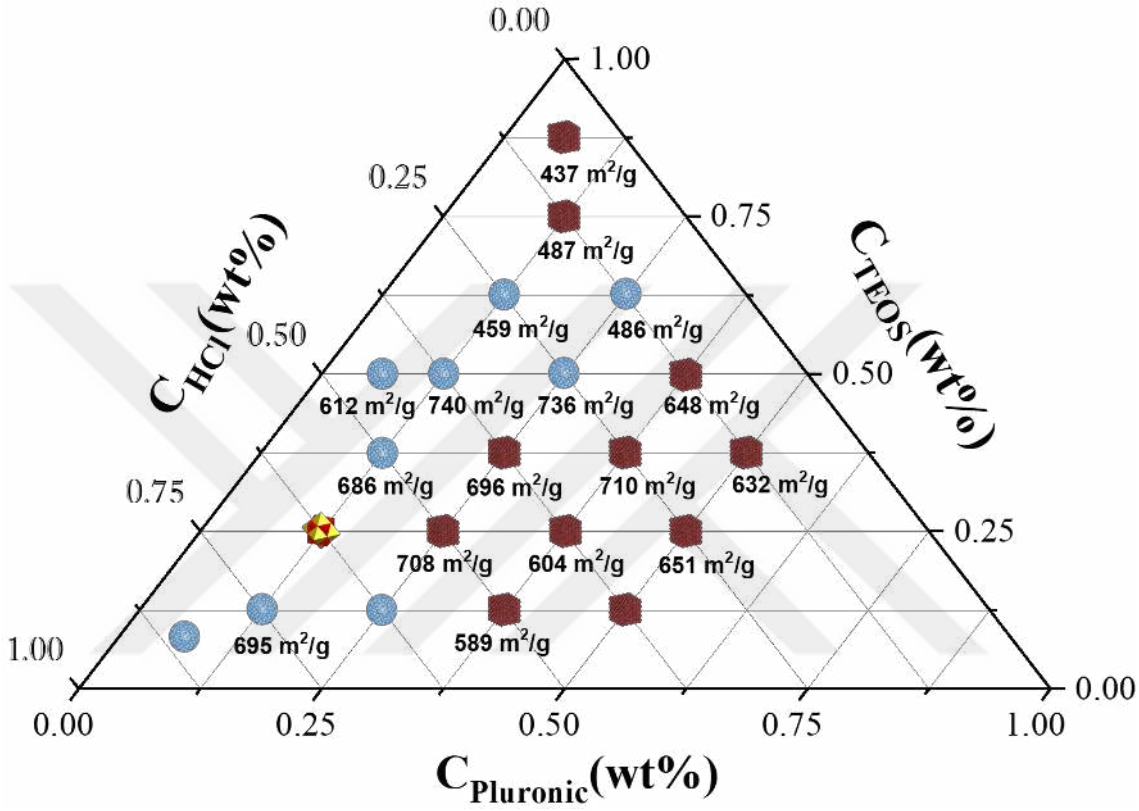

Figure 2.7 Specific surface area of the MSPs which were synthesized with constant TEOS concentration as 200 µL/mL was determined with BET method from nitrogen adsorption measurements.

XRD analysis of silica particles showed that all of the particles have an amorphous structure. Figure 2.8. represents only one analysis from all measurements. Because of the same structure of the plots from all samples in the designed matrix, only one sample is shown here as representative. Similar results of XRD analysis for amorphous silica particles in the reported studies were obtained from MSPs synthesized with HCl/Pluronic F127/TEOS system [99].

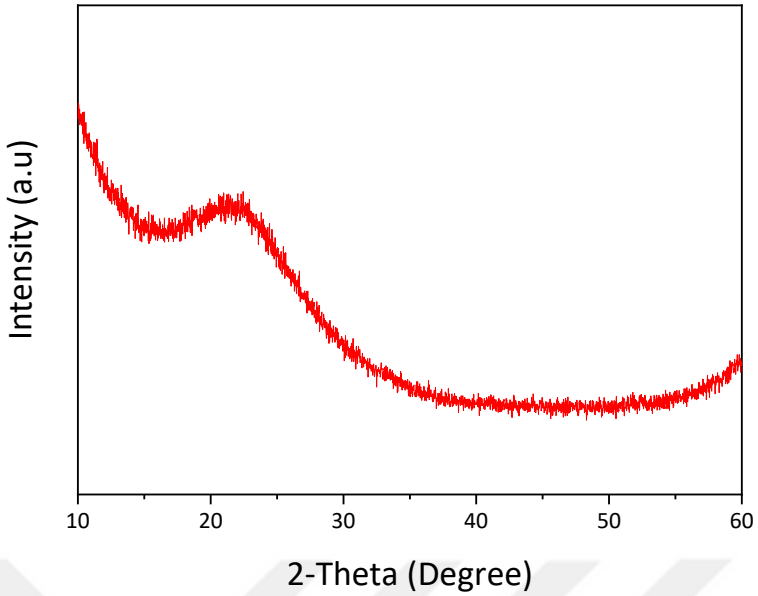

Figure 2.8 Representative XRD analysis of MSPs in the phase diagram.

2.3.2 The Effects Of Concentration Parameters on the Synthesis of MSPs by HCl/Pluronic F127/TEOS System

After the investigation of ternary phase diagram of morphology of silica structures, we tried to understand the effect of reactants on morphology and pore structure of MSPs. The effect of acid concentration on the morphology of MSPs is already investigated by the previous study. HCl concentration was varied in a range of $10^{-4.0}$ – 8.0 M and obtained monolith to spherical particles with increasing the HCl concentration. It is found that the hierarchical morphology of MSPs was synthesized by two steps. First, the ordered cylindrical pores which have 3-5 nm diameter came together to form primary porous silica particles with a hexagonal shape, then those primary particles agglomerated to create spherical secondary particles. By higher acid concentrations formation of silica gels was found faster and the yield of the reaction was higher. On the other hand, lower acid concentration made the speed and yield lower, but pores were more ordered in the structure.

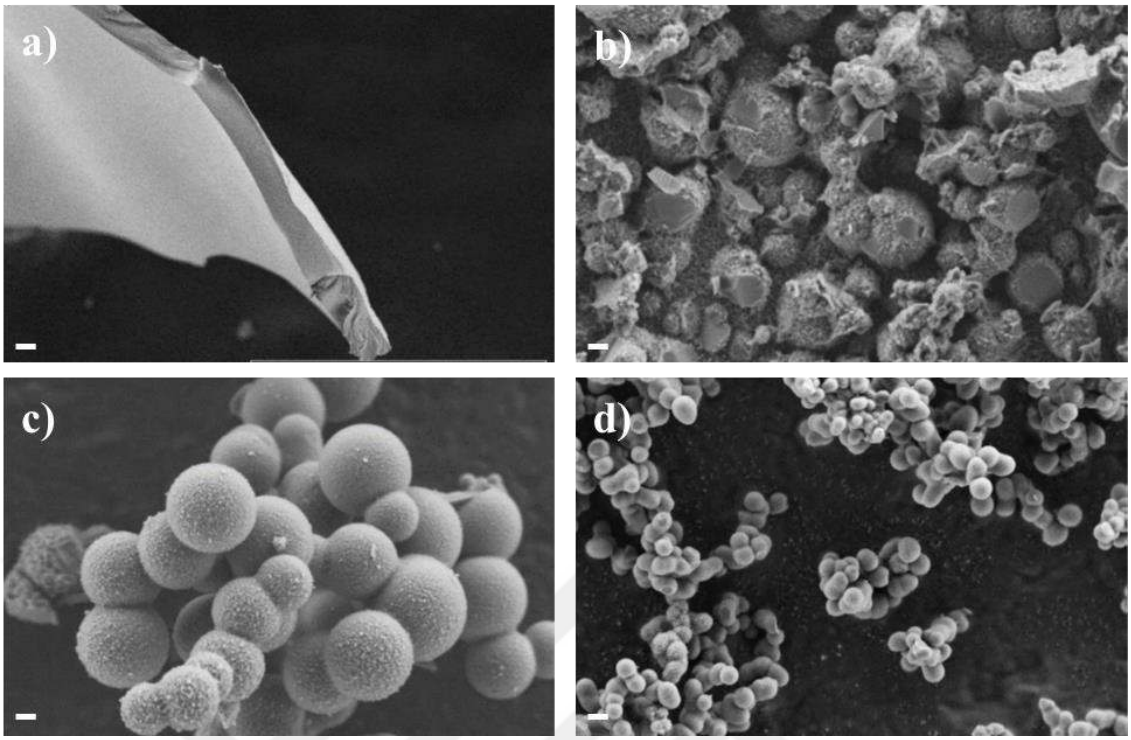

Figure 2.9 Morphology of the mesoporous silica structures synthesized in the synthesis solution which had 200 µL/mL TEOS, 0.01 g/mL Pluronic F127 at varied HCl concentrations as a)10^{-4}M, b) 1.00 M, c) 3.00 M , and d) 8.00 M. [7].*Scale bars correspond to 10 µm for a), and 1 µm for b,c,d).*

In this part of thesis work, we investigated the effect of surfactant concentration, silica precursor concentration on morphology and pore structure of silica structures. Additionally, we investigated the effect of dilution of reaction mixture by keeping the composition constant on properties of MSPs. The reaction system was modified by changing two important factors during the synthesis. First, the solution of HCl/Pluronic F127 was prepared according to the concentrations in the final volume of the reaction mixture. Secondly, reactions were carried out in the closed systems to avoid evaporation of TEOS. These modifications resulted in enhancing the surface area of the porous silica structures.

The Effect of Pluronic F127 Concentration on The Morphology of MSPs

The surfactant in the reaction mixture can help to stabilize the particle formation and affect the pore formation mechanism. In this part of the study the effect of Pluronic F127 concentration on particle stabilization and pore formation was investigated. The synthesis of MSPs was carried out by varying concentrations of Pluronic F127 in the reaction

mixtures in the range of 0.01 to 0.05 mg/mL. The concentrations of reaction mixtures and N_2 adsorption/desorption results are summarized in Table 2.2.

Table 2.2 Summary of silica synthesis concentrations which have different amounts of Pluronic F127, specific surface area (SSA), pore size (d_p), and pore volume (V_p).

Sample No:	Pluronic F127 (g/ml)	TEOS (µL/mL)	HCl (M)	SSA (m2/g)	d_p (nm)	V_p (cm^3/g)
KS15	0.01	200	4.00	583	7.52	0.41
KS16	0.03	200	4.00	789	6.50	0.34
KS17	0.05	200	4.00	719	4.16	0.17

Previous results [7] showed that higher acid concentration results in spherical particles as morphology. So, we fixed the HCl concentration as 4.00 M in reaction mixture. We changed the concentration of Pluronic to investigate its effect on the morphology and pore structure. As it is shown by SEM images in Fig 2.10., aggregation of spherical silica particles was lower and particle size was smaller by the increase of surfactant concentration. In the nature of the sol-gel method, larger particles are more favorable energetically. So, smaller silica nuclei aggregate during the gelation process to create the final structure of the 3D morphology. However, increasing the amount of surfactant affect the micelle formation and templating ability. Interaction between silica precursor and Pluronic starts in more micelles when the amount of Pluronic increased. Then, many small reaction cells would be formed to create silica nuclei in many different places of the mixture. So, slightly smaller (Fig 2.10) and less aggregated particles were formed because the difference between the two nuclei was narrower with the increase of surfactant. KS15 and KS16 samples showed closer mean particle sizes as 2.34 ± 0.57 µm and 2.29 ± 0.39 µm, respectively, with ImageJ analysis of SEM images. However, the KS17 sample which has the highest amount of Pluronic in the synthesis showed a higher decrease in the mean particle size as 1.77 ± 0.37 µm. Also, the surface quality of silica particles was better by increasing the concentration of Pluronic F127.

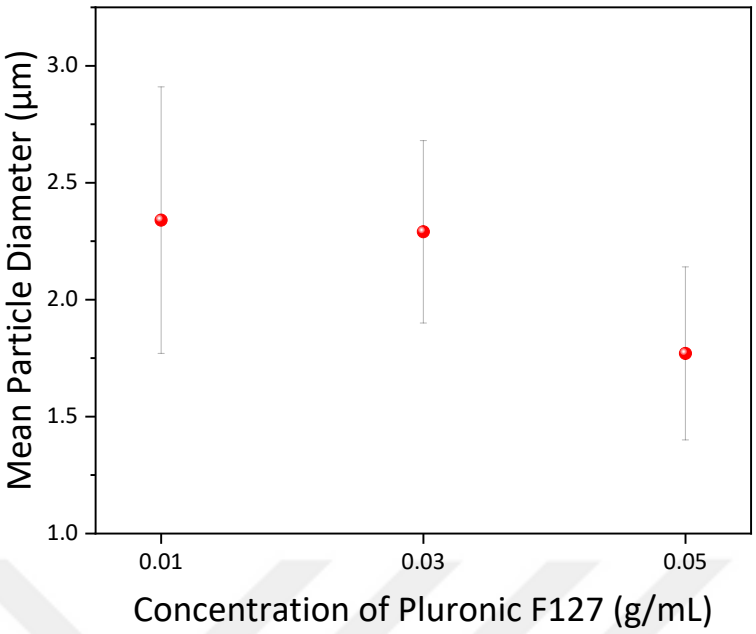

Figure 2.10 The change of spherical secondary particle size as a function of the concentration of Pluronic F127.

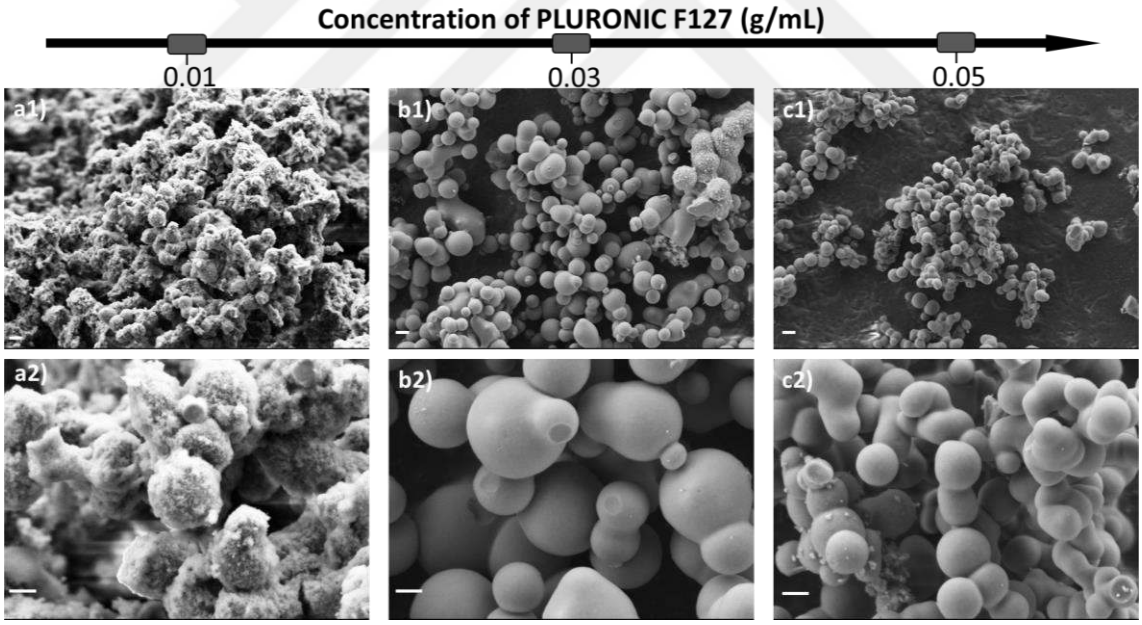

Figure 2.11 SEM images of mesoporous silica structures synthesized by different Pluronic F127 concentrations as a1-2) KS15, b1-2) KS16, and c1-2) KS17. The concentrations are summarized in Table 2.2. Scale bars are 2 µm for the images at top (a1,b1,c1) and 1 µm for the images at down (a2,b2,c2).

These results showed that the increase in the concentration of surfactant resulted in smaller particle size, smaller pore volume, pore diameter, and higher specific surface area of the particles. The decrease in the size of the particles can be attributed to the ability of Pluronic F127 to stabilize the particle formation. Similar results for pore diameter and

pore volume were also obtained with the increase in the amount of Pluronic. The decrease in pore sizes from 7.52 nm to 4.16 nm and pore volumes from 0.41 cm^3/g to 0.17 cm^3/g can be attributed to the number of micelles formed by the surfactant. Higher concentrations of Pluronic F127 results in formation of a greater number of micelles. It means that more reaction sites were formed, and smaller sizes of primary particles were able to be formed. These smaller size of primary silica particles fuses to form secondary particles as it was described above. Agglomeration of smaller size primary particles results in smaller size pore diameters and less volume of the pores.

Figure 2.12 represents the adsorption isotherms of silica particles synthesized by different amounts of Pluronic. KS16 and KS17 showed Type II adsorption isotherm. The adsorbed quantity by those samples increased by the increase of pressures and both have saturation points below 0.2 relative pressure of nitrogen. However, the isotherm obtained from KS15 had a shape more like a mixture of Type II and Type IV. As described in section 1.2.2.3., this large space between adsorption and desorption can be obtained when the critical pore width is exceeded. KS15 was the sample that had the highest pore width at 7.52 nm. Therefore, the gap between adsorption and desorption curves can be attributed to the pore sizes. Smaller pore sizes, the smaller gap can be clearly seen from the isotherms of the samples. The last increase in the quantity adsorbed by higher relative pressures is due to the multilayer adsorption of nitrogen during the physisorption analysis. Pluronic F127 acts as a porogen in the reaction mixture. Silica clusters are attached by hydrogen bonding interactions to the micelles formed by Pluronic in the reaction mixture. Cooperative self-assembly of TEOS and Pluronic forms hexagonally ordered structures which are filled by surfactant molecules (micelles) in the primary particles. After calcination of the particles, evaluated temperature removes Pluronic from the structure and the porous structure of the silica is obtained. Therefore, higher surface areas will be produced by higher amounts of Pluronic F127. On the other hand, the results showed that 0.05 g/mL concentration showed a slightly lower surface area than 0.03 g/mL. The difference in that range (>700 m^2/g) is negligible but this difference can be the result of losing order on the pores. The high number of small size pores in small particles results in lower specific surface areas by blocking effect of randomly oriented pores.

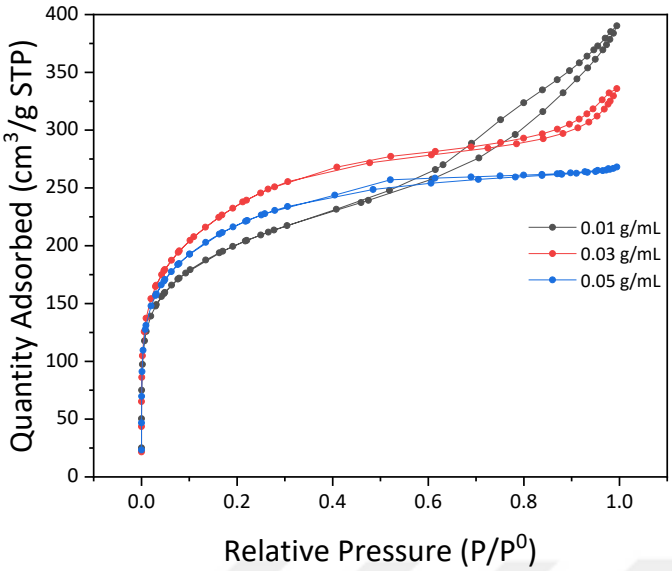

Figure 2.12 Adsorption isotherm plots of silica particles synthesized by different amounts of Pluronic F127. Isotherm plots of KS15 (0.01 g/mL), KS16 (0.03 g/mL), and KS17 (0.05 g/mL) are represented by black, red, and blue, respectively.

Dilution of Three Reactant of The Synthesis (HCl/Pluronic F127/TEOS) and Effect of Dilution Ratio on The Morphology of MSPs

Typically, mesoporous silica particles were synthesized under the same conditions such as room temperature reactions, and same calcination temperatures as 450 °C, without stirring. After investigating the influence of the surfactant concentration on the morphology of MSPs, the effect of the concentrations of all three reactants, HCl/Pluronic F127/ TEOS, was also investigated by serial dilutions of all in the constant composition of three reactants. A detailed concentration list is given in Table 2.3. Calculations of the concentrations of reactants were derived from the concentrations of the KS16 sample from the previous section.

Table 2.3 Summary of silica synthesis concentrations which have different dilution rates of all three reactants HCl/Pluronic F127/TEOS

Sample No:	Pluronic F127 (g/ml)	TEOS (µL/mL)	HCl (M)
KS16	0.03	200	4.00
KS19	0.0075	50	1.00
KS20	0.015	100	2.00
KS21	0.0225	150	3.00
KS22	0.0525	350	7.00

Previous studies showed that acid concentration is significantly effective on the morphologies of MSPs. When the acid concentration was lower than 3.00 M, monolith silica particles were the main morphology besides spherical silica particles. Higher reaction kinetics due to higher concentrations of the acid catalyst made the particles not only spherical but also decreased the ordering of their pores. Moreover, the mean particle size of MSPs decreased from approximately 4.00 μm to approximately 1.00 μm [7]. However, the synthesis of KS19-22 samples resulted in different morphologies at the same acid concentration reported previously. As it is represented in Fig 2.13., concentrations of all reactants are effective on changing the morphology and porous structure even if the ratio between them is not changed. Mainly monolith particles were obtained in low acid concentrations (below 3.00 M). However, monolith particles were also produced in the high concentration of HCl acid as 7.00 M (Fig 2.13. e1-2). KS22 was the proof that the morphology of MSPs would not be estimated by only acid concentration. The amounts of TEOS and Pluronic F127 are also effective in morphology variations. Especially the amount of surfactant is very important for the resulting morphology of silica particles, as is discussed in the previous chapter. An accurate ratio between silica precursor and surfactant should be chosen to get spherical particles. Otherwise, too low and too high ratios about surfactant to the precursor have resulted in monoliths even if the reaction kinetic would be very fast due to the acid concentration. That can be attributed to the binding effect of extra surfactant in the reaction. Due to large amounts of Pluronic F127, there are excess polymeric parts in the reaction mixture which makes spherical particles covered and fused more. In the previous synthesis, it is observed that particles were fully spherical in 7.00 M HCl acid concentrations but when the amounts of Pluronic and TEOS increased, monolith particles were produced. The concentration is of TEOS is also effective on that result, but it is not as effective as the amount of the surfactant.

KS21 has shown the best spherical structure among those samples with morphology and individuality. The effect of lowering the ratio between Pluronic F127 and TEOS will be explained in the next chapter.

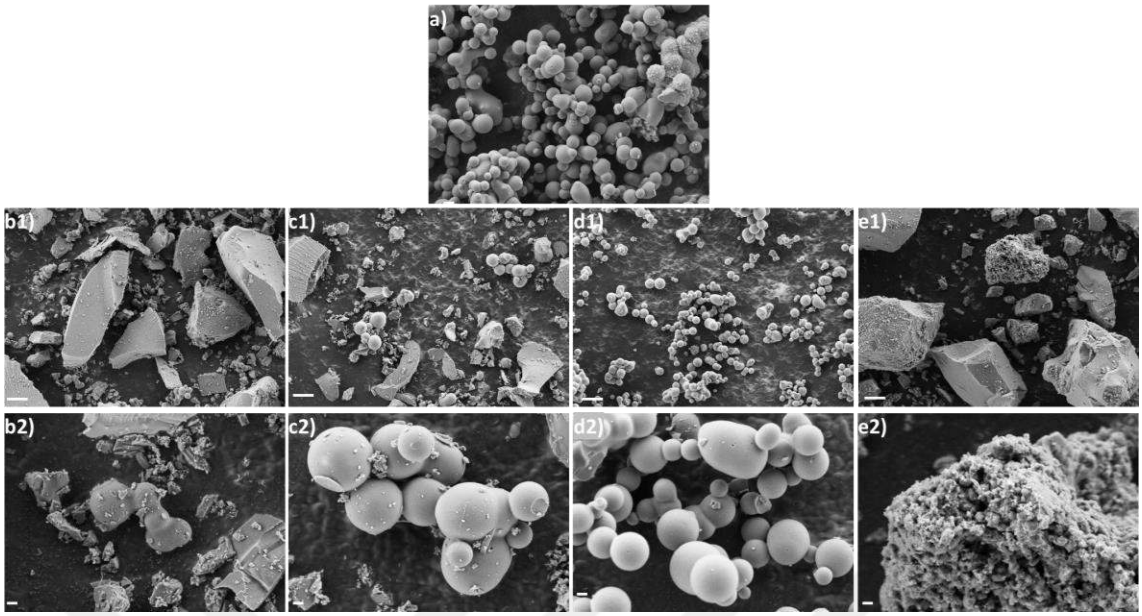

Figure 2.13 SEM images of MSPs synthesized by different dilution ratios on concentrations of three reactants, HCl/Pluronic F127/TEOS without changing their ratios in between. The scale bar on the images corresponds to 1 μm for (b2), 2 μm for (a,c2,d2,e2), and 10 μm for (b1,c1,d1,e1). The samples are represented by a) KS16, b1-2) KS19, c1-2) KS20, d1-2) KS21, and e1-2)KS22.

The SEM images of KS22 particles which have the highest concentrations among the full set proved that micron-sized monoliths were formed by agglomeration of secondary spherical particles. Because of high amounts of Pluronic F127 and TEOS, the morphology of silica particles could not be controlled by the kinetics of the reaction which was very high due to the high concentration of HCl acid. After removing the Pluronic F127 from the structure by calcination pores were formed with secondary spherical particles which were connected with the excess amount of TEOS. This kind of morphology is promising for applications that do not require a certain shape of the particles such as wastewater treatment.

Figure 2.14. represents the adsorption isotherms of samples named by KS19-21 (a) and KS22 (b). KS19-21 samples which were diluted showed from KS16 (Fig 2.14.) showed similar adsorption isotherm as Type II with KS16 (Fig 2.12). The saturation points of those particles were below 0.2 relative pressure, and the curves did not have any hysteresis curve by adsorption and desorption processes. These type of adsorption behaviors means that the particles do not have pore sizes higher than 4 nm which is the critical diameter size to have large hysteresis of adsorption and desorption curves. On the other hand, KS22 (Fig 2.14 b) had a completely different adsorption isotherm than the

other pairs of it with the same ratios of HCl/Pluronic F127/TEOS. The shape of its adsorption isotherm was similar to Type IV(a). The hysteresis curve between adsorption and desorption of the gas is large enough to understand that particles have pore sizes larger than 4 nm. Also, the average pore width was calculated for adsorption and desorption as 6.37 nm and 4.63 nm, respectively. The difference between KS22 and others showed how the particle properties like shape, pore size and SSA can change at one composition by different concentrations. Same composition created by higher amount of HCl acid concentration and TEOS effected the morphology of the particles because of higher rates of hydrolysis and condensation reactions. As it was clear in SEM images, KS22 particles were formed by spherical particles bound with bridges that are formed by extra TEOS in the reaction mixture. In addition, the larger amount of surfactant also contributed to the formation of these particles. Because of different solubility of surfactant in different concentrations of HCl acid and the number of micelles can affect the particle properties. So, the secondary spherical particles do not consist of high pore sizes, but the last structure has gaps in between spherical particles.

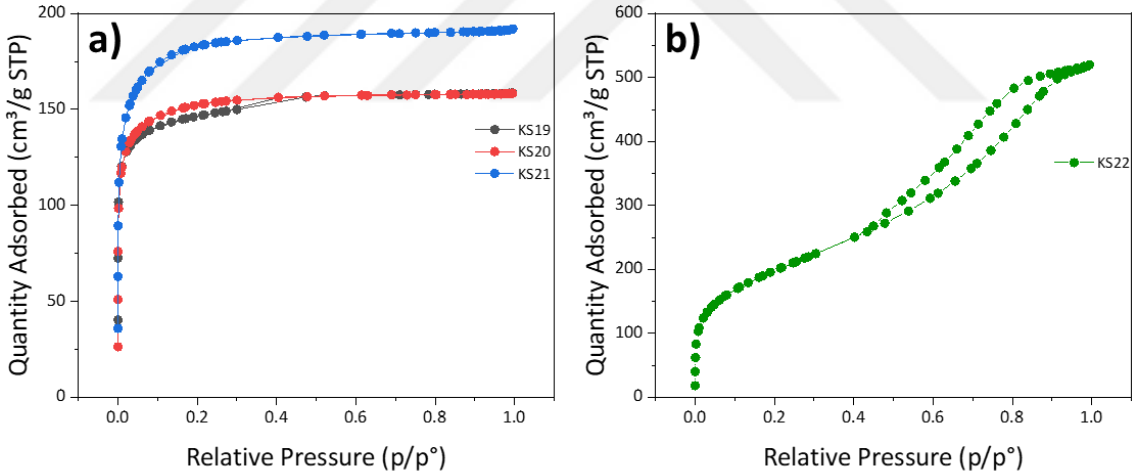

Figure 2.14 Adsorption isotherm plots of silica particles synthesized by the concentrations given in Table 2.3. Isotherm plots of KS19, KS20, and KS21 are represented in a) by black, red, and blue, respectively. The isotherm plot of KS22 is represented in b) by green.

Effect of Lowering the Pluronic/TEOS Ratio on Morphology of MSPs in the Same Concentrations of Aqueous Acid Solution

The investigation of the effect of dilution rate of all reactants showed that morphology of MSPs can be tuned by not only acid concentration but also the ratio between TEOS and Pluronic F127 in the reaction mixture. The particles were synthesized with different

amounts of TEPS to understand the effect of the Pluronic/TEOS ratio. Typically, the concentrations were selected based on the concentrations of KS21 from the previous section due to its spherical morphology and more individual formation. As it is summarized in Table 2.4., the amount of TEOS was varied in the range of 50-500 µL/mL when the concentrations of HCl acid and Pluronic F127 were kept constant. The influence of TEOS concentration on morphology and specific surface area of MSPs was investigated by SEM images and BET analysis, respectively.

Table 2.4 Summary of silica synthesis concentrations which have different amounts of TEOS in constant HCl acid and Pluronic F127 concentrations.

Sample No:	Pluronic F127 (g/ml)	TEOS (µL/mL)	HCl (M)
KS28	0.0225	50	3.00
KS29	0.0225	100	3.00
KS21	0.0225	150	3.00
KS30	0.0225	200	3.00
KS31	0.0225	250	3.00
KS32	0.0225	500	3.00

Figure 2.15. representing the SEM images of MSPs listed in Table 2.4. showed that increasing the amount of TEOS in the reaction mixture changes the morphology of MSPs from spherical to highly fused particles after some level. This can be attributed to the high number of nuclei formed by hydrolysis and condensation reactions of TEOS. When the ratio between Pluronic F127/TEOS decreased by increasing the amount of TEOS, silica excess amounts of nuclei are formed for templating and shape stabilizing ability of the surfactant. The continuous hydrolysis of extra TEOS molecules in the reaction mixture perform as a binder to the secondary particles formed by agglomeration of primary particles. Fig. 2.15. d,i) shows that KS32 has very small-sized (~30 nm) spherical particles that were bound and formed micron-sized monolith particles. The results showed that the synthesis of individual spherical particles is almost impossible. Because the excess amount of silica precursor obtained by increasing the concentration above 500 µL/mL agglutinate spherical secondary particles. So, micron sized monolith like structure was formed by decreasing the ratio between surfactant and silica precursor.

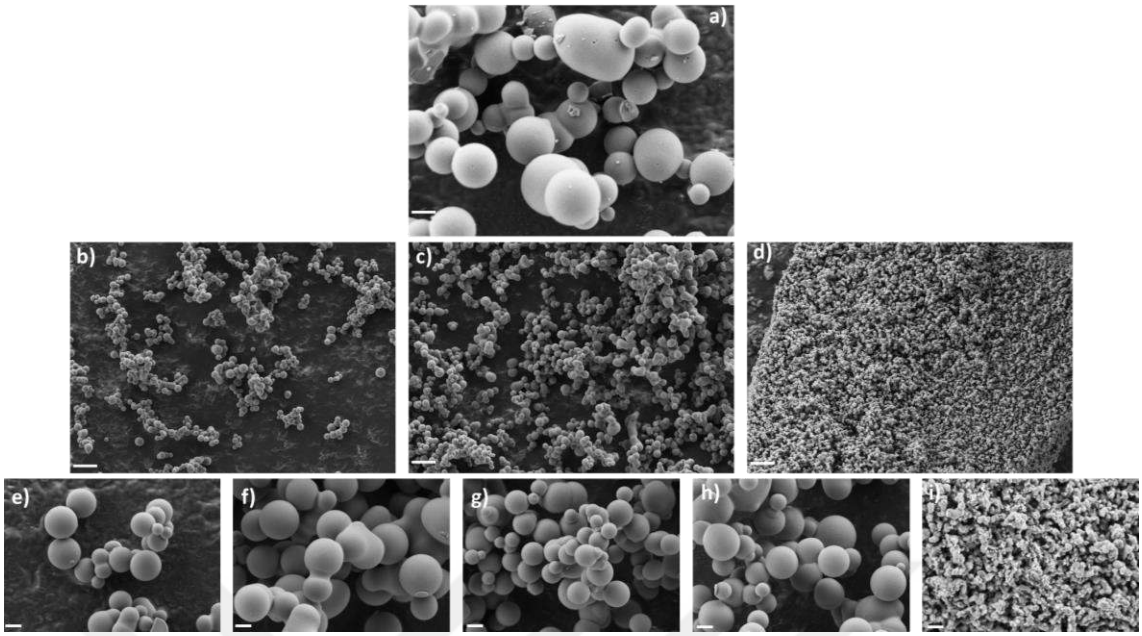

Figure 2.15 SEM images of MSPs synthesized by different amounts of TEOS in the reaction mixture with constant HCl acid and Pluronic F127 concentrations. The scale bar on the images corresponds to 2 µm for (a,e,f,g,h,i) and 10 µm for (b,c,d). The samples are represented by a) KS21, b,e) KS28, c,g) KS30, d,i) KS32, f) KS29, and h) KS31.

Figure 2.16. represents the adsorption isotherms of silica particles synthesized under the conditions that are summarized in Table 2.4. The samples which were synthesized with a relatively lower amount of TEOS (KS28-31) showed an isotherm that is a mixture of Type I(b) and Type II. Their saturation points were around 0.1 relative pressure and the hysteresis between adsorption and desorption curve was small. It means that the particles were mainly microporous. In addition, the specific surface area of the particles was increased by increasing the amount of TEOS in the system. The SSA of the particles increased from 483 m^2/g to 653 m^2/g. The specific surface area of the sample KS30 was higher than KS31 although KS31 was synthesized with a higher amount of TEOS. Since the values were very near to each other, the difference can be negligible and be commented as that SSA can be increased up to some limiting value of approximately 650 m^2/g. On the other hand, the sample KS32 which was a monolith formed by smaller spherical primary particles showed an isotherm that was the mixture of Type II and Type IV(a). After the first saturation point, the quantity adsorbed was continuously increased by increasing the relative pressure. The hysteresis between adsorption and desorption of N_2 gas was also larger than in other samples. These results were in good agreement with the previous results obtained in earlier sections. Due to the interspaces between spherical

particles, they show this type of isotherms. Also, the specific surface area of the sample KS32 was the highest in that set of samples. Its SSA was 680 m^2/g.

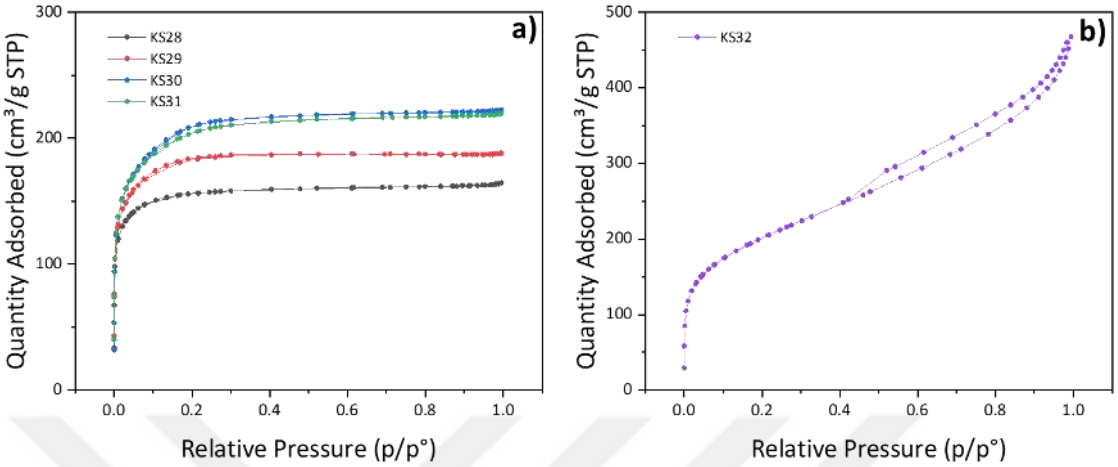

Figure 2.16 Adsorption isotherm plots of silica particles synthesized by different amounts of TEOS in the reaction mixture with constant HCl acid and Pluronic F127 concentrations. Isotherm plots of KS28, KS29, KS30, and KS31 are represented in a), and the isotherm plot of KS32 is represented in b).

2.3.3 The Effect of Processes Conditions and Parameters to Morphology o the MSPs Synthesized By HCl/Pluronic F127/TEOS System

In addition to determining SSA and morphology of MSPs with concentration control over three components, we also studied the effects of external process parameters such as hydrothermal treatment and stirring on the particles. These processes are applied on different particles not only from the phase diagram matrix but also from previous studies.

The Effect of Hydrothermal Treatment on SSA of Particles Synthesized with HCl/Pluronic F127/TEOS System

It was found in the literature that hydrothermal treatment (HT) helps the ordering of the pores and enhances the SSA of silica particles [100], [101]. To understand the influence of the process in the HCl/Pluronic F127/TEOS system, spherical and monolith particles from the phase diagram matrix with particles size of ~3.00 micrometer were hydrothermally treated. Also, the post-treatment process was applied to the sample which has a composition of 4.00 M HCl, 0.01 g/mL Pluronic F127 and 200 µL/mL TEOS. All of the samples were synthesized under two different conditions. When the first condition was the same as all other samples in previous sections of the chapter, TEOS was added

with increasing the temperature of HCl/Pluronic 45 °C for the heat-treated counterparts of the samples. After completely adding TEOS, the second type of the samples was kept under 80 °C in an autoclave for 24h. After that, drying and calcination processes were applied equally on both samples. The specification of the investigated samples is summarized in Table 2.5. including the SSA results before and after hydrothermal treatment.

Table 2.5 Effect of hydrothermal treatment on the selected samples.

Synthesis Concentrations				Properties				
Sample No:	Pluronic F127 (g/ml)	TEOS (µL/mL)	HCl (M)	Shape	Size (nm)	SSA no HT (m^2/g)	SSA HT (m^2/g)	Improvement with HT (%)
PD08	0.05	200	3.84	S	3000	739.56	829.81	12.20
PD10	0.14	200	1.28	M	-	648.16	872.25	34.57
KS14	0.01	200	4.00	S	2500	331.03	912.92	175.78

Investigation of the samples which were synthesized with HT or without HT by SEM and Scanning Transmission Electron Microscope (STEM) images showed that the shape of the samples was not influenced by HT. As it is represented in Fig 2.17, spherical PD08 particles remained spherical when HT was included in the synthesis. Unfortunately, the detailed analysis for pore structure and order was very difficult because that given high voltage from STEM damaged the walls in 1 minute. On the other hand, lower voltages were not able to visualize pore structure. Moreover, the specific surface area and pore structure of the samples were analyzed by BET and BJH methods in N_2 adsorption/desorption tests. Those measurements were summarized as the HT process possibly enlarged the pores and enhanced the order of pores and resulted in higher surface areas than normally synthesized particles. As it is summarized in Table 2.5., specific surface areas of the particles were increased significantly after HT. However, the sample (PD08) which has SSA higher than 700 m2/g was influenced less than the other particles. Especially KS14 which has a mixture of micropores and larger pores, mostly micropores, was the most influenced sample from HT. This can be attributed to the capacity of the HT process to enlarge the pores and enhance the order. KS14 and PD08 have the approximately same amount of HCl acid but the amount of Pluronic F127 in PD08 is five times larger than KS14. We showed in Section 1.3.1 that increasing the amount of surfactant, not only increases the number of pores but also makes the pores smaller. So, the larger number of smaller pores would be especially harder to enhance the order. On

the other hand, the sample PD10 had the largest amount of Pluronic F127 but it was affected more than PD08 because of the morphology. Due to its monolith morphology, HT would affect not the only order of pores from primary particles, but also the gap between secondary spherical particles forming monolith. Moreover, that sample had the lowest amount of acid catalyst in the system, so pores were more ordered and had space be enhanced.

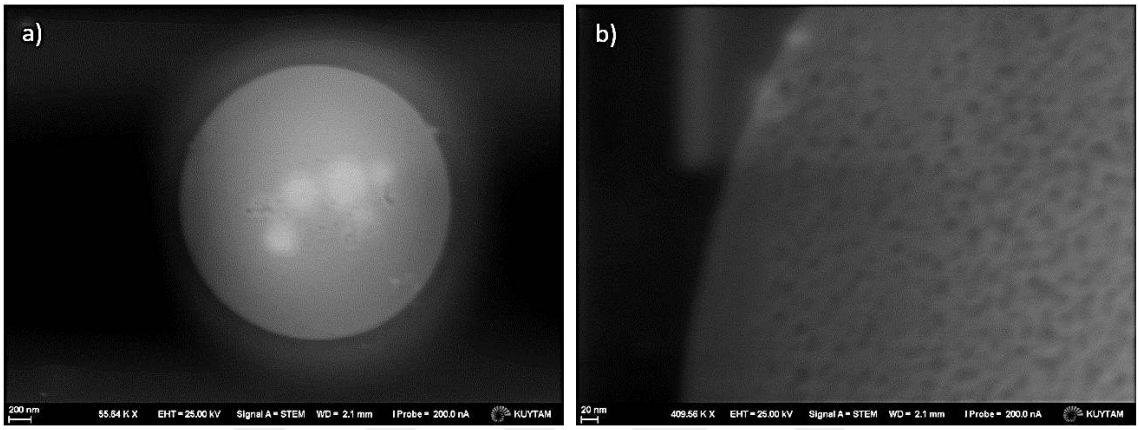

Figure 2.17 STEM image of hydrothermally treated sample PD08 with different magnifications. Scale bars on the images correspond to 200 nm and 20 nm for a) and b), respectively.

Figure 2.18. represents the nitrogen adsorption-desorption isotherms obtained from the sample KS14 (HT and no HT). Both samples showed Type II isotherm. The sample which was not treated had a very low saturation point when it is compared to the sample which is hydrothermally treated. Also, the hysteresis between adsorption and desorption curves of the hydrothermally treated sample was much larger than the normally synthesized particles. The shape of the isotherm plots and BJH measurements showed that HT contributed to the micropores and enlarged them up to 5 μm.

Based on these results, it was concluded that high surface area samples with improved pore size and order can be successfully produced with the acid-catalyzed synthesis route of HCl/Pluronic F127/TEOS.

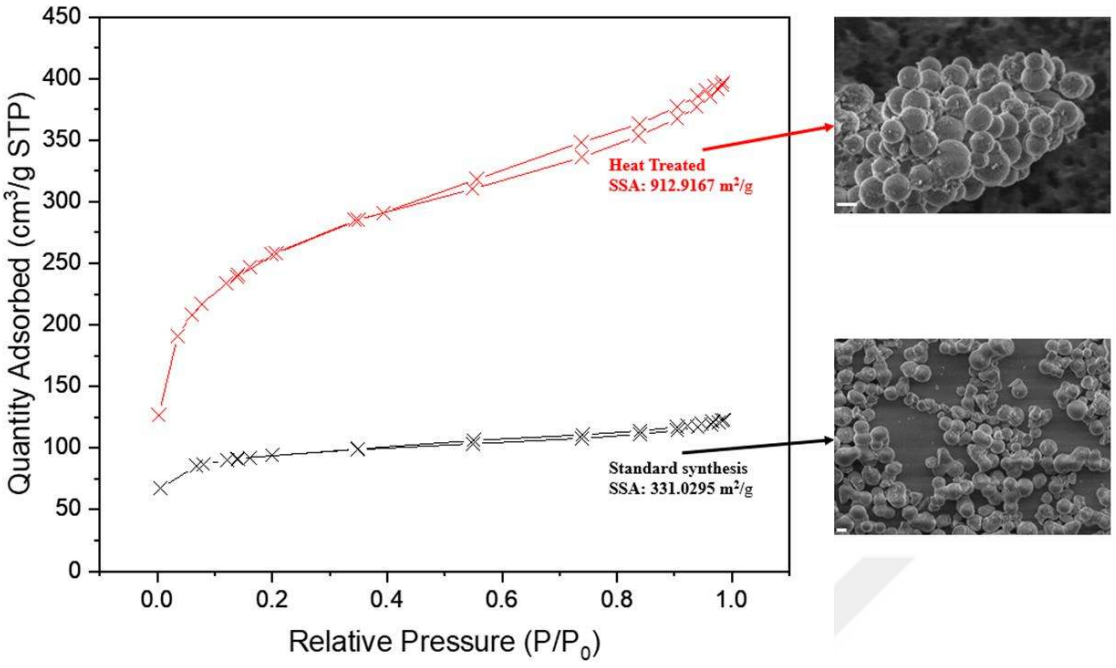

Figure 2.18 Nitrogen adsorption-desorption isotherms of mesoporous silica samples synthesized under different conditions (heat treatment and non-treated) with the same solution of 0.01 g/mL Pluronic F127, 200 µL/mL TEOS, and 4.00 M HCl (KS14). The scale bars in SEM images are 2 µm.

The Effect of Stirring Rate and Stirring Time on The Morphology of Mesoporous Silica Particles

All the reported samples in previous chapters were vigorously stirred by shaking for few minutes (2-3 mins) after adding TEOS to the reaction mixture. Understanding the influence of stirring on the system was investigated by different sets of particles. In the first set, we changed the stirring rate and duration for the synthesis in two different pH. The synthesis conditions are summarized in Table 2.6. The mixture of Pluronic F127 and HCl solutions was prepared by manually shaking similar to the samples in previous sections. The reaction mixtures were stirred with a magnetic stirrer by different stirring rates during the hydrolysis and condensation reactions of TEOS. The magnetic stirring processes were applied for 5 mins and 30 mins to understand the effect of duration.

According to the SEM images and particle sizes, the samples which were stirred with 500 rpm showed similar properties such as particle size and surface texture with vigorously stirred samples. Increasing the stirring rate affected the surface of silica particles and made the surfaces rougher. In addition, the increase in stirring rate, as well as prolonged time resulted in more merged and larger sized particles, were observed. Therefore, a

higher stirring rate and longer stirring times influenced the morphology of the particles negatively and 5 mins stirring with 500 rpm was the optimum for the particles if stirring is necessary. However, vigorously mixing synthesis can result in more standard samples and make the products more reproducible. The results showed that the stirring process for our synthesis route is not advantageous and makes the system more complicated.

Table 2.6 Summary of silica synthesis concentrations and process parameters for stirring process applied on the system.

Synthesis Concentrations				Process Parameters	
Sample No:	Pluronic F127 (g/ml)	TEOS (µL/mL)	HCl (M)	Stirring Rate (rpm)	Stirring Time (min)
SE01	0.01	200	7.00	100	5
SE02	0.01	200	7.00	300	5
SE03	0.01	200	7.00	500	5
SE04	0.01	200	7.00	500	30
SE05	0.01	200	7.00	750	5
SE06	0.01	200	7.00	750	30
SE07	0.01	200	5.00	500	5
SE08	0.01	200	5.00	500	30
SE09	0.01	200	5.00	750	5
SE10	0.01	200	5.00	750	30

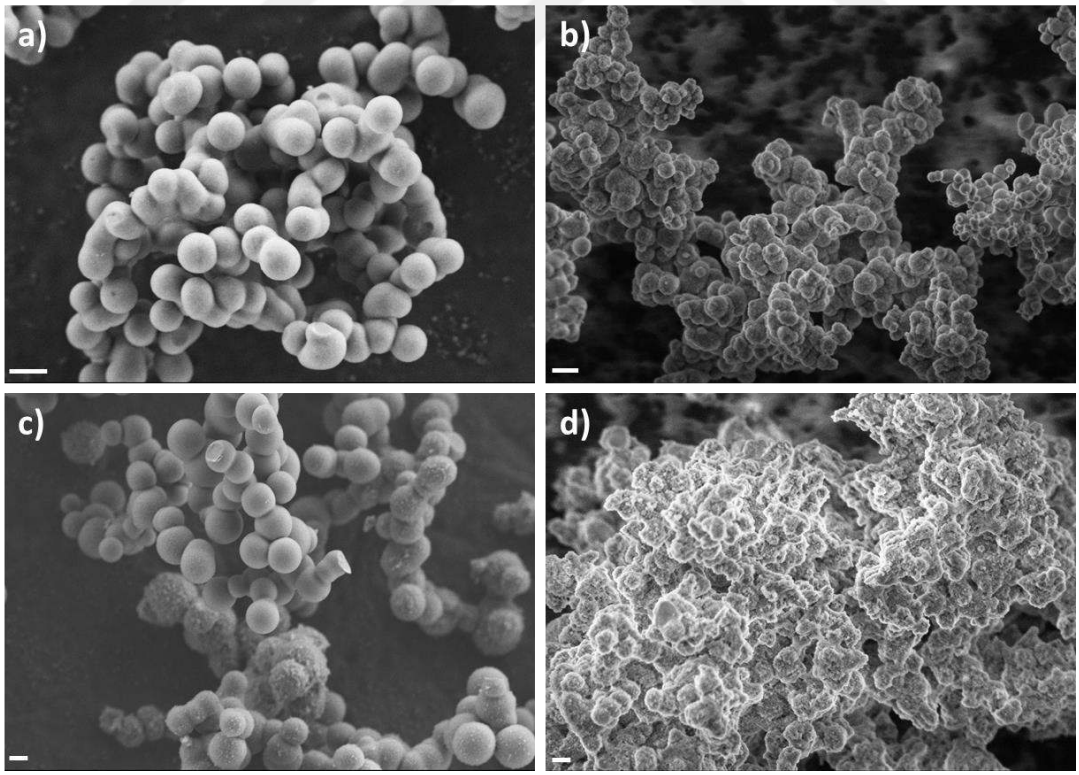

Figure 2.19 SEM images of the silica samples that were not stirred (a,c) and stirred (b,d) during the synthesis. The samples in a) and b) were synthesized with 7.00 M HCl and b) were stirred by 750 rpm for 30 mins. The samples in c) and d) were synthesized with 5.00 M HCl and d) were stirred under the same conditions with b). The scale bars correspond to 1 µm for a),c) and 2 µm for b),d).

The average particle size 1.2 ± 0.85 μm for the samples synthesized with 7.00 M HCl acid and 1.9 ± 0.2 μm for the samples that were synthesized with 5.00 M HCl acid. The particle sizes after stirring are mainly in the standard deviation of manually stirred samples but stirring made the standard deviations larger. Moreover, the particle size analysis of the samples made it harder than manually stirred samples due to more fused particles.

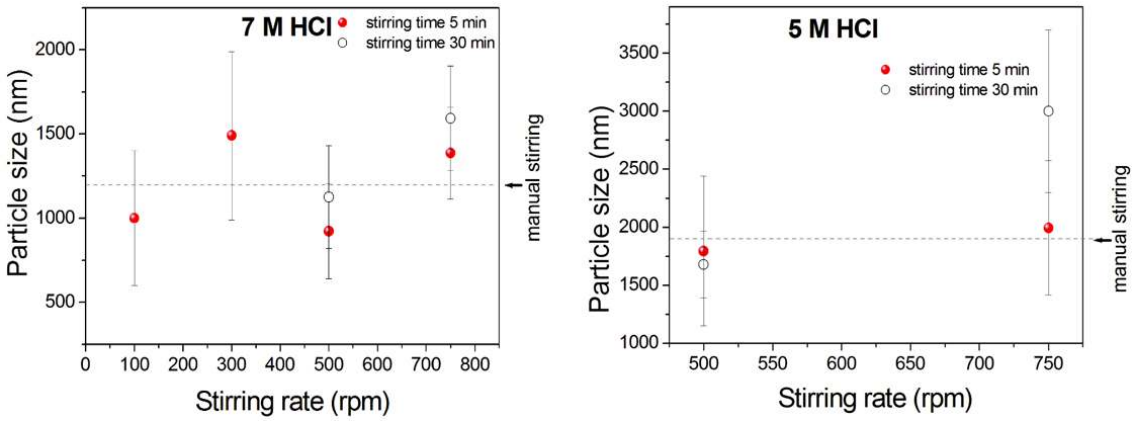

Figure 2.20 Effect of stirring rate and stirring time on the particle size of the samples.

Investigation of the effect of stirring on the morphology of the particles and mechanism of the synthesis we prepared the second set of the samples. The particles were synthesized with concentrations of KS21 (Section 1.3.2) but with lower amounts of TEOS. Serial dilutions to see the mechanism of particle formation under stirring were made in a range from 1:50 to 1:5. Otherwise, it was very hard to apply the stirring process with a magnetic stirrer for a long time. 500 rpm was chosen as the stirring rate due to the last results that were showing the closest properties by the products. The experimental conditions of the second set of samples were summarized in Table 2.7.

Table 2.7 Summary of silica synthesis concentrations and process parameters for the second set of samples that were analyzed to understand the mechanism of particle formation under stirring.

Synthesis Concentrations				Process Parameters	
Sample No:	Pluronic F127 (g/ml)	TEOS (μL/mL)	HCl (M)	Stirring Rate (rpm)	Stirring Time (h)
ST01	0.0225	3.00	3.00	500	24
ST02	0.0225	15.00	3.00	500	24
ST03	0.0225	18.75	3.00	500	24
ST04	0.0225	21.43	3.00	500	24
ST05	0.0225	30.00	3.00	500	24

The SEM images showed that stirring made the particles more fused when the amount of TEOS increased. After the first sample, ST01, all of the particles have spherical morphology. However, those spherical particles were fused and formed monolithic particles with the increase in TEOS concentration. Although the number of small (a few nm) spherical particles increased, their sizes were lower by the increase in the amount of TEOS. It can be attributed to the effect of stirring during the hydrolysis and condensation reaction. Because of the stirring process nuclei formation starts in many places, more than manually stirred samples, and formed particles reached their energy to be stabilized in monolithic particles. Also, silica precursor, TEOS, could behave like a binder in between small spherical particles to form a fused structure. On the other hand, the first sample showed some not clear spherical shapes, but it was mainly micrometer-scale bulks.

Those results showed that nm scale spherical particles can be produced by stirring the reaction mixture which has a relatively low amount of TEOS. The particles in the second set can be used in many studies in vivo. However, the system is needed to be more investigated to individualize those particles.

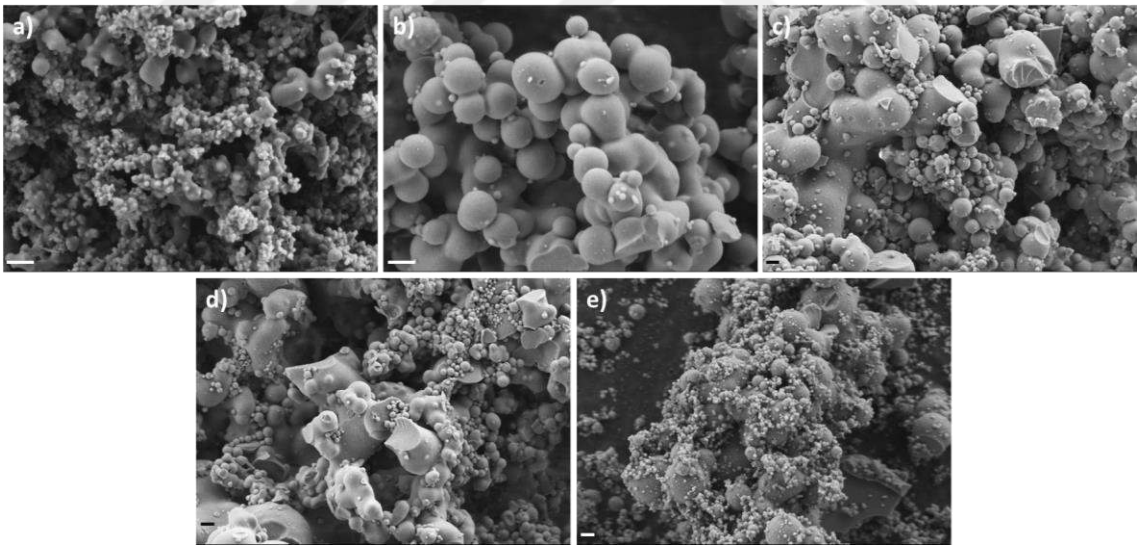

Figure 2.21 SEM images of the silica samples from the set of samples that were analyzed to investigate the mechanism of the particle formation under stirring. The samples were shown by letters as a) ST01, b) ST02, c) ST03, d) ST04, e) ST05 and scale bars correspond to 1 μm for each image.

2.4 Conclusion

Mesoporous silica structures for various applications were successfully synthesized by using Pluronic F127 as structure directing agent and TEOS as silica precursor in acidic

solutions. Various types of mesoporous silica particles (above 150 samples) having different particle properties such as morphology, size, pore size and specific surface area were successfully synthesized. Porous silica structures with monolith, spherical and polyhedron shaped samples were obtained by this template-directed synthesis method of surfactants. The effect of surfactant concentration, TEOS concentration, the Pluronic/TEOS ratio, composition of the reaction mixture, stirring and hydrothermal treatment processes was investigated particularly. It was clearly demonstrated that high surface are samples with various morphology can be produced with this method. The effect of those synthesis parameters mentioned above were systematically studied to understand mechanism of the synthesis method. The morphology of mesoporous silica samples changed from spherical particles to highly fused structures (can also be called monolith) by increasing the TEOS concentration from 50 µL/mL to 500 µL/mL in synthesis mixture. The morphology of the samples changed from spherical particles to monoliths as well by changing the concentrations of reactants in one composition. The composition which has 0.03 g/mL Pluronic, 200 µL/mL TEOS and 4.00 M HCl changed by the ratios as 1:4, 1:2, 3:4 and 7:4. The morphologies of the samples observed as monolith for 1:4 and 7:4 ratios when the others were spherical particles.

The combined effects of all the influences from concentration changes of the reactants were studied to have phase diagram of the synthesis. The main morphological areas were identified in the phase diagram and the specific surface area of the samples were determined and was found to be as high as 740 m^2/ g. The particles exhibited main contribution to the SSA from the microporosity (2-4 nm pore diameter) and mesopore size of average 6-8 nm was detected is several samples. The domination of each morphology is defined by this study in the phase diagram. Additionally, it was demonstrated that the morphology of polyhedron is the transitional step from spherical to monolith.

The enhancement of the specific surface area of mesoporous silica samples by ordered pore channels, increased pore size was also studied in this thesis work by hydrothermal treatment processes. The highest specific surface area, near 1000 m^2/g, was observed by carrying out the synthesis in autoclaves under 80 ^oC. Although the shape of particles remained as spherical, more fused particles were observed by this technique.

This study showed the ability of this cost effective and simple method to produce highly promising porous silica structures. Significantly high surface areas and pore volumes show promise to use them in applications such as drug delivery, adsorption, catalyst etc. Additionally, tuning the particle properties by the method will be easier due to the phase diagram and detailed report on effects. Synthesized mesoporous silica samples of this study were used in the next chapters to investigate the possible applications.

Chapter 3:

ADSORPTION OF RHODAMINE 6G BY MESOPOROUS SILICA PARTICLES SYNTHESIZED WITH DIFFERENT ACID CATALYZED SYSTEMS

3.1 Motivation

Wastewater effluent of the textile industry is an important environmental concern because of the used dyes during the coloring of the products. Mostly, textile industries discharge their wastewater in large volumes into clean sources such as rivers and streams [8]. Furthermore, these dye molecules can be carcinogenic, highly toxic and have low biodegradable due to their chemical structures which are complex and aromatic molecular structures [102]. Because of these hazardous features and coloring ability of the dyes, they have a negative effect on the aquatic life by decreasing the incoming light and increasing the values of Chemical Oxygen Demand (COD) [9]. Various approaches have been studied by researchers to remove these dyes to have better environmental health measures. These approaches can be listed as coagulation, flocculation, chemical oxidation, decolorization, ozonation, filtration by membranes, and adsorption [10]–[15]. Adsorption is among the most commonly applied method to clean wastewater from dyes. This method is considered to be simple, cost-effective, and efficient [16].

Typically, dyes used in the textile industry are composed of two main components: chromophore and auxochromes [24], [26]. Chromophore produces the color and auxochromes are ionizable groups to improve the affinity of the dye towards the material to be dyed. Chromophores typically formed by chemical groups which are the azo group (–N=N–), carbonyl group (=C=O), carbon-nitrogen (=C=NH; –CH=N–), carbon-sulphur (=C=S; ≡C–S–S–C≡), ethylene group (=C=C=), methine group (–CH=), nitro (–NO_2; –NO–OH), and nitroso (–N=O; =N–OH). On the other hand, auxochrome parts are amino (–NH_2), carboxyl (–COOH), hydroxyl (-OH), and sulphonate (–SO_3H) [103], [104].

Textile dyes can be classified when only their general structure and charges are considered as ionic (cationic and anionic) and nonionic [23], [24]. Anionic dyes are negatively charged, named also acid dye, and highly reactive in aqueous solutions. Their discharge into clean water sources is not preferred because the hydrolysis of free dye

molecules results in formations of reactive and toxic groups in the liquid phase [25], [26]. Nonionic dyes do not ionize in water, so they can be dispersed in aqueous medium [10]. Cationic dyes are positively charged, basic dyes which have various chemical structures based on their aromatic groups. Although some of them have been used in medicine as antiseptics [104], those groups are significantly toxic and can be hazardous for health and can cause allergic reaction, skin irritation, mutations in the cells, and cancer [26], [105].

Several organic and inorganic materials have been used as adsorbent species to treat wastewater consisting of textile dyes. Alumina (Al_2O_3), silica (SiO_2), magnetic nanoparticles (for instance Fe_3O_4), carbon nanotubes, graphene oxide, and activated carbon are the most used inorganic (or synthetic) materials as adsorbents [17]–[22]. MSPs are of interest for adsorption because of their high surface area, tunable porous structure, large pore sizes, and high pore volumes, thermal and mechanical stability [32], [106], [107]. Also, utilizing the MSPs as selective adsorbents is possible with functionalizing their particles by different chemical groups such as amine, carboxyl, etc. onto the inner and external surface of the particles. This functionalization of the surfaces makes the particles selective and increases their capacities for adsorbing textile dyes [27]–[32]. Three steps follow each other in sequence during the adsorption of dyes on MSPs. These steps can be listed as:

i) Transportation of the dye to the outer surface of the MSPs, called film diffusion.

ii) Transportation of the dye molecules into the pores of MSPs, called particle diffusion.

iii) Adsorption of the dye molecules by the inner surface of the MSPs [108].

Silica particles are negatively charged (above the pH of isoelectric point, generally close to pH≈2) due to the -OH groups and they adsorb positively charged dyes by the strong electrostatic interactions. Because of the large variations of the dye molecules with their structural properties, silica particles are needed to be functionalized on their surfaces by different groups to adsorb different types of dye molecules [108]. Also, the adsorption of negatively and positively charged dyes by silica particles can be enhanced by functionalization processes. For instance, Wang et. al. showed that MCM type MSPs which have 5.6 nm pore size and 1222 m^2/g SSA, have 0.07 mmol/g adsorption capacity for Methylene Blue (MB) cationic dye, without any functionalization [109]. Then Ho et al. showed that MSPs which have 2.55 nm pore size and 754 m2/g SSA, can adsorb 0.3

mmol/g MB by carboxylic functionalization onto the silica surfaces [110]. On the other hand, amine (-NH_2) functionalization of silica surfaces makes particles able to adsorb anionic dyes such as Acid Blue, Methylene Orange (MO), etc. efficiently [53], [111], [112]. Some adsorption studies by mesoporous silica particles are listed in Table 3.1. However, these functionalization processes have two important drawbacks of high cost and complexity.

Table 3.1 Adsorption of Different Dyes by MSPs with various functionalization [108].

Mesoporous Silica				Dye		Removal Eficiency	
Type	SSA (m_2/g)	Pore Size (nm)	Functional Group	Class	Name	R%	Q_e (mmol/g)
MCM	1647	3.8	-	Cationic	Methylene Blue (MB)	-	0.14
	1149	3.0	-		Methylene Blue (MB)	-	0.04
	1222	5.6	-		Methylene Blue (MB)	-	0.07
	754	2.6	Carboxylic		Methylene Blue (MB)	-	0.30
	1448	-	Al		Yellow Dye (YD)	92.0	-
	774	2.5	NH_2	Anionic	Acid Blue 25 (AB-25)	-	0.60
	215	1.8	NH_2		Remazol Red	99.1	-
SBA	659	5.2	-	Cationic	Methylene Blue (MB)	99.1	0.15
	659	5.2	-		Janus Green B (JGB)	-	0.13
	707	1.9	Hyperbrancedpolyglycerol		Methylene Blue (MB)	-	<0.5
	768	8.9	-		Safranine T (ST) Malachite Green (MG)	83.6 95.7	-
	1005	21.6	Ethylenediamine Aminopropyl penta ethylene hexamine	Anionic	Acid Blue 113	83.6	-
	1435	19.2			Acid Red 114	85.5	-
	1290	16.8			Acid Green 28	95.9	-
	1092	16.3			Acid Yellow 127	88.2	-
MPS	285	19.0	Dimethyldecylamine	Anionic	Dark Yellow GG	-	1.71
	285	19.0			Red Violet X-2R	-	0.90
	313	-	NH_2		Acid Red 14 (AR-14)	75.0	-
	313	-	NH_2		Acid Black 1 (AB-1)	83.0	-
	516	4.6	Dimethyldecylamine		Yellow GG (YGG)	-	1.96
	516	4.6	Dimethyldecylamine		Red Violet X-2R	-	0.96

The bare mesoporous silica particles without any coating introduced in the previous chapter are prospective candidate for cationic dye removal in wastewater treatment applications. In the previous chapter synthesis of high surface area MSPs were successfully synthesized by HCl acid as the catalyst of the system. Here the samples were prepared by different acids such as HNO_3 and H_2SO_4 used as the catalyst. We expected to have different properties such as morphology, pore size, pore volume, and surface charge of the samples by changing the catalyst of the synthesis. The pH of the reaction mixture was one of the most effective parameters on product parameters. Changing the type of acid even when the concentration is same can change the pH of the mixture. On the other hand, the counter ion of the acid can also influence the particle properties. The first aim of this study was to understand the effect of acid type on particle properties.

Additionally, adsorption behavior of the particles (Si-HCl, Si-HNO_3, and Si-H_2SO_4) under different conditions such as different pH, temperature, contact time, amount of adsorbent, and initial concentration of the dye to describe the optimum conditions for removing dyes from water sources. All of the parameters were systematically studied in detail to determine the maximum removing capacity of each sample. These cost-effectively obtained adsorbent particles with larger removing capacity can make industries to use them for sustainable water. The mechanism of the adsorption process of each sample was modeled by using the linearized Langmuir and the Freundlich isotherms. Also, the kinetic parameters of the adsorption processes were studied by Pseudo-First Order and Pseudo-Second Order kinetic models. By changing the reaction temperature, the changes in Gibb's free energy, enthalpy and entropy of the reaction were calculated to determine spontaneity of the processes. The results showed that these mesoporous silica particles can be used as efficient adsorbents to remove cationic dyes in wastewater of textile industries. As described in the first chapter, the particle properties can be tuned by changing the concentrations of three components to control the surface area, the pore size and adjust the morphology. These parameters significantly influence the adsorption capacity of the particles. In this chapter we will investigate the adsorption capacity of MSPs synthesized by using various acid catalyzed solution in TEOS/Pluronic F127 system. The adsorption capacity of these particles can give us an insight about their possibility to be employed in wastewater treatment applications of textile industry.

3.2 Materials And Methods

3.2.1 Materials

The synthesis of silica samples was carried on by the synthesis method that is described in the first chapter. The samples were synthesized at room temperature by using Pluronic F127 as the surfactant and TEOS as the silica precursor. Although the method was applied similarly in the first chapter, acid catalysts were varied in this chapter as HCl, HNO_3 and H_2SO_4. The amphiphilic triblock copolymer, Pluronic F127 (poly(ethylene oxide)$_{106}$–poly(propylene oxide)$_{70}$–poly(ethylene oxide)$_{106}$ ($PEO_{106}PPO_{70}$-PEO_{106}) from Sigma Aldrich was used as a structure-directing agent and the molecular weight of Pluronic F127 is 12600 g/mol. Tetraethyl orthosilicate (TEOS) with 208.33 g/mol molecular weight was purchased from MERCK. HCl, HNO_3, and H_2SO_4 acids from Sigma Aldrich were used

as catalysts of the synthesis. Rhodamine 6G (R6G) was used as the model dye to be adsorbed in aqueous solutions and HCl, NaOH from MERCK were used to adjust the pH of the solutions.

3.2.2 Synthesis of the MSPs As Adsorbents

The silica samples were synthesized under the same conditions in Chapter 1 such as room temperature, without stirring, and without any post treatment processes such as hydrothermal treatment. All of the samples were synthesized by the same concentrations of each component to understand the effect of catalysts on the adsorption behavior of the products. Pluronic F127 (0.01 g/mL) was dissolved in 7.00 M aqueous acidic solutions prepared using HCl, HNO_3 and H_2SO_4 concentrated solutions. The time for dissolution was short in such high acid concentration. To the Pluronic solution 200 µL/mL of TEOS was added to the mixture and the sample was stirred for 3-5 mins. The mixtures were kept at room temperature and atmospheric pressure for 24 hours. Normally, gel formation and precipitation of white powders occurred in a few minutes with those high concentrations of HCl acid. However, gel formation took several hours (~12 h) in the mixtures that were prepared with H_2SO_4 acid. On the other hand, the mixture prepared by HNO_3 acid showed similar behaviors with HCl acid. The dried samples were calcined under 500 ^oC (heating rate of 1 ^oC/min) for 8 h to remove the surfactant. After the calcination silica powders were grinded and used for further processes.

3.2.3 Characterization of the MSPs

The size, morphology, porosity, and surface quality of the synthesized MSPs were analyzed by FE-SEM (ZEISS Ultra Plus SEM). The specific surface area of the particles was determined by measuring N_2 adsorption isotherms at 77 ^oK. The measurements were done by Micromeritics ASAP 2020 HD instrument. Before the measurements, the samples were degassed under vacuum then analyzed by applying Brunauer-Emmet-Theory (BET) method for the specific surface area assessment. The specific surface area was calculated automatically by the instrument from the linear part of the BET plot. The cumulative surface area of the pores and pore sizes were determined by BJH analysis of the adsorption data.

3.2.4 Adsorption Studies

The R6G adsorption capacities of the MSPs synthesized with different catalysts were investigated by changing several important parameters. These parameters; pH, temperature, initial concentration of the dye, contact time, and amount of adsorbent. On the other hand, the stirring rate and volume of the aqueous solution were kept constant at 350 rpm and 10 mL. Firstly, the calibration curve of R6G was investigated to measure the concentration of it by UV/vis spectrophotometer at λ_{max} of 526 nm. Then the adsorption processes were completed under the decided conditions by dispersing the particles in dye solutions. At the end of each adsorption process, supernatant solutions were centrifuged for 10 min with 8000 rpm to avoid a baseline shift on the analysis.

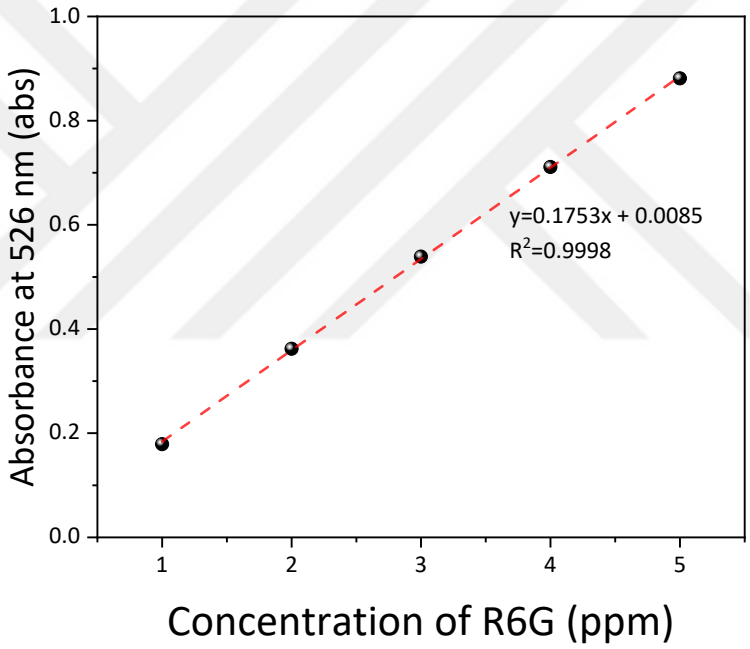

Figure 3.1 Calibration curve of R6G under the conditions that are room temperature and pH=6.

The investigation of the parameters (pH, temperature, amount of adsorbent) was studied under optimized contact time (10 mins) and initial concentration (10 ppm). The maximum adsorption capacity of the samples was determined by the experiments in 24 h and under room temperature at pH=6 which is the pH of DI water.

The following equation is used to calculate the amount of R6G adsorbed by silica samples at equilibrium q_e (mg/g)

$$q_e = \frac{(C_0 - C_e)V}{W} \quad (1)$$

where q_e is the equilibrium adsorption capacity (mg/g) of the samples, C_0 and C_e (mg/L or ppm) are the starting and equilibrium concentrations of R6G, W is the mass of silica powders in gram, and V is the volume of an aqueous solution which was 10 L for our experiments.

3.2.5 Adsorption Isotherms

There are several mathematical models to make a reliable prediction over an adsorption behavior by the isotherms such as Freundlich, Langmuir, BET, Temkin, Redlich-Peterson etc. [108]. These isotherms are used to predict the maximum capacity of an adsorbent under decided conditions as pH, temperature, dye type, or the adsorbent type. Also, the shape of the isotherms is used to predict whether the adsorption system is favorable or unfavorable. When designing the optimum adsorption systems, the investigation of the most accurate equilibrium curve is very important [113]. The most commonly used models to determine the isotherm of the adsorption of dye molecules onto solid surfaces in aqueous systems are the Langmuir and Freundlich models [114], [115]. Langmuir model describes the adsorption process as the adsorbent sites have equal energies and each adsorbate molecule is attached to one site. Which can be summarized as monolayer adsorption of the dye molecules onto the adsorbent surface. If the adsorption curve fits that model, it means that the adsorbate molecules which are the dye molecules in our situation form a monolayer homogeneously on the adsorbent surface. The dimensionless separation factor (R_L) is typically used to describe the feasibility of the process and power of the attachment of dye molecules onto the adsorbent surface. The quantity of that value describes the isotherm to be either unfavorable ($R_L>1$), linear ($R_L=1$), favorable ($0<R_L<1$), or irreversible ($RL=0$) [116]. The separation factor is calculated by the following equation.

$$R_L = \frac{1}{K_L C_0 + 1} \quad (2)$$

Where C_0 (mg/L) is the initial concentration of adsorbate which is MSP for our study.

On the other hand, the Freundlich model does not only express the monolayer formation but also involves the heterogeneous adsorption on the surfaces. This purely empirical formula remains linear until the saturation level of the adsorption by the adsorbate. After that, it takes a non-linear form in the graph, which is the point that adsorbate cannot adsorb

anymore, and the exact value of removal remains constant. The isotherm constant K_f changes with the temperature. Typically, the adsorption saturation point enlarges with increasing the temperature.

Table 3.2 Mathematical Equations of non-linear for of the isotherms [117].

ISOTHERM	EQUATION
Langmuir	$q_e=(K_L\, q_{max}\, C_e) / (1+K_L\, C_e)$
Freundlich	$q_e = K_f C_e^{1/n}$

Where q_e: the amount of adsorbate adsorbed per unit amount of adsorbent at equilibrium (mg/g); C_e: equilibrium dye concentration (mg/L); q_{max}: maximum adsorption capacity of the adsorbent (mg/g); K_L: Langmuir isotherm constant related to the energy change during adsorption (L/mg); K_f: the Freundlich constant representing adsorption capacity (mg/g); 1/n: the Freundlich isotherm constant representing curve of the plot.

Adsorption of R6G onto silica particles was investigated by Langmuir and Freundlich Isotherm models in this study to understand the mechanism of the process and maximum capacity of the silica samples. (Table 3.2). Investigations of isotherms were studied by varying the initial concentration of the dye from 1 ppm to 70 ppm under conditions that are room temperature and natural pH of the DI water. After dispersing 10 mg of silica samples into 10 mL of dye solutions, the mixture stirred at 350 rpm for 24 hours. Then the mixture was centrifuged with 8000 rpm for 10 mins to have the top solution for UV/vis analysis. The equilibrium concentration was calculated from the calibration curve.

3.2.6 Adsorption Kinetics

Scale-up operations of experiments done in a laboratory to industrial levels are important for wastewater treatment applications in the textile industry [118], [119]. Kinetics of the reactions that are calculated from time-dependent measurements are important to understand the dynamics of the adsorption processes for those operations [120]. As it described in the introduction there are three important steps following each other when the adsorbent is a porous structure. Kinetic modeling allows estimation of all steps in total to understand the mass transfer rate and adsorption speed of the process. These parameters are as important as the maximum adsorption capacity of an adsorbent to be used in the industry [108], [110], [116].

There are three different kinetic models which are commonly used for wastewater treatment applications to evaluate the kinetic parameters of MSPs for dye adsorption. As it is listed in Table 3.3, the models are; pseudo-first-order (Lagergren) kinetic model, pseudo-second-order (Ho and McKay) kinetic model, and intraparticle diffusion (Webber and Morris) model [112], [121], [122].

Table 3.3 Mathematical equations of three most popular kinetic models [112], [121], [122].

KINETIC MODEL	EQUATION
Pseudo-first-order	$q_t = q_e(1 - exp^{-k_1 t})$
Pseudo-second- order	$q_t = \frac{q_e^2 k_2 t}{1 + q_e k_2 t}$
Intraparticle diffusion	$q_t = k_i t^{1/2} + c$

The variables in Table 3.3: q_t and q_e are the adsorption capacities (mg/g) at exact time t and equilibrium, respectively; k_1 is the rate constant for pseudo-first-order kinetic model (L/min), k_2 is the pseudo-second-order rate constant (g/mg) [120].

In some cases, the pseudo-first-order model may not correctly predict the amount of adsorbed quantity due to the failure over large ranges of contact times. The pseudo-second-order model that counts chemisorption-controlled reaction and sorption capacity of the solid part can be used in such reactions to having better estimations [26].

Any of the described three consecutive steps which explain the dye adsorption by MSPs can be the controlling factor of the reaction rate. The film diffusion of dye molecules migrates to the outer surface of the particles, then the dye molecules start diffusing into the interior active sites by either from the pores and/or surface diffusion. In the final step, dye molecules are started to be absorbed by the inner surfaces of the silica particles. These steps can dominate the adsorption rate of the process according to the particle properties such as pore size and pore volume. However, the last step is much faster than the first and second steps. So, it is not considered in kinetic investigations [108].

In our study, we investigated the dynamics of Rhodamine 6G adsorption by our silica samples with pseudo-first-order and pseudo-second-order kinetic models. Contact time of the adsorption processes was changed in a range between 5-20 min under the

conditions that are room temperature and natural pH=6. After dispersing 10 mg of silica samples into 10 mL of dye solutions which had 10 ppm initial concentration, the mixture stirred with 350 rpm. Then the mixture was centrifuged with 8000 rpm for 10 mins to have supernatant for UV/vis analysis. The equilibrium concentration was calculated from the calibration curve.

3.3 Results And Discussion

3.3.1 Properties of the Synthesized MSPs

The morphology of the samples was determined by SEM images. Also, particle sizes were measured by ImageJ processing of the SEM images of the samples. All of the samples showed similar morphology as fused spherical particles, which were expected due to the previous results described in the first chapter. A higher concentration of the acid catalyst resulted in smaller diameter particles due to fast hydrolysis and condensation reactions of TEOS during the sol-gel system with HCl acid. In this set of particles concentrations of all three acids were the same as 7.00 M. Although the particle size of the samples synthesized with HCl and HNO_3 were approximately similar, the samples synthesized with H_2SO_4 were smaller than the other samples. When the particle sizes for Si/HCl and Si/HNO_3 were 1.24 ± 0.23 µm and 1.59 ± 0.24 µm, respectively, the particle size of Si/H_2SO_4 particles was obtained as 0.68 ± 0.10 µm. This can be attributed to the effect of acidity of the reaction mixture because the H_2SO_4 is a diprotic acid which can serve double numbers of protons come from H_2SO_4 acid. As it is previously established that the acid concentration has a stronger effect on the particle size when it is compared to the other effects such as the amount of surfactant and TEOS. However, the gel formation during the synthesis was slower with the H_2SO_4 acid catalyst when it was compared with the HCl and HNO_3 acids. The mixture turned to solid gel and liquid after a few minutes when the catalyst was HCl or HNO_3 but even after 24 h, the mixture was still viscous liquid. Due to the oily liquid structure of the H_2SO_4 phase separation was slow but it is understood from the particle sizes that silica formation was still faster than the other two acid catalyzed synthesis solution mixtures.

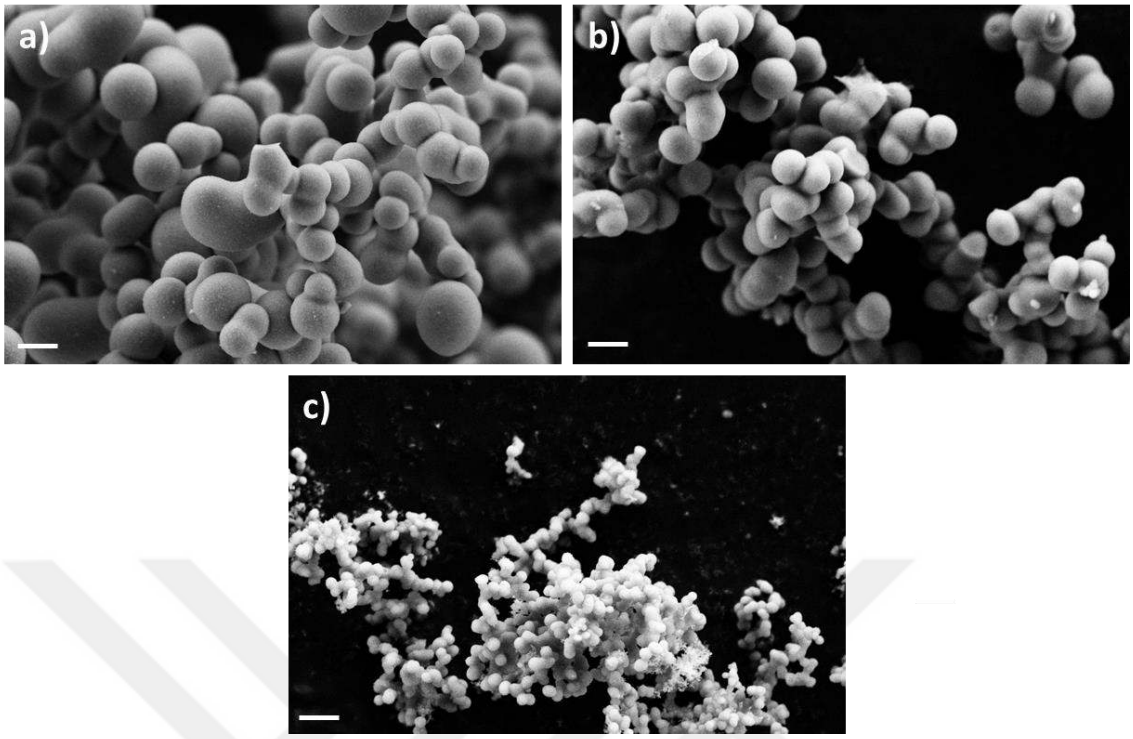

Figure 3.2 SEM images of the silica samples synthesized with different acid catalysts as a) HCl, b) HNO_3 and c) H_2SO_4 acids. The scale bars of the images correspond to 1 µm for a), and 2 µm for b),c).

Figure 3.3 represents the adsorption isotherms of silica particles synthesized under the catalyst effect of HCl, HNO_3, and H_2SO_4 acids. Si/HCl and Si/HNO_3 samples showed Type II adsorption isotherm. The adsorbed quantity by those samples increased until a saturation points by the increase of pressures. Si/HCl particles have saturation points below 0.2 relative pressure of nitrogen, similar to the previous spherical samples. Si/HNO_3 particles reached the saturation points with higher relative pressure. Moreover, both samples have pore sizes smaller than the critical value (4.00 nm) to have larger hysteresis between their adsorption and desorption curves. However, Si/HNO_3 particles had larger SSA as 784 m^2/g when Si/HCl particles had SSA of 497 m^2/g. It can be attributed to the more porous structure when it is compared to Si/HCl samples. Because when the particle sizes were similar (even slightly larger) and pore sizes were approximate (~3.5 nm), the surface area should be smaller. This may be the result of the counter ion, which was taking the role as bridging ion, was larger when it was NO_3^- instead of Cl^-. An interesting observation was that the adsorption isotherm of Si/H_2SO_4 particles showed an isotherm with a similar shape to Type IV(a) isotherm. This type of isotherm was observed by the monolith particles in the previous analysis. Although the particles had spherical morphology, they showed the isotherm. The type of the isotherm

was also supported by the pore size which was calculated as ~14.0 nm. That pore size was much larger than the critical value to have Type IV(a) isotherm. Because of this large pore size, the surface area of the particles was 287 m^2/g even when the particle size was much smaller than the others.

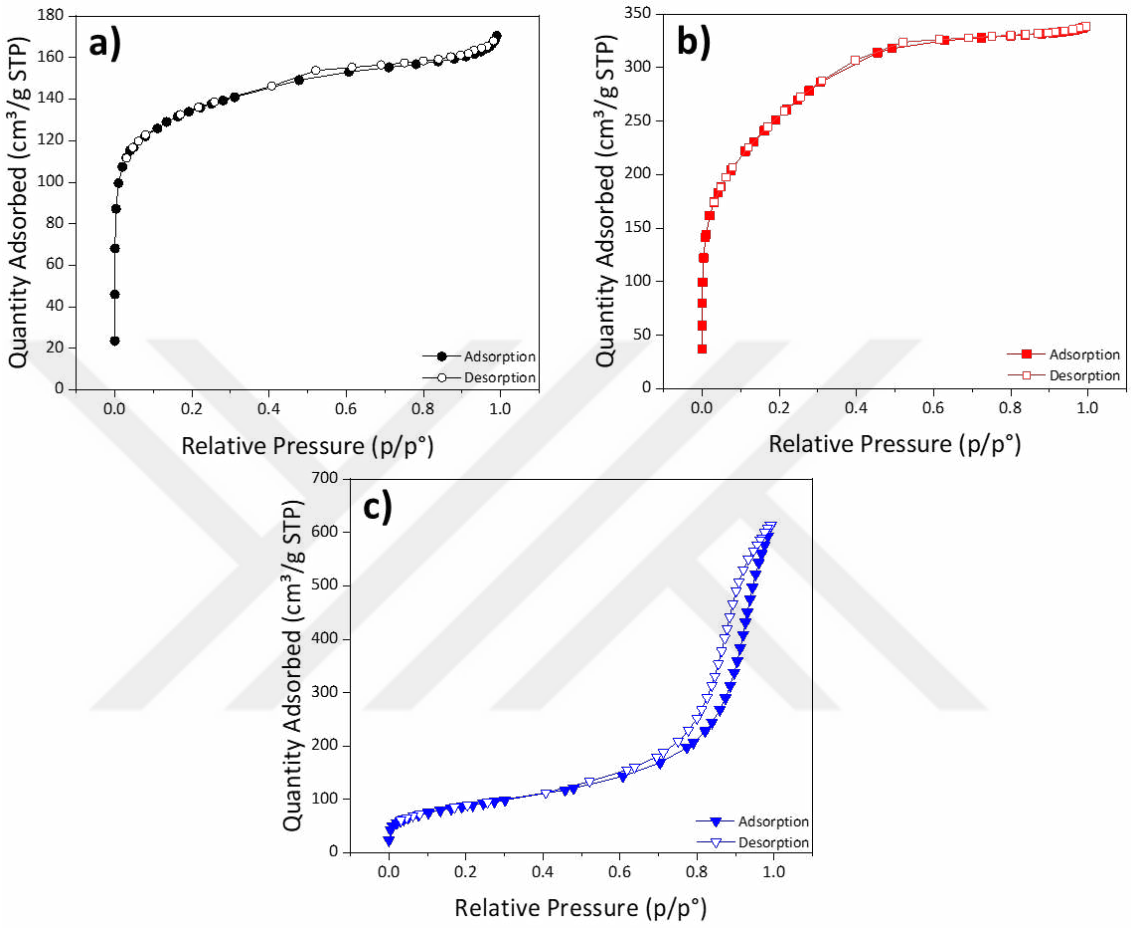

Figure 3.3 Adsorption isotherm plots of silica particles synthesized with different acid catalysts as a) HCl, b) HNO_3 and c) H_2SO_4 acids.

As it is seen from the literature, increasing the pore size is more positively effective on adsorption processes than the surface area of the particles. After the BET analysis, it could be estimated that the best performance would be observed from Si/H_2SO_4 samples, even when their surface charges were approximately equal to -35.0 mV, roughly, in a pH=7 solution.

3.3.2 Effect of Adsorbent Dosage

The influence of the amount of silica particles on the removal of R6G was studied at room temperature to determine the optimum adsorbent dose for further experiments.

Amount of silica particles in 10 mL of 10 ppm dye solutions were varied in a range from 5 mg to 25 mg. Figure 3.4 shows that for all particles adsorption percent increases by increasing the adsorbent dose and then reaches to a saturation point. Si/H_2SO_4 particles showed the maximum percent removal (76.5 % - 98.5 %) of R6G as compared to Si/HCl (31.7 %)- 53.7%) and Si/HNO_3 (58.6 % - 87.5 %) for all adsorbent concentrations (5-25 mg) investigated. In case of Si/H_2SO_4 samples the removal of R6G reached to the saturation point. However, Si/HCl and Si/HNO_3 reached to their saturation point after 15 and 20 mg respectively.

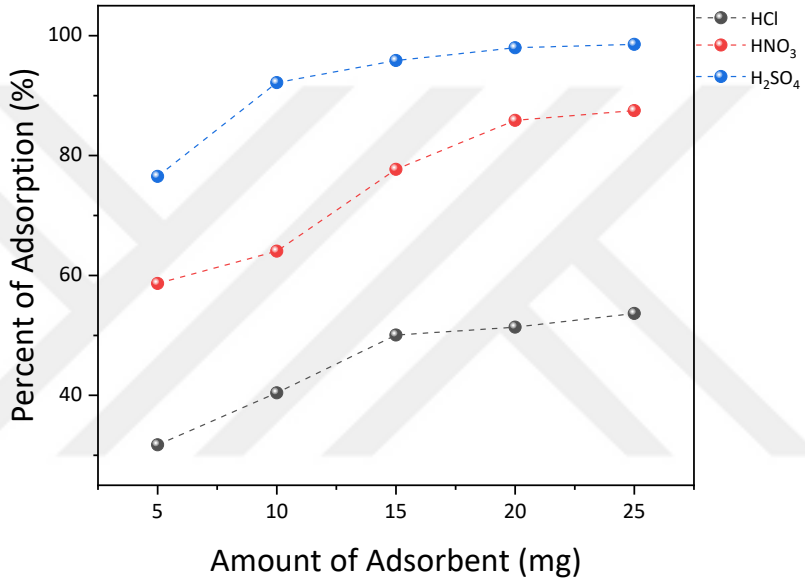

Figure 3.4 Effect of amount of adsorbent on the percent of adsorption of R6G on the samples that were synthesized with different acids. The experimental conditions were; pH = 6, t = 10 min, T= 25 °C, initial concentration of the dye = 10 ppm.

The adsorption mechanism of R6G with the silica particles are typically electrostatic interactions between positively charged -NH groups of the dye and negatively charged silica particles. However, the other effect is existing due to the pore size of the particles which enables the particle diffusion to the interior surfaces. Larger pore-sized particles showed higher adsorption capacities.

3.3.3 Effect of Contact Time

The ideal contact time for the process was determined by varying the mixing time in the range between 1-20 mins at pH=6. 10 mg of silica samples were dispersed in 10 mL of 10 ppm R6G aqueous solutions at room temperature and stirred by a magnetic stirrer

with 350 rpm. As it is represented in Fig 3.5. the maximum removal was obtained in 5 mins for Si/HCl by 39% removal when it was still increasing for Si/HNO_3. That can be attributed to the large surface area of the Si/HNO_3 samples due to the particle diffusion to the interior surface by the silica surfaces. On the other hand, Si/H_2SO_4 particles showed a small increase from 1 to 5 mins that reached its maximum of 90% removal. This higher removal in shorter durations by Si/H_2SO_4 (d_p= ~14 nm) as compared to Si/HCl (d_p= ~4 nm) and Si/HNO_3 (d_p= ~3 nm) can be attributed to their larger pore size which makes the second consecutive step (particle diffusion) faster. Whereas the maximum removals after 20 mins were 40%, 65%, and 92% for Si/HCl, Si/HNO_3 and Si/H_2SO_4, respectively. Reaction kinetics will be established in the next sections of the chapter.

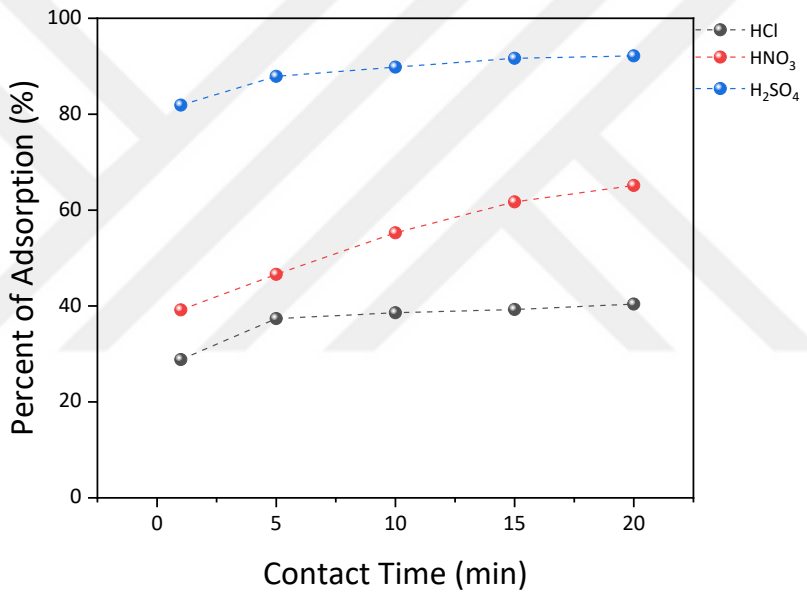

Figure 3.5 Influence of contact time on the percent of R6G removal by the silica particles that were synthesized with different acids. The experimental conditions were pH = 6, T= 25 °C, amount of adsorbent = 10 mg, and initial concentration of the dye = 10 ppm

3.3.4 Effect of Temperature

The reaction temperature is one of the most important parameters for adsorption parameters to explain the process thermodynamically and understand the adsorption type whether it is physical adsorption or chemisorption. To study the effect of temperature on the silica samples' adsorption capacities, the temperature of the reaction changed from 25 °C to 65 °C by a heater systematically. 10 mg of each silica sample were dispersed into 10 mL, 10 ppm dye solutions which were heated up before. As it is represented in Fig 3.6. all of the samples showed a correlation between temperature and removal percent of

R6G. Each of the samples showed the same behavior as lower removal capacity with higher temperatures. The percent removal of dye molecules by MSPs decreases due to the exothermic nature of the adsorption processes. Because of the electrostatic interaction between two oppositely charged parts of the process, the system releases heat to the environment during the adsorption process. Increasing the temperature commonly decreases the solubility limits and reduces the removal efficiency by decreasing physical interactions between dyes and adsorbents [123]. From the observed trend presented on Fig 3.5. it is expected that the interaction between dye molecules and silica particles is physical adsorption, not chemisorption and a reversible electrostatic interaction.

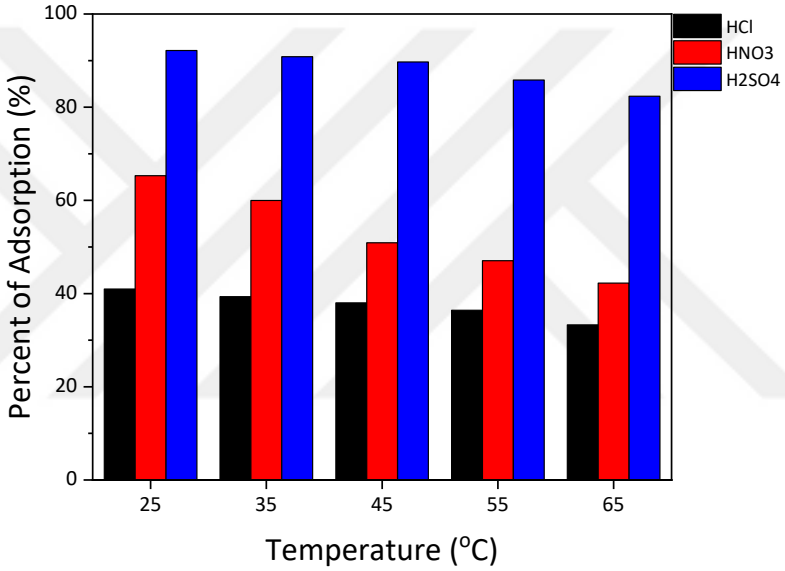

Figure 3.6 Effect of temperature on percent removal of R6G by silica particles that were synthesized with different acids. The experimental conditions were pH = 6, t= 10 mins, amount of adsorbent = 10 mg, and initial concentration of the dye = 10 ppm

Within every temperature, Si/H2SO4 particles showed the highest adsorption capacity when it is compared with the others. The lowest percentages of removal of R6G by the silica samples were 33%, %42, and %82 for HCl, HNO_3, and H_2SO_4 catalyzed synthesis, respectively. The decrease in performances of all samples showed that they adsorbed R6G molecules by ionic interaction.

3.3.5 Effect of Solution pH

The dominated parameter of the adsorption processes which are based on electrostatic interactions as the mechanism is the pH value of the reactions. To investigate the

influence of pH changes, the solution pH range was varied between 2 and 12. 0.1 M HCl and 0.5 M NaOH solutions were used to adjust the pH of the reaction mixture. Influences are effective for both sides of the reaction as the dye and the adsorbent part. In different pH values, adsorbents show different surface charges. Typically, MSPs have isoelectric point at pH=2, then the surface charge of particles decreases with increasing the pH value. From our observations, capacity of adsorbing positively charged molecules by silica particles should be increasing up to pH=10, then it should decrease around pH=12 (Surface charge ≈ -40 mV). However, as it is represented in Fig 3.7. The adsorption of R6G molecules by all of the silica samples was the lowest. This behavior can be attributed to the deterioration of the dye molecules. The interaction ability of cationic dyes at high pH values decreases due to their interactions with free OH groups in the solution. On the other hand, the surface of the mesoporous silica particles was discharged under a high level of acidity. When the pH value of the solutions was closer to the isoelectric point of MSPs, their adsorption capacities were decreased.

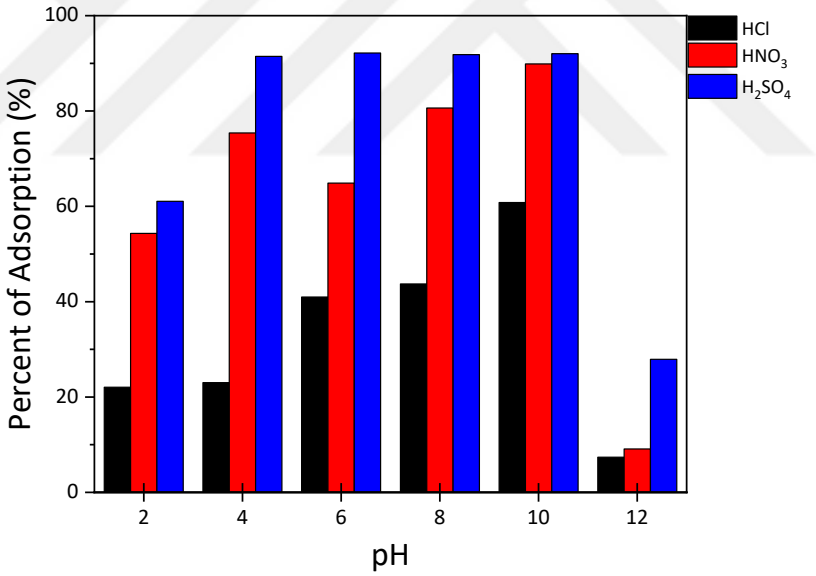

Figure 3.7 Effect of pH of the reaction mixture on percent removal of R6G by silica particles that were synthesized with different acids. The experimental conditions were T = 25 °C, t= 10 mins, amount of adsorbent = 10 mg, and initial concentration of the dye = 10 ppm

The most influenced sample was Si/HCl particles during the experiments. The percentage removal of R6G molecules by Si/HCl particles changed in a range between 7 and 60% from lowest to the highest. Moreover, all of the samples showed their best adsorption performances in pH=10. Si/H_2SO_4 did not show any change by changing the pH from 4 to 10 because of their adsorption saturation limit was achieved already. The percent of

R6G adsorption by Si/HCl, Si/HNO_3, and Si/H_2SO_4 particles was 60%, 89%, and 92%, respectively.

3.3.6 Adsorption Isotherms

Investigation of the mechanism and adsorption capacity of the samples towards R6G dye molecules were studied by the two most common adsorption isotherms. Langmuir and Freundlich adsorption isotherms which are frequently used isotherms for dye adsorption studies were employed in this work. Figure 3.8. represents the percent removal of R6G by silica samples against the initial concentration of R6G. Investigation of the isotherm was studied by varying the initial concentration of the dye in a range between 10 and 70 ppm under equal conditions such as T = 25 °C, t = 24 h, pH = 6, and amount of adsorbent = 10 mg. The samples were constantly stirred by a magnetic stirrer at rate of 350 rpm. After that, all of the solutions were centrifuged by 8000 rpm for 10 mins to have the top solution for UV/vis analysis. All three samples showed a similar trend as lower adsorption performances with increasing the initial concentration of the dye molecules. The largest decay was observed by Si/H_2SO_4 particles from 92% to 29%. However, it cannot be attributed to decrease in performance of the particles. The absolute quantity of adsorbed molecules was similar to the different initial concentrations of the dye.

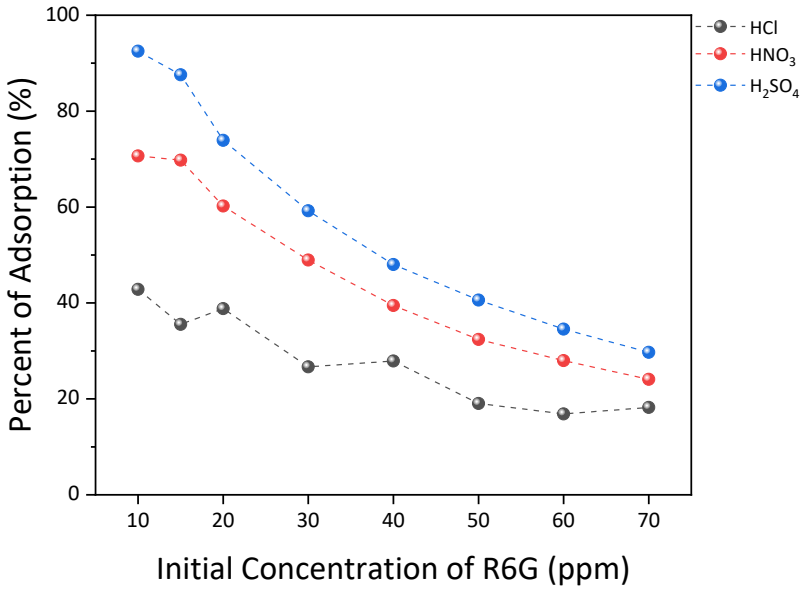

Figure 3.8 Effect of initial concentration of R6G molecules in the reaction mixture on percent removal by silica particles that were synthesized with different acids. The experimental conditions were T = 25 °C, t = 24 h, pH = 6, and amount of adsorbent = 10 mg

Table 3.4 represents the comparison of adsorption isotherms employed in the work. The adsorption of R6G molecules was better estimated by Langmuir isotherm with Si/H_2SO_4 particles (R^2 = 0.993), the Freundlich isotherm model fitted better for the adsorption process by Si/HCl and Si/HNO_3 particles (R^2 values were 0.990 and 0.950, respectively). Si/H_2SO_4 particles were able to complete the second consecutive step of adsorption which was about particle diffusion. However, the other samples showed heterogeneous adsorption. This adsorption behavior of the samples can be attributed to the pore sizes. The large pore size of Si/H_2SO_4 particles make them able use their inner surface for monolayer adsorption of the dye molecules. But the other samples could use just their external surfaces for the formation of heterogeneous layers of dye molecules. because they were able to use only the external surfaces. The larger pore size can also be the reason to have the maximum adsorption capacity of 20.092 mg/g which is approximately twice better than the other two silica samples. Maximum adsorption capacities were estimated by Langmuir isotherm as 9.890, 14.213, and 20.092 mg/g for Si/HCl, Si/HNO_3, and Si/H_2SO_4 samples, respectively.

Table 3.4 Adsorption parameters of the silica samples obtained from a linear form of Langmuir and Freundlich isotherm models at room temperature and pH =6 for the removal of R6G from water

		Silica Samples		
	Parameters	**Si/HCl**	**Si/HNO_3**	**Si/H_2SO_4**
Langmuir	q_{max} (mg/g)	9.890	14.213	20.092
	R_L	0.551	0.196	0.167
	R^2	0.968	0.899	0.993
Freundlich	K_F (mg/g)	2.024	5.710	8.708
	1/n	0.428	0.313	0.268
	R^2	0.990	0.950	0.890

On the other hand, incoherent adsorption parameters for R6G adsorption on all three samples clearly showed that there were specific interactions between particle surfaces and dye molecules. Dimensionless Separation Factor (R_L) and 1/n values were in between 0-1. It means that the adsorption of cationic dye molecules by mesoporous silica particles was favorable under the conditions. Moreover, the adsorption process done by Si/H_2SO_4 particles was more favorable than the others when we examine the R_L and 1/n values. Si/HCl particles showed a tendency to be fitted by both isotherms. The R^2 values were 0.968 and 0.990 for Langmuir and Freundlich isotherms, respectively. These results can

only be observed from an adsorbent that does not have strong interactions with the dye molecules and low adsorption capacities. Si/HCl samples showed the lowest performance in all investigated conditions. So, it was expected to observe this kind of behavior from this sample because of very low removal capacity.

3.3.7 Adsorption Kinetics of R6g Removal by MSPs

Pseudo-first order and pseudo-second-order kinetics models were employed in this study (Fig 3.5.) to investigate the reaction pathways and the dye uptake rate. The summary of the parameters of both models is given in Table 3.5. Kinetic model parameters are important to understand the possibility of the silica samples whether they can be scaled up as an adsorbent in the textile industry or not. If the adsorption processes require very short time to remove all of the pollutants from wastewater, the adsorbent would be used in industrial level. Also, the rate of the reactions indicates how fast are the adsorption processes by MSPs.

Table 3.5 Kinetic parameters of adsorption reaction of R6G by the silica samples. Values were obtained from the linear form of pseudo-first-order and pseudo-second-order models.

		Silica Samples		
	Parameters	**Si/HCl**	**Si/HNO_3**	**Si/H_2SO_4**
	q_e (mg/g) experimental	4.284	7.065	9.250
pseudo-first-order	q_e (mg/g) calculated	1.113	3.738	1.278
	K_1 (min^{-1})	-0.004	-0.004	-0.009
	R^2	0.890	0.997	0.991
	q_e (mg/g) experimental	4.284	7.065	9.250
pseudo-second-order	q_e (mg/g) calculated	4.109	6.896	9.299
	K_2 (g/mg min)	0.469	0.085	0.455
	R^2	1.000	0.990	1.000

As it is represented in Table 3.5, the linear regression coefficient values depicted that the adsorption of R6G proceeded by the pseudo-second-order kinetics model which was slightly better explained than the pseudo-first-order kinetics, similarly with the results in the literature. Moreover, the relationship between the calculated and experimental values of q_e was clearly better fixed with the pseudo-second-order kinetics model. For instance, the experimental adsorption capacity of Si/H_2SO_4 was calculated as 9.299 mg/g by

pseudo-second-order model when it was 9.250 mg/g as experimental. But pseudo-first-order calculated the adsorption capacity as 1.278 mg/g which is very much lower than the experimental value.

3.3.8 Investigation of the Thermodynamic Parameters for The Adsorption Process

The energy changes during the adsorption process are important to determine the spontaneity of the adsorption reaction of the dyes by adsorbents. Moreover, the thermodynamic parameters such as the Gibbs' free energy (ΔG°), the standard enthalpy change (ΔH°) and the standard entropy change (ΔS°) were studied to understand the effect of temperature on the adsorption process [124]–[126]. the Gibbs' free energy (ΔG°) of the reaction is calculated by the following equation:

$$\Delta G^o = -R\,T\,lnK_c \quad (3)$$

where the equilibrium constant K_c for Langmuir Isotherm is calculated from;

$$K_L = \frac{{}^{q_e}/_{C_e\left(\frac{10^{-3}}{MW_{R6G}}\right)x(NA)x\,d_{R6G}}}{SSA_{SiO_2}} \quad (4)$$

and T is the absolute temperature of the reaction in Kelvin (K) and R is the universal gas constant which equals 8.317 J/mol K. Also, q_e is the equilibrium adsorption capacity of the adsorbent (mg/g), C_e is the equilibrium constant in solution (mol/L), d is the molecular size of R6G and SSA is the surface area of the adsorbents (m^2/g).

van't Hoff equation is employed to calculate the energy changes of enthalpy (ΔH°) and entropy (ΔS°):

$$\ln K_L = \frac{\Delta S^\circ}{R} - \frac{\Delta H^\circ}{RT} \quad (5)$$

The calculated thermodynamic parameters are summarized in Table 3.6.

Table 3.6 The thermodynamic parameters of adsorption of R6G by the silica samples according to Langmuir Model.

	Silica Samples		
Parameters	**Si/HCl**	**Si/HNO_3**	**Si/H_2SO_4**
ΔG° (kJ/mol)	-22.501	-23.471	-30.499
ΔH° (kJ/mol)	-6.531	-20.260	-19.485
ΔS° (kJ/mol.K)	0.054	0.011	0.038

The negative values of ΔH° indicate that the adsorption reaction of R6G by silica samples was exothermic, which was also determined in the previous section by Figure 3.6. Moreover, decreases in the entropies showed that the freedom of the molecular movement during the adsorption process was also decreased. Because of capturing the free dye molecules in the aqueous system, the entropy of the system decreases. On the other hand, negative values ΔG° indicated that adsorption of R6G by all of the silica samples were spontaneous the conditions that were pH = 6, room temperature, 10 ppm initial concentration and 10 mg of silica particles in the mixture. In addition, Si/H_2SO_4 samples showed the highest energy change as -30.499 kJ/mol for Gibbs Free Energy.

3.4 Conclusion

Porous silica particles could be successfully synthesized by the method that was investigated in the first chapter by changing the acid catalyst in the system. The influence of the type of acid was analyzed by the characterization techniques such as SEM, BET, and zeta potential measurements. After the characterization studies, it was observed that the particle size and pore size of the silica particles can be tuned by changing the acid in the same system. Under the same conditions such as temperature and amounts of surfactant and/or silica precursor, the samples that were synthesized by H_2SO_4 acid catalyst produced smaller size (0.68 ± 0.10 μm) spherical particles with larger pore sizes (~14 nm). The effect of additional proton served from diprotic acid as the catalyst was the main role of these types of particles formation. On the other hand, the other samples, synthesized by HCl and HNO_3, resulted in similar pore sizes (~3 nm) but particle size and surface area values were influenced dramatically. When the particle size was increased by using HNO_3 as the catalyst, specific surface area was also increased. This increase in the SSA was not an expected result when the pore sizes was similar and particle size was higher. It can be attributed to the smaller pore sizes formed by agglomeration of smaller primary particles. The synthesized silica particles were demonstrated as a simple and cost-effective adsorbent for the effective removal of a cationic dye (R6G) from water. The adsorption capacities of the samples were compared with each other under different conditions such as pH, temperature, amount of adsorbent, contact time, and initial concentration of the dye. The adsorption studies showed superior uptake capacity of Si/H_2SO_4 compared to Si/HCl and Si/HNO_3. The uptake capacity of the samples in 10

minutes was obtained as 9.25 mg/g, 7.07 mg/g, and 4.28 mg/g for Si/H_2SO_4, Si/HCl, and Si/HNO_3, respectively. In addition, Si/H_2SO_4 particles showed the maximum adsorption capacity of 19.562 mg/g after 24 h which is importantly promising for wastewater treatment applications. The main reason to have better adsorption performances with Si/H_2SO_4 particles can be attributed to the three consecutive steps of dye adsorption by porous particles. Especially after the diffusion of dye film on top of the particle surfaces, pore size and pore volume of the particles were found critical to have higher adsorption capacities. Larger pore sizes make particles available to use their inner surfaces when the smaller pore sized particles form heterogeneous layer formation of adsorbed molecules. Because of the larger pore sizes, the diffusion of dye molecules into the interior surface were larger in the second step of adsorption reactions. When we look at the reports in the literature, those consequences were expected from Si/H_2SO_4 particles. Indeed, adsorption isotherm studies done by employing Langmuir and Freundlich isotherm have supported the results. The mechanisms for adsorption of R6G molecules by Si/HCl and Si/HNO_3 particles were better fitted to the linearized Freundlich isotherm. However, the mechanism happened with Si/H_2SO_4 particles was better fitted to the linearized Langmuir Isotherm. This can be attributed to that within smaller pore sizes, second step of the adsorption process were carried out by low diffusion rates with Si/HCl and Si/HNO_3 samples. So, the adsorption of R6G by these particles was more heterogeneous multilayer formation rather than monolayer formation. On the other hand, the monolayer formation of dye molecules on the silica surfaces was dominantly controlling the adsorption process when Si/H_2SO_4 particles were the adsorbent.

Dynamics of the removal of R6G by silica particles synthesized with the Acid/Pluronic F127/TEOS system were also investigated by employing pseudo-first-order and pseudo-second-order kinetic models. The adsorption capacities in equilibrium were better estimated by the pseudo-second-order kinetic model for all of the samples, similar to the studies in the literature. Moreover, it was determined by the kinetic calculations that the fastest adsorption rate belongs to Si/HCl particles, then Si/H_2SO_4 (0.49 g mg^{-1} min^{-1} and 0.36 g mg^{-1} min^{-1}, respectively). But due to the lower saturation points of Si/HCl particles, the equilibrium adsorption capacity was much lower than the Si/H_2SO_4 samples. Additionally, thermodynamic parameters of the adsorption processes were calculated by investigating the effect of temperature of the adsorption processes. Gibbs Free Energy

values showed that the adsorption processes of R6G were completed when the silica particles synthesized under different acid catalyst were used as adsorbents. The adsorption with Si/H_2SO_4 sowed the highest Gibbs' free energy than other silica particles (-29.64 kJ/mol, Si/HCl: -22.49 kJ/mol and Si/HNO_3: -23.46 kj/mol).

The results of adsorption studies, especially maximum adsorption capacity and kinetic parameters, showed that Si/H_2SO_4 particles are promising candidates for wastewater treatment of the textile industry. The adsorption behavior of the sample was high without any coating and/or complex process. These particles may also be beneficial for the adsorption of anionic dyes after functionalizing by the amine group or different groups to make the surface positively charged. On the other hand, the reusability of those samples should be investigated to determine that these particles can be employed at the industrial level of wastewater treatments. Also, the benefits of uptake performances of Si/H_2SO_4 may also be used in other applications such as drug delivery and host material for catalytic purposes.

Chapter 4:
DEVELOPMENT OF ACTIVE CATALYST MATERIALS BY METAL LOADING ONTO SILICA PARTICLES

4.1 Motivation

In the last decades, wastewater treatment processes have been significant challenges for cleaning water sources to have sustainable development goals. Because of hazardous ingredients in wastewater, environmental health is especially threatened for aquatic life. Particularly in textile industries, wastewater treatment has received a great deal of attention due to the dye molecules which have been used for coloring agents during mass production. As it is reported, approximately 20% of worldwide dye products are lost in wastewater effluents [34]. Discharging these toxic dye molecules into natural water sources by wastewater causes serious problems for aquatic life. Dye molecules generally are not biodegradable, toxic and carcinogenic and therefore dangerous for aquatic life. In addition these colorful compounds block the incoming light and increase the Chemical Oxygen Demand (COD) [9] causes adverse effect in aquatic ecosystem. Several approaches such as coagulation, flocculation, reverse osmosis, filtration, and adsorption have been developed to purify wastewater of industries [10]–[15]. However, these traditional physical solutions are limited by their low efficiency. Also, these techniques create secondary pollution for the environment due to their mechanisms. Especially the adsorption and filtration processes complete the treatment process by transferring the toxic ingredients from water to solid phase. So, they require further steps to remove created solid wastes for decreasing the actual pollution and regenerate the adsorbents to have the operational balance of budget spent on wastewater treatment processes [127]. To increase the efficiencies of wastewater treatment processes, various approaches as Advanced Oxidation Processes (AOPs) have been studied for removing the toxic dye molecules [34]–[37]. AOPs are generally versatile, and very effective methods to decrease the pollution in water [33]. These processes typically consist of Fenton, photo-Fenton catalytic reactions, and H_2O_2/UV processes (photocatalysis) to produce OH· radicals. The pollutant is oxidized with the highly reactive hydroxyl radicals and remove them from the water [38], [39]. In addition, the efficiency of these techniques can be improved by the use of incoming sunlight which is not harmful to environmental health,

and the most available energy source [128]. There are several materials to be used in these processes as the photocatalyst [20], [33], [129]–[131]. Titanium Oxide or Titania (TiO_2) semiconductor materials are the most studied photocatalyst. The first study, published by Fujishima, reported that TiO_2 electrode is able to do electrochemical photolysis of water [132]. Because of the large energy band gap of TiO_2, UV light can be absorbed by the material and it decreases the efficiency to generate OH· radicals that are the main actor in the oxidation destruction of the pollutant [33]. Some other materials such as single-phase semiconductors have been investigated to achieve higher efficiencies for the generation of the hydroxyl radicals [133], [134]. On the other hand, photo-Fenton reactions require process controls such as pH adjustment which are high-cost methods [40]. Since the wastewater treatment processes need to be as much as simple, effective, and cost-friendly, different types of catalysts have been studied to overcome all the drawbacks.

The studies have been directed to use composite materials such as catalyst-loaded unique structures to increase the efficiency of those processes [41]. The superior properties of MSPs, such as chemical/thermal stability, tunable pore size and order, high surface area, high loading capacity, and ease of their surface functionalization by different groups have made them a great option to be supporting host matrix for catalysts [42]. Loading different metals, metal oxides or metal sulfides on MSPs increased the heterogeneous catalyst efficiency as the composite materials [43]. Due to the larger and more oriented porous structure, MSPs have been used more in catalyst systems in liquid phases when they are compared with zeolites. The ability of these particles to remove pollutants from water is promising for future industrial wastewater treatment processes [135]. Because of these reasons, we intended

- To prepare metal/MSP composites,
- To investigate metal/metal oxide loading capacity of MSPs synthesized with TEOS/Pluronic F127/HCl system
- To investigate the degradation ability of the composites over decolorization of Methylene Blue (MB)
- To compare the capacity of composites containing different metal and metal oxides.

The photocatalytic agents prepared by TEOS/Pluronic F127/HCl system will reduce the cost of the product significantly. The pore structure and high specific surface area of silica particles enhance the loading of active catalyst which will ultimately increase the efficiency of oxidation process. A room temperature simple synthesis method of catalytic composites is promising for wastewater treatment processes by photocatalytic or photo-Fenton methods.

4.1.1 The Importance of MSPs as Catalyst Support Materials

Catalyst support or host materials requires several important properties for increasing the efficiency of supported catalysts such as metals or metal oxides by acting as the active center for the processes [136]. First of all, the support materials are required to be highly stable in the reaction phases to keep the active catalyst material in the desired form. If the host is not a highly stable material under reaction conditions, the efficiency and reusability of the method dramatically decrease [137]. In addition, the support material should have a high surface area and large pore volumes to disperse active catalyst sites on the surface [43]. It is very important when the supported active catalyst agents are high-priced metals such as palladium, platinum, gold, silver, etc. because the host material must serve the highest possible active surface for the catalysts [138]–[140]. On the other hand, the host material must be easily functionalized by different groups such as amine or carboxyl to make the synthesis processes simple and cost-effective. These requirements can be fulfilled by various oxides, carbon compounds or metal-organic frameworks and therefore they are the most frequent used compounds as catalyst support or host materials. However, MSPs have great advantages among all these materials because of their excellent chemical and physical properties. The main role to outstand the challenges in catalyst supporting is the unique and tunable porous structure of silica-based materials [43], [136].

X. Chu et al. used MSPs to support Au nanoparticles for aerobic oxidation of alcohols [141]. They used amine functionalized MCM-41 type MSPs. These functionalized particles were used to support the highly active Au nanoparticles. It was reported that using the mesoporous silica particles as support allowed to synthesize size-controlled metal catalysts which improve the efficiency up to >99.5 %. Also, it was shown that because of the stability of the product, the catalyst process could be recycled five times.

J. Gonzalez et al. investigated the catalysis properties of mesoporous silica host material for oxidative removal of 4,6-dimethyldibenzothiophene [142]. SBA-15 type silica particles were utilized to support the WO_3 active catalysts which readily oxidized 4,6-dimethyldibenzothiophene. They concluded that 25 wt.% WO_3/SBA-15 catalyst composite removed 99% of undesired 4,6-dimethyldibenzothiophene molecules.

M. Zheng et al. studied the photocatalytic water oxidation process by using SBA-15 type mesoporous silica particles [143]. They used electrostatic interaction between amine-functionalized silica particles and tetra iron(III)-substituted polyoxotungstate $[Fe(III)_4(H_2O)_2(P_2W_{15}O_{56})_2]^{12-}$ to form stable photocatalyst composite. Due to the high stability of mesoporous silica particles in the liquid phase, they could recycle the catalyst up to four runs. It was concluded that the supporting silica particles create great opportunities as highly reusable photocatalytic materials for water oxidation in heterogeneous catalyst systems.

I. Barroso-Martin et al. reported catalyst composites supported on SBA-15 ordered silica-based mesoporous structure for photodegradation of Methylene Blue (MB) [144]. They loaded Au and AuCu nanoparticles on mesoporous silica and titania-silica particles to improve the degradation efficiency for MB under UV light. They reported the presence of support material improves the photodegradation ability of active catalyst nanoparticles. The results showed that after 120 min of UV light irradiation, the dye molecules were oxidized up 99 % when AuCu catalyst nanoparticle was supported with titania-silica. The improved performance from titania-silica supporting material was attributed to the Schottky barrier formation with the presence of TiO_2 molecules.

Also, F. Chang et al. investigated the photocatalytic degradation of MB and reduction of Cr(VI) by using mesoporous silica as a supporting material for Fe-TiO_2 active catalyst under UV light [145]. They reported the degradation efficiency as 82 % Fe/Ti/Si composites with the molar ratio of 1:1:1-Fe:Ti:Si. According to their results, the degradation and reduction processes were completed in 180 mins. Also, the silica-supported catalyst composites could be used up to four cycles with a small decrease in efficiency.

In addition to these instances, mesoporous silica particles are used as supporting materials for many applications such as dehydration transfer hydrogenation [146], CO_2 adsorption [147]–[149], and hydrogenation of methanol [150].

4.1.2 Main Advances in Advanced Oxidation Systems

Advanced oxidation processes (AOPs) are considered as efficient methods to remove toxic pollutants having high stability from industrial wastewater due to the degradation ability of catalytic materials. [151]–[155]. Especially in the degradation of textile dye molecules, AOPs have been defined as very powerful approaches at ambient conditions (temperature and pressure) because of producing significantly active radicals [156]. Typically, these processes include a group of methods that are based on the utilization of O_3 and H_2O_2 as oxidants. Their effect is enhanced by the presence of light, catalytic agents (generally metal ions like Fe^{2+}/Fe^{3+} and metal oxides mostly TiO_2), and combinations of the processes such as Fenton (H_2O_2/Fe^{2+}), photo-Fenton (Fenton + UV light), etc. [153], [157]–[160]. These processes exhibited biocompatibility, cost-effectiveness and simplicity and therefore have been used in many applications including reduction of Chemical Oxygen Demand (COD), removing pollutants, treatment of sludges, removal of micropollutants, and removal of color and odor [155], [158], [161]–[166].

Fenton-based reactions and processes are known to produce highly reactive OH· radicals by the decomposition of H_2O_2 with the aid of iron ions catalyst [167], [168]. These radicals are able to degrade organic pollutants [167], [168]. The reaction mechanism can be described as the reaction equations below;

$$H_2O_2 + Fe^{2+} \rightarrow Fe^{3+} + OH^- + \cdot OH \quad (1)$$

and

$$Fe^{3+} + H_2O_2 \rightarrow Fe^{2+} + HO_2\cdot + H^+ \quad (2)$$

Spin-trapping experiments have been used to prove the existence of hydroxyl radicals in the Fenton reaction [169]. The OH· radicals that are produced by the Eq. (1) have the main role in the degradation of pollutants such as dye molecules. On the other hand, initiation of the Fenton reactions is also possible with other metals which are at lower oxidation states like Cu^{2+}, Co^{2+}, or Fe^{3+}. These reactions are named by Fenton-like

reaction (Eq. (2)) [155]. However, it is found that Fenton-like reactions are slower than Fenton reactions [170].

Abo-Farha reported the comparative study of some azo dyes by different AOPs which are Fenton, Fenton-like, light-induced Fenton/Fenton-like reactions in 2010 [170]. Comparison of oxidation agents as Fe^{2+} and Fe^{3+} proved that Fenton reactions are faster and more efficient than Fenton-like reactions. The removal rates were calculated as 42-79 L/mol S and 0.002-0.01 L/mol S by Fenton and Fenton-like reactions on the degradation of Acid Orange 8 and Acid Red 17 textile dyes. In addition, removal of Acid orange and Acid Red dyes was found 93% and 98%, respectively by Fenton reactions while the removal was 89% and 78% by Fenton-like reactions.

Another important technique in AOPs is light-induced Fenton reactions which are named by photo-Fenton (PH-Fenton) processes. That method is the fine combination of Fenton of Fenton-like catalysts and radiation of UV-vis light which has a wavelength lower than 600 nm [171]. These reactions can produce an extra amount of hydroxyl radicals by two additional reactions described in Eq. (3) and Eq. (4) [172]:

$$Fe(OH)^{2+} + h\nu \rightarrow Fe^{2+} + OH \cdot \text{ when } \lambda < 580 \text{ nm} \quad (3)$$

$$H_2O_2 + h\nu \rightarrow 2\,OH \cdot \text{ when } \lambda < 310 \text{ nm} \quad (4)$$

The supplemental radicals formed by the help of energy coming from UV-vis light enhance the efficiency of Fenton reactions and accelerates the degradation of pollutions [172]. Also, the increased efficiency and higher oxidation rate make the Fenton reactions able to use a fewer amount of metal ion catalysts in the system [173]. Due to the ability of those reactions to using sunlight as the source of energy needed in oxidation processes, ph-Fenton methods have been considered as a versatile and effective way to purify water for a more sustainable environment [165], [174]–[176].

In this study, we developed metal loaded mesoporous silica particles as highly efficient catalytic materials. The addition of metal ions into mesoporous silica particles enhance the efficiency of the catalytic material by Fenton reactions. Mesoporous silica particles were loaded with Fe^{2+} and Cu^{2+} metal ions by adding metal salts in simple and cost-effective mesoporous silica synthesis method described in Chapter 2. The degradation

efficiency of Fe/MSP and Cu/MSP was investigated by the degradation of Methylene Blue (MB) molecules.

4.2 Materials And Methods

4.2.1 Materials

Metal loaded silica samples were synthesized at room temperature by using Pluronic F127 as the surfactant, TEOS as silica precursor, and HCl as acid catalyst. The amphiphilic triblock copolymer, Pluronic F127 from Sigma Aldrich was used as a structure directing agent. Tetraethyl orthosilicate (TEOS) with 208.33 g/mol molecular weight was purchased from MERCK. HCl (37 wt.%.) was purchased from Sigma Aldrich. $FeCl_2 \cdot 4H_2O$ (MW=198.81 g/mol) and $CuCl_2 \cdot 2H_2O$ (MW=170.48 g/mL) salts were used in the synthesis for loading the silica samples with active catalysts. Both salts were purchased from MERCK. Methylene Blue (MB) was used for the experiments as a model textile dye.

4.2.2 Preparation And Characterization Of Fe/SiO_2 And Cu/SiO_2 Catalyst

The catalyst samples were synthesized by modifying the already utilized method in TEOS/Pluronic F127/HCl system. 0.225 g/mL Pluronic F127 was dissolved in a 3.00 M HCl acid aqueous solution. Then metal salts ($FeCl_2$ and $CuCl_2$) were dissolved in the solution mixture. The concentration of the metals was varied in a range between 0.01 M and 0.10 M (Table 4.1). 200 µL/mL TEOS was added to the solution to have the composite catalysts formed by Fe^{2+}, $Cu^{2+,}$ and silica.

Table 4.1 The summary of concentrations used to synthesize metal loaded mesoporous silica catalysts

Sample No:	Loaded Metal Ion	Concentration of Metal Ion (M)	Concentration of Pluronic (g/mL)	Concentration of TEOS (µL/mL)	Concentration of Acid (M)
CS01	Cu^{2+}	0.01	0.0225	150	3.00
CS02	Cu^{2+}	0.02	0.0225	150	3.00
CS03	Cu^{2+}	0.05	0.0225	150	3.00
CS04	Cu^{2+}	0.1	0.0225	150	3.00
CS05	Fe^{2+}	0.01	0.0225	150	3.00
CS06	Fe^{2+}	0.02	0.0225	150	3.00
CS07	Fe^{2+}	0.05	0.0225	150	3.00
CS08	Fe^{2+}	0.1	0.0225	150	3.00

Instead of colorless gel formation, yellow and blue gel formations were obtained in those syntheses as is shown in Fig 4.1. Typically, gelation of reaction mixture is completed in

a few hours at 3.00 M HCl concentration. The samples were aged overnight after TEOS addition, the liquid phase was removed by vaporization at room temperature and atmospheric pressure (24 h). As the last step, the dry powders were calcined at 500 ^{o}C to remove surfactant from the particles to have a porous structure.

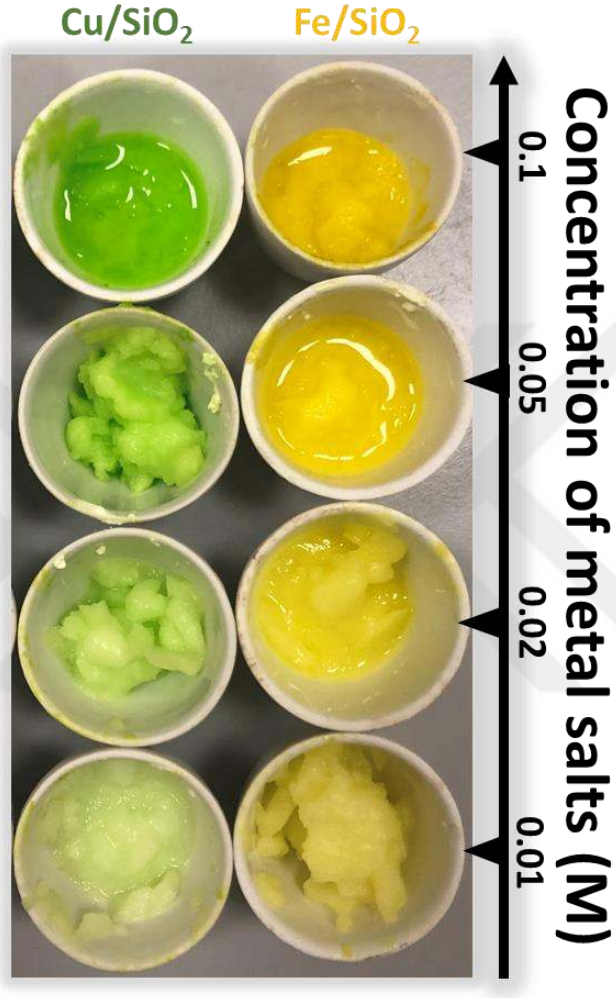

Figure 4.1 The metal loaded silica samples before the calcination process step.

Field Emission Scanning Electron Microscopy (FE-SEM) images and Energy Dispersive X-Ray Spectroscopy (EDX) results were obtained using a ZEISS Ultra Plus scanning electron microscope equipped with Bruker EDX detector. Particle sizes of the catalysts were determined by analyzing SEM images by ImageJ software. The images were taken by different magnifications varied as 2.00K, 5.00K, and 10.00K. Chemical structure mapping of the catalyst particles was investigated by the EDX spectroscopy analysis to see the distribution of metal ions in the silica host.

4.2.3 Experimental Procedure

Investigation of catalytic activity of Fe/SiO_2 and Cu/SiO_2 composite particles were studied under two different conditions under exposure to UV light and dark. In both cases, 100 ppm of MB solutions were used to evaluate the catalytic activity of the samples. 10 mg of composite catalyst particles were dispersed into a 6 mL dye solution. After that 2 mL of 30 wt.% H_2O_2 solutions was added to the solution mixture. For the experiments under UV light, 500 W Xe lamp were used and the distance between the lamp and testing solution was 30 cm. The experiments were completed in 60 mins and degradation ratios were measured by UV-vis spectroscopy analysis. To calculate the concentrations after the tests, 0.1 mL of the supernatant solution was taken and diluted with 2.9 mL of DI water to get trustable results from the UV/vis spectroscopy analysis. Then the solution was centrifuged for 3 mins with 8000 rpm to avoid baseline shift by remaining particles. The concentrations of resulted solutions were computed by the calibration curve which was drawn by serial dilutions. The maximum UV/vis absorption wavelength of methylene blue solutions was obtained as 664 nm in line with the literature data [177].

The reaction rates of MB degradation were calculated by Langmuir-Hinshelwood pseudo-first-order kinetic model which is shown blew to investigate the photocatalytic activity of the composite photocatalyst particles [178];

$$\ln\left({}^{C_0}/_{C_t}\right) = kt \quad (5)$$

where C_0 and C_t are the initial concentration and the concentration after the relative exposure time of MB, respectively, k is the rate constant and t is the exposure time. The results of degradation ratios and the rate of the reactions will be introduced in the next sections of the chapter.

4.3 Results And Discussion

4.3.1 Characterization Of The Catalysts

Figure 4.2 represents the SEM images of the particles synthesized with the TEOS/Pluronic F127/HCl/Metal system. It was clearly shown that loading the metals on the MSPs did not have any negative influence on the shape of the particles. This can be attributed to the effect of ions in the synthesis. Metal chlorides were used as source of

metal ions. So, the counter ions remained same with HCl. KS21 samples which were introduced in previous chapters were also clear spherical-shaped particles. Although the size of spherical particles was not affected significantly, it was observed that the fusion of the particles was lower when they were loaded with Cu^{2+}.

On the other hand, free metal oxides were observed by increasing the amount of iron(II) chloride in the reaction mixture as shown in the SEM images of loaded samples (Fig. 4.2). The homogeneous distribution of Cu loaded mesoporous silica particles can be explained by the inorganic chemical properties of the material [179]. Copper can make ligand exchange processes relatively easier than iron due to electron configurations of their ions. Fe^{2+} gets a more stable orbital by giving an electron and forming Fe^{3+} which is the electron configuration of Fe_2O_3. However, Cu^{2+} needs one more electron to be more stable by completing the orbital symmetry of 3d orbital. Due to those behaviors of the ions, it can be summarized as iron would more prefer oxidizing and forming its complex rather than attaching to the silica surfaces when it is compared with copper(II) ions. In addition, the small particles on the surface of MSP (Fig 4.2.) were proven as Fe_2O_3 molecules by EDX spectroscopy (Fig 4.3 & Fig 4.4). The small particles on the external surface of spheres were detected as Fe with the EDX mapping analysis. On the other hand, the homogeneous distribution of Cu^{2+} ions into the structure of silica particles were clearly seen by mapping the particles even with 0.10 M of salt concentration during the synthesis.

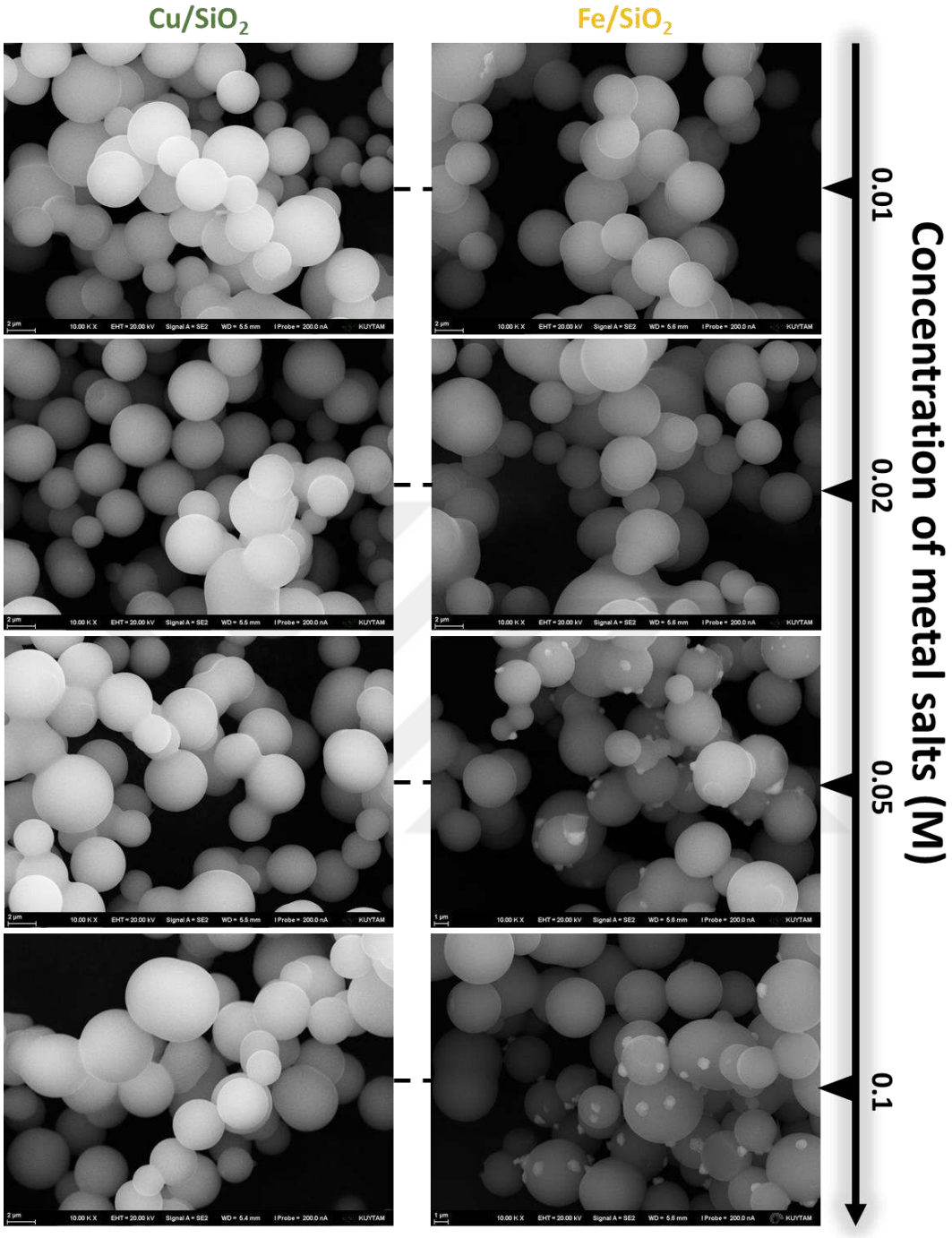

Figure 4.2 SEM images of the metal loaded silica particles, taken by secondary electron detector. The scale bars of the images correspond to 2 µm.

The loading capacity of MSPs can be enhanced by orienting the pores, enlarging the pore size and increasing the SSA of mesoporous silica particles. Controlling of these parameters can enhance the loading of metal ions onto the silica surfaces which will ultimately improve their catalytic activities.

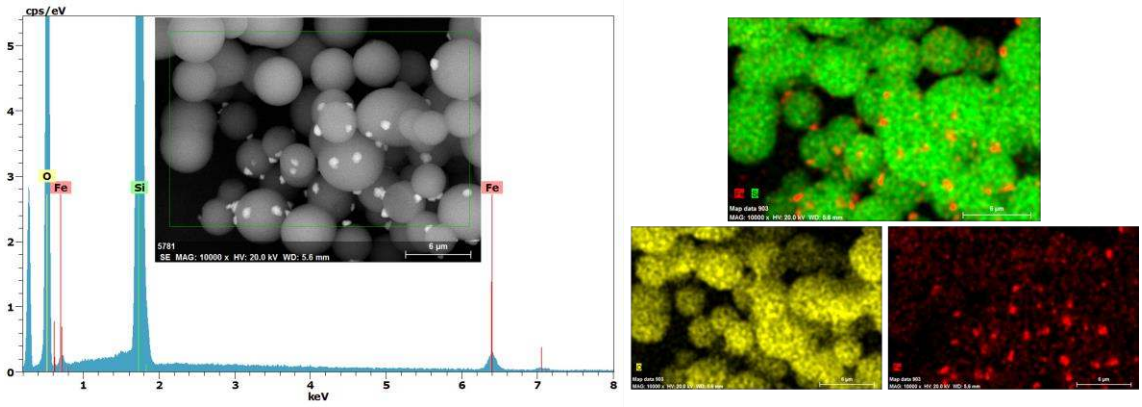

Figure 4.3 EDX spectroscopy results of Fe2+ loaded silica particles with 0.10 M of ions. The colors represent elements as green: silicon, red: iron and yellow: oxygen

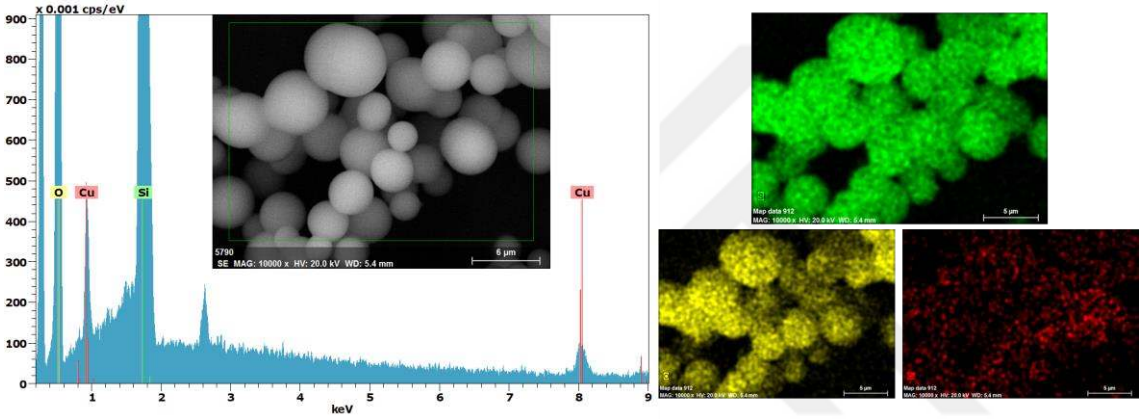

Figure 4.4 EDX spectroscopy results of Cu^{2+} loaded silica particles with 0.10 M of ions. The colors represent elements as green: silicon, red: cupper and yellow: oxygen.

The SEM images and chemical analysis of the samples showed the successful inclusion of metal ions onto mesoporous silica particles. The easy parameter control of the synthesis route may be a great opportunity for wastewater treatment and other catalyst applications by reducing the cost while increasing efficiency. In general, catalytic materials consist of expensive materials such as silver, gold, titanium, or platinum. In addition, micron-sized MSPs can be synthesized with relatively higher cost methods. Here we combined the simpler and cost-effective method to synthesize MSPs and relatively cheaper metals to synthesize catalytic materials.

4.3.2 Catalytic Activity Of Fe/SiO_2 And Cu/SiO_2 Catalysts In Dark (Fenton And Fenton-Like Reactions)

It is well known that Fe^{2+} and Cu^{2+} are the initiators of Fenton and Fenton-like reactions, respectively [155], [169]. In this study, investigation of catalytic activity of Fe/SiO_2 and Cu/SiO_2 composite catalytic particles under room temperature, ambient temperature,

neutral pH, and complete dark conditions was performed. The summary of the parameters of the experiments was listed in Table 4.1. The results of catalytic degradation of MB showed that iron-loaded silica particles were more efficient catalysts when they were compared with copper-loaded silica particles. Very high % removal rates (> 99%) were obtained by the composite catalyst particles that were composed of Fe^{2+} ions in the structure. On the other hand, copper-loaded silica particles removed %76.71 of MB after 60 mins by the highest concentration of dopped active catalyst. These results can be attributed to the type of catalytic activities. When the iron-loaded particles formed the hydroxyl radicals by Fenton reactions in the presence of H_2O_2, copper-loaded particles formed the radicals by Fenton-like reactions due to lower oxidation states of copper ions. The results proved the fact that Fenton reactions are more efficient and have higher reaction rates compared to Fenton-like reactions.

Table 4.2 Summary of the properties and experimental results of composite catalysts synthesized at room temperature with 0.0225 g/mL Pluronic F127, 200 µL/mL TEOS, and 3.00 M HCl acid.

Sample No:	Loaded Metal Ion	Concentration of Metal Ion (M)	Max. % Removal of MB (in dark)	Complete Degredation Time (min)
CS01	Cu^{2+}	0.01	58.27	> 60
CS02	Cu^{2+}	0.02	61.34	> 60
CS03	Cu^{2+}	0.05	71.76	> 60
CS04	Cu^{2+}	0.1	76.71	> 60
CS05	Fe^{2+}	0.01	92.59	≈ 60
CS06	Fe^{2+}	0.02	99.65	30
CS07	Fe^{2+}	0.05	99.65	20
CS08	Fe^{2+}	0.1	99.82	≈20

Figure 4.5 represents the degradation rate of MB dye by Fenton (iron ions) and Fenton-like (copper ions) reactions completed with the presence of H_2O_2 and catalyst composites. The efficiency difference of the particles was clearly understood by the concentrations of MB after the experiments. The iron ion-loaded silica particles with the highest concentration of the Fe^{2+} completed the removal of MB near 20 mins. Although copper ion-loaded silica particles showed lower efficiency and reaction rates than iron ion-loaded silica particles in the current conditions, they showed a systematic increase in the efficiency by increasing the number of loaded ions on the silica particles. The catalytic efficiency can be further improved by loading more metal ions . Moreover, these performances of the composite catalysts were found as a great option for wastewater treatment of textile industries even in industries that have a lack of sunlight or other light sources.

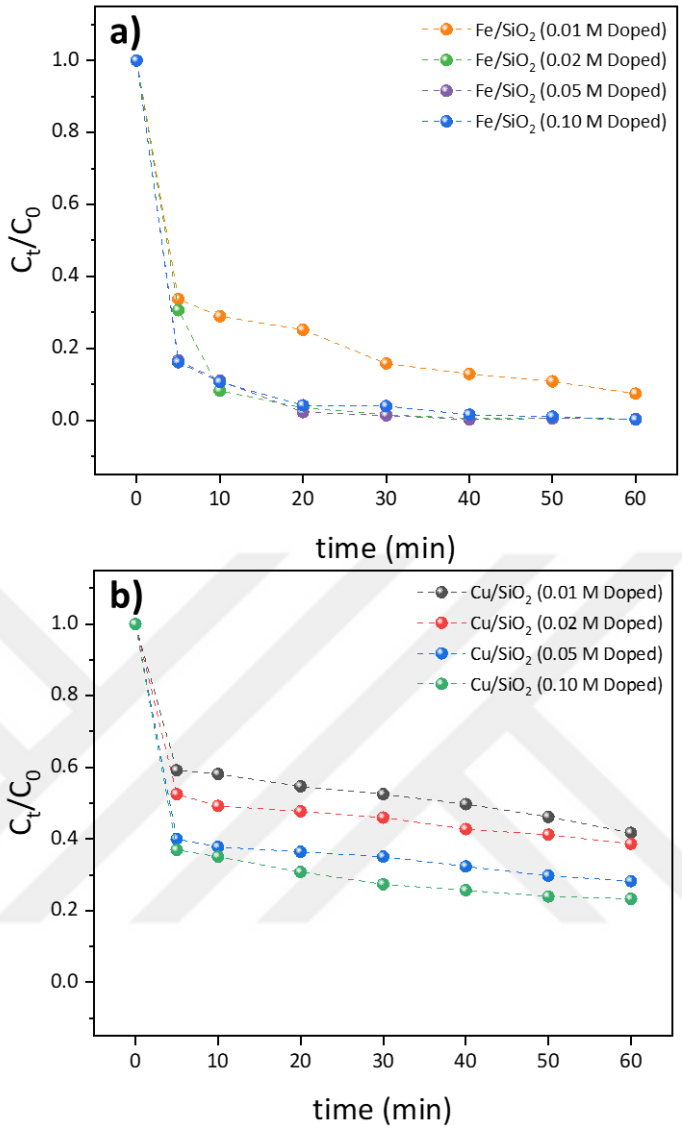

Figure 4.5 Degeneration curves of the catalyst composites synthesized by TEOS/Pluronic F127/HCl and metal salt-induced systems. The degradation rate of MB in dark with the presence of H_2O_2 by the composite catalysts; a) Fe^{2+} loaded, and b) Cu^{2+} loaded silica particles.

The apparent rate constants (k) were calculated as 0.015, 0.016, 0.021, and 0.029 min^{-1} with 0.01, 0.02, 0.05, and 0.10 M copper ion loaded particles in maximum removal of MB, respectively. The rate constants (k) with increasing the amount of iron ion loaded particles were calculated as 0.043, 0.094, 0.094, and 0.11 min^{-1} in maximum removal of MB. It means that iron ion-loaded particles were about 4 times faster than copper ion-loaded particles in all concentrations.

4.3.3 Catalytic Activity Of Fe/SiO_2 And Cu/SiO_2 Catalysts Under Uv Light (PH-Fenton And PH-Fenton-Like Reactions)

After investigation of Fenton and Fenton-like reactions completed with catalyst composite particles, the experiments were also done under the presence of a light source. A UV lamp that had a 500 W Xe lamp source was employed in the experiment setup from a 30 cm distance to investigate the photocatalytic activity of metal loaded silica particles with PH-Fenton and PH-Fenton-like reactions. Nevertheless, the effect of the light source on MB dye and the combined effect of light and H_2O_2 were analyzed firstly without any dispersion of the metal loaded silica particles (Fig 4.6.). The summary of parameters of the experiments under UV lamp was listed in Table 4.2. The maximum % removal of MB results showed that loading metal ions onto MSPs enhanced the catalytic activity of the particles significantly. When bare silica particles removed only 41.95% of the dye molecules from an aqueous solution in the presence of H_2O_2 and UV light, loaded particles successfully removed about 100% of dye molecules.

Improvement of the dye removal was approximately equal by the metal loaded silica s which had either Fe^{2+} or Cu^{2+} metal ions. Nevertheless, PH-Fenton reactions done by Fe^{2+} ions were faster than PH-Fenton-like reactions done by Cu^{2+} ions due to the higher oxidation state of iron ions. The highest metal ion-loaded composites (0.1 M of each ion) completed the total degradation of MB in about 10 mins and 20 mins by Fe^{2+} and Cu^{2+}, respectively.

Table 4.3 Summary of the properties and PH-Fenton / PH-Fenton-like reactions results of composite catalysts synthesized at room temperature with 0.0225 g/mL Pluronic F127, 200 µL/mL TEOS, and 3.00 M HCl acid.

Sample No:	Loaded Metal Ion	Concentration of Metal Ion (M)	Max. % Removal of MB (in dark)	Complete Degredation Time (min)
Blank	-	-	2.16	∞
H_2O_2	-	-	26.38	∞
Bare SiO_2	-	-	41.95	∞
CS01	Cu^{2+}	0.01	99.995	50
CS02	Cu^{2+}	0.02	99.997	40
CS03	Cu^{2+}	0.05	99.998	30
CS04	Cu^{2+}	0.1	99.998	20
CS05	Fe^{2+}	0.01	99.997	40
CS06	Fe^{2+}	0.02	99.998	20
CS07	Fe^{2+}	0.05	100.000	10
CS08	Fe^{2+}	0.1	100.000	10

Figure 4.6. represents the results obtained by the photocatalytic experiments under UV light exposure. As it was described by Eq. (4), the presence of H_2O_2 supported the hydroxyl radical formation under light by breaking the forms with the energy of light. 26.38% removal of MB dye molecules enhanced the photocatalytic activity of the metal loaded silica particles and bare silica particles. However, pure MB solution was not affected by the incoming light energy and dye molecules could be removed by only 2.16%. On the other hand, it was understood that even bare MSPs would destroy MB dye molecules by about 40% in the presence of light and H_2O_2. However, that much removal of MB under a strong light source would not be effective for wastewater treatment of the textile industry. Since the removal yield was saturated on approximately 42% percent, bare silica particles would never clean the wastewater fully if the number of particles was not increased. The feasibility concerns of the wastewater treatment processes prevent the use of large amounts of MSPs in the systems due to the high cost. On the other hand, metal ion-loaded silica particles showed highly promising degradation rates of MB. Especially Fe^{2+} loaded silica particles completed the oxidation process in a very short time as 10 mins.

Another observation during the experiments was bubble formation in reaction mixtures with the presence of H_2O_2 and metal loaded silica particles. This formation of bubbles can be attributed to the $CO_2 + H_2O$ formation which was done by the attack of OH· radical to the dye molecules. Evolution of CO_2 was faster when the UV light was exposed to the reaction mixtures. Due to the extra OH· radical formation by two different paths: the first path was the chemically generated OH· radicals with the Fenton and Fenton-like reactions of metal ions and H_2O_2 and the second path was photogenerated electron on the metal loaded silica particles can transfer from the valence band to the conduction band for the formation of a photogenerated hole. These photogenerated holes can be formed by the interaction between the hole and water molecules. Also, H_2O_2 is an important electron acceptor, and it supports the separation of photogenerated holes and electrons to form more hydroxyl radicals. The higher number of OH· radicals, the higher efficiency in degradation of MB dye molecules.

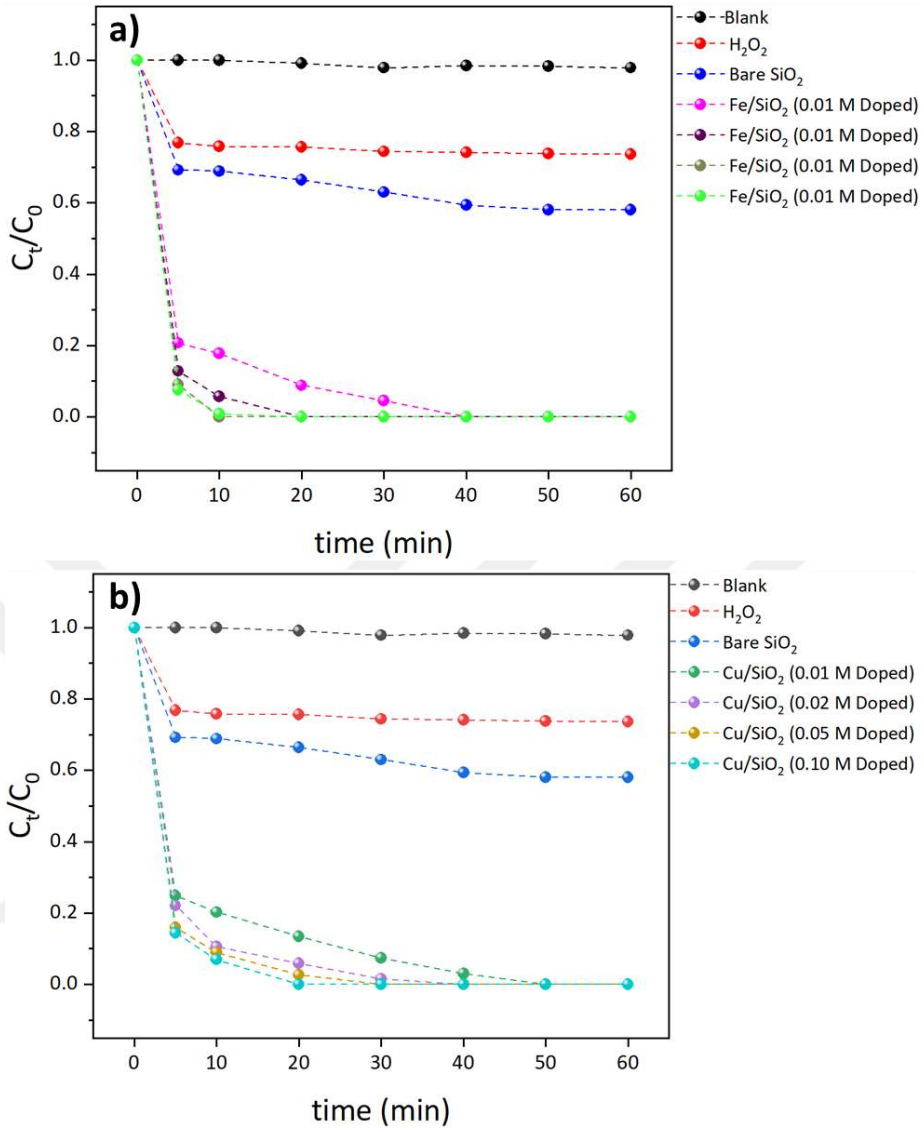

Figure 4.6 Degeneration curves of the metal loaded silica particles synthesized with the metal loaded silica particles. Degradation of MB dye was analyzed under different conditions; Blank: pure dye solution, H2O2: only H2O2 present, and dispersion of bare silica particles under the light exposure. Results were obtained by a) Fe^{2+} and b) Cu^{2+} loaded silica particles.

Higher efficiencies and faster reactions were obtained by PH-Fenton and PH-Fenton-like reactions in the presence of metal ions loading on MSPs. When the reaction rate constant (k) of the degradation process was calculated as 0.009 min^{-1} by the reactions with bare MSPs, 0.18 and 0.26 min^{-1} were calculated with the 0.10 M loading of Cu^{2+} and Fe^{2+} ions, respectively after 60 mins. In addition, the reaction rate constant was reached its highest value by 0.01 M loaded Fe^{2+} ions in 5 mins as 0.52 min^{-1}. These reaction rates were also shown that light-induced catalytic performances of the Cu^{2+} loaded samples were enhanced about 10 times. The increase in Fe^{2+} ion-loaded particles was not as high as the ones with Cu^{2+} since they were already working great without light. Moreover, both of

the metal loaded silica samples shown highly promising solutions for wastewater treatment processes in the textile industry.

4.4 Conclusion

Silica-based active catalyst materials could be successfully synthesized with the novel, simple and cost-effective methods. Active photocatalyst metals were loaded on the MSPs without any requirement of additional post-heating, stirring, or etching processes. The metal ions could be distributed homogeneously in the composite structure. Overloading was observed after a certain amount of $FeCl_2$ salts as 0.05 M during the synthesis, but additional Fe_2O_3 particles were not free in the powder. They were attached to the silica surfaces and contributed to the catalyst activity of the samples by Fenton-like reactions between Fe^{3+} and H_2O_2 molecules. In addition, it was understood by the SEM images that joint synthesis of metal loaded silica catalyst materials by the method of synthesizing MSPs did not affect the morphology of the particles. As it was shown in the previous chapters, KS21 samples remained spherical after adding metal ions to the system. Moreover, the samples showed less fusion of the secondary particles after the agglomeration of primary particles. The concentration of surfactant, TEOS, and HCl acid resulted in micro/mesoporous structures (Chapter 1). It can be estimated that larger pore size and higher surface area of the silica particles would have higher loading efficiency of metal ions with this technique. However, the effect of synthesis reaction time and amounts of compositions should be investigated to have optimum conditions for synthesizing metal loaded silica catalyst structures.

The catalytic activity of the samples was studied by different reaction mechanisms as Fenton, Fenton-like, PH-Fenton, and PH-Fenton-like reactions. The efficiencies of metal ion-loaded silica hosted composite catalysts were investigated by systematic experiments. It was found that Fe^{2+} ion-loaded samples were better in efficiency and speed of the reactions under every condition. The effectiveness of the reactions on wastewater treatment by degradation of MB was observed as; PH-Fenton (Fe^{2+}) > PH-Fenton-like (Cu^{2+}) > Fenton (Fe^{2+}) > Fenton-like (Cu^{2+}). The results showed that the method produces highly efficient solutions for wastewater treatment processes, especially in the textile industry. MB dye molecules were successfully degraded by 100 % removal with PH-Fenton and PH-Fenton-like reactions done by metal ion-loaded silica particles. 0.52 min^{-}

[1] reaction rate constant could be obtained by Fe^{2+} loaded silica structures. After 10 mins and 20 mins, the concentration of MB was decreased from 100 ppm to zero 0.01 M Fe^{2+} and Cu^{2+} loaded particles, respectively. That removal makes maximum removal capacity as approximately 800 mg/g for MB dye and it could be obtained by larger amounts of the initial concentration of the dye.

Moreover, higher amounts of hydroxyl groups produced by the metal loaded silica catalyst particles may also be effective for other organic compounds which are dangerous for aquatic life and sustainable environment. However, the effect of reaction conditions must be studied more to have the optimum condition to have maximum removal efficiency of pollutants. Especially in the larger industries, these optimum conditions would be promising to purify water, odor removal, sludge treatment, and removal of macrobiotics.

Additionally, the effect of MSPs as a host material was also proven by the results. Bare silica particles contributed to the degradation of MB in this study by about 40 % with the presence of H_2O_2. Like metal loaded silica catalyst samples, the effect of properties of MSPs must be also investigated to have optimum combinations.

Instead of expensive metals such as palladium, platinum, gold, or silver using cheaper metals like iron or copper to synthesize highly active catalytic materials is a very promising development for wastewater treatment processes. Also, our simple and cost-friendly method to synthesize those particles by TEOS/Pluronic F127/HCl system decreases the cost to produce these highly catalytic and photocatalytic composites. Increasing the efficiency of the metal loaded silica catalyst samples about 10 times by just exposure to UV light for 10 mins makes those particles very applicable to treatment applications. Because sunlight is a free energy source that does not create any pollution for the environmental health.

Chapter 5:
INVESTIGATION OF SELF-PROPELLED MESOPOROUS SILICA MICROMOTORS

5.1 Motivation

In recent year, micromotors have been attracted developments in nanotechnology [180]. Well-designed micromotors offer great potential to be structures can be employed in various applications in materials science such as microprobes/sensors, monitoring in micro/nano level investigations [181]–[185]. Therefore, lots of researchers have investigated the dynamic behaviors and improve the efficiency of different kinds of micromotors to meet various requirements. The development of micromotors is a significant advancement towards the realization of micro/nanoscale world.

R.F. Ismagilov established the first micromotor by designing a system having catalytic decomposition of hydrogen peroxide by the platinum-coated surface of a metal to be the fuel of propulsion [186]. Decomposition of H_2O_2 formed bubbles to push the metal platinum-coated metal microparticle. After the first invention of self-propelled micro/nanomotors, many approaches have been studied to control these types of self-locomotion by controlling the surface modifications, loading agents to be fuel, responsive feed-back of the particles to the media, or structural properties (e.g. size, morphology), etc. [187]–[193].

Most of the micro/nanomotors use bubble formation and separation from them as the fuel of the locomotion. These types of self-driven locomotion can be classified into three main groups which are i) self-diffusiophoresis, ii) self-electrophoresis and ii) bubble propulsion [44], [45]. Self-diffusiophoresis is a type of spontaneous locomotion using the concentration gradient of a substance in a liquid to move colloidal particles [46], [47]. The self-electrophoresis mechanism uses the power electric field which is formed by the decomposition of H_2O_2 and the formation of water molecules [48], [49]. Electrocatalytic decomposition of hydrogen peroxide forms H^+ cations on anode surfaces and those protons are consumed by the cathode side of the JPs. The asymmetric ion distribution on the system yields fuel for locomotion. On the other hand, bubble propulsion is a more facile system as the formation of bubbles by CO_2, O_2, etc. in an aqueous environment to

push the colloids for locomotion [45]. In this study, we have focused on bubble propulsion and diffusiophoresis to have self-propelled motion with mesoporous silica Micromotors.

Although self-propelled locomotion by bubble propulsion mechanism is relatively easier and faster, the speed and start/stop of the motion are hard to control [180]. Catalytic decomposition of hydrogen peroxide into oxygen gas and water molecules is the most common fuel for the bubble propulsion mechanism. The geometry of the particles to be driven is one of the most important key factors to control the movement [194]. W. Huang et al. reported shell micromotors to control the bubble nucleation for controlling the motion [195]. They synthesized shell structured particles consisting of Pt, Ag, and Au layers on top of silica beads with different particle sizes in a range between 2-30 μm. They reported the control of the movement by speed and opening diameter of pore which is the non-coated part. They also concluded that shell motors were much faster than the JPs motors. However, instead of bubble formation by catalytic degradation of H_2O_2, a fuel that is non-toxic and produces enough movement is needed for self-propelled micromotors. The best alternative for this approach is water. W. Gao et al. reported the first micromotors that use water as the fuel for autonomous movement [196]. They used titanium coating o half of the Al-Ga alloy to have the JPs. Ga-Al alloy presents as a catalyst for water-splitting reactions. One year after that investigation, F. Mou et al. used catalytic water-splitting reaction to use water as the fuel for their self-propelled micromotor. They used Mg and Pt to synthesize bubble-driven micromotor. The locomotion of this novel particles was driven by the reaction between water and MB with the support of $NaHCO_3$. These investigations were very important developments for biomedical applications such as targeted drug deliver due to the high biocompatible reactants and products.

On the other hand, using MSPs as micro/nano micromotor and various applications of them have been well described in a review paper reported by X. Ma and co-workers [197]. The applications are summarized as targeted drug delivery, gene co-delivery, monitoring in biological systems, and photodynamic therapy. The superior properties such as high surface area, uniform structure, and large pore sizes make MSPs great micro/nanocarriers. Different types of chemicals to be used as fuel of the motion have been loaded to mesoporous silica and obtained motion by bubble propulsion. Lastly, Guix et al. reported a synthesis method to form $CaCO_3$ particles from substitution reaction between $CaCl_2$

and Na_2CO_3 [198]. $CaCO_3$ particles can produce CO_2 gas under slightly acidic solutions and move by the bubble propulsion with the given reaction mechanism:

$$Ca^{2+}{}_{(aq)} + 2Cl^{-}{}_{(aq)} + 2Na^{+}{}_{(aq)} + {CO_3}^{2-}{}_{(aq)} \rightarrow CaCO_{3(s)} + 2Na^{+}{}_{(aq)} + 2Cl^{-}{}_{(aq)} \quad (1)$$

$${CO_3}^{2-} + 2H_3O^{+} \rightarrow CO_{2(g)} + 3\,H_2O \quad (2)$$

In our study, we loaded the MSPs that were synthesized in previous chapters with high surface area and spherical shape and loaded with $CaCO_3$ using in situ precipitation on the silica particles. Due to the size of the particles non-Brownian motion was not detected for the unloaded silica particles. Bubble propulsion and self-diffusiophoresis was observed as main driving forces for the motion of the particles. Particles with different size, SSA and pore size were compared to deduce information about the loading capacity and movement of the particles. The in situ precipitative loading of the particles was found to be a successful route for the production of self-propelled mesoporous silica particles which have great potential to be used as Janus particles. Also, the biocompatibility and low toxicity of the composition and bubble formation are great advantages.

5.2 Materials And Methods

5.2.1 Materials

MSPs to be utilized as self-propelled Micromotors were synthesized by using TEOS/Pluronic F127/TEOS system that was studied in Chapter 2. $CaCl_2{\cdot}2H_2O$ and Na_2O_3 chemicals were used to load MSPs with $CaCO_3$ and both were purchased from MERCK. Rinsing of loaded silica particles for faster evaporation of the solvent and drying was completed by ethanol, acetone, and toluene purchased from Sigma Aldrich. Dimethyl Sulfoxide (DMSO from MERCK) was used to enhance the stability of the $CaCO_3$ vaterite phase.

5.2.2 Characterization Techniques

Scanning Electron Microscope (SEM) and Energy-Dispersive X-Ray Spectroscopy (EDX)

The morphology of the silica particles before and after utilizing them as self-propelled Micromotors were analyzed by using Field Emission Scanning Electron Microscope

(FE-SEM) and Environmental Scanning Electron Microscope for ZEISS UltraPlus SEM and ZEISS EVO LS15, respectively. The shape and size of the particles were analyzed by the images taken with the secondary electron detector by different magnifications. Chemical compositions of the samples were analyzed by the EDX analysis by FE-SEM which has a Bruker detector. Ca, C, O, and Cl compositions were analyzed by mapping and listing of chemical compositions at 5-9 acceleration voltage.

Surface Area Measurements

The same technique in previous chapters was used to analyze the properties of porous structure such as pore volume, pore diameter, and specific surface area of MSPs. Micromeritics ASAP 2020 physisorption instrument was employed to measure adsorption/desorption isotherms of MSPs. The SSA of the samples was calculated by using the BET model to fit the resulted isotherms. All of the experimental data is plotted by the amount of gas adsorbed and desorbed against relative pressure. The pore diameter and pore volume values of the samples were obtained by the BJH method.

Surface Charge Of The Samples (Zeta Potential)

Zeta potential measurements of bare silica particles, and loaded silica particles were determined by the Brookhaven ZetaPals instrument. These measurements were applied not only to investigate the colloidal stability of particles but also to determine the pH of maximum attraction by electrostatic interactions between silica and Ca^{2+} ions. Moreover, the results were evidence of utilizing the bare silica particles as micromotors.

Conductivity Measurements

To determine the uptake and release of the Ca^{2+} ions of MSPs, a conductometer HI98303 (HANNA) was used. First silica particles were dispersed in the loading solution containing Ca^{2+} ions and were left undisturbed. The solid particles sedimented within 10 min. From this dispersion 500 µL to 1500 µL sample was taken (using the clear top solution) and was diluted by added to 50 mL deionized water (conductivity = 0-1 µS/cm). Conductivity measurements were completed in these diluted solutions.

Monitoring The Locomotion Of The Samples

The locomotion of mesoporous silica micromotors was visualized by using Leica DMLM optical microscope with MShot MDX4-T camera. The videos of the motions were recorded at varied magnification from 5x to 50x. The velocity of the particles was calculated manually from recorded videos.

5.2.3 Experimental Procedure

Synthesis Of MSPs

The synthesis of the silica sample was carried on by the synthesis method that is described in the second chapter. The samples were synthesized at room temperature by using Pluronic F127 as the surfactant and TEOS as the silica precursor. The concentrations of the samples were varied in the spherical region of the established ternary phase diagram of TEOS/Pluronic F127/HCl. Moreover, the synthesis of hydrothermally treated samples was also used to investigate the effect of pore size and order in this part of the study. The hydrothermally treated particles were synthesized under 80 °C evaluated temperature after adding TEOS in autoclaves. The experimental conditions and concentrations of the used particles to be utilized as micromotors were summarized in Table 5.1.

Table 5.1 The summary of experimental conditions to synthesize MSPs to be utilized as micromotors

Sample No:	$C_{Pluronic\ F127}$ (g/ml)	C_{TEOS} (µL/mL)	C_{HCl} (M)	Hydrothermal Treatment
KS16	0.03	200	4.00	-
HTK16	0.03	200	4.00	80 °C, 24 h
KS17	0.05	200	4.00	-
PD09	0.09	200	2.56	-
HTPD09	0.09	200	2.56	80 °C, 24 h
CA	Commercially available			

$CaCO_3$ Loading on Mesoporous Silica Particles

To achieve the locomotion by bubble propulsion, MSPs were loaded with $CaCO_3$ due to the tendency of carbonates to produce CO_2 gas in an acidic medium. CO_2 gas can form bubbles on the surface of loaded particles and push them forward. Direct synthesis of $CaCO_3$ on the external surface and inside of the pores of MSPs was used to functionalize samples as fuel-loaded particles. First of all, MSPs were dispersed in $CaCl_2$ solution to

attract Ca^{2+} ions to silica surface. The main driving force for that step was electrostatic interactions of naturally negatively charged MSPs and positively charged ions. Then the coating of silica particles by Ca^{2+} ions was completed by centrifuging and the top solution was removed. Secondly, the centrifuged and dried particles were dispersed in Na_2CO_3 solution to form $CaCO_3$ on MSPs. The concentration of $CaCl_2$ solution was varied in a range between 0.0125 M and 0.07 M to determine the optimum loading condition. Then these concentrations were combined with three different concentrations of Na_2CO_3 solution which were 0.01 M, 0.02 M, and 0.05 M. The resulted particles were characterized by SEM images and EDX analysis, and an insufficient amount of incorporation was observed. Thus, further experiments were studied to increase the loading amount of $CaCO_3$.

The processes were continued with increasing the amount of $CaCl_2$ and Na_2CO_3 concentrations to 1.0 M. The results showed that increasing the concentration of salts was not the solution for increasing the efficiency of $CaCO_3$ loading.

To have the highest attraction of Ca^{2+} by silica samples, MSPs were carried out with the presence of NH_3 in solutions to decrease the zeta potential of the particles. It was well known from the Zeta potential results, described in the next sections, of our MSPs that particle surface charge has larger negativity with increasing the pH. Within that system of loading Ca^{2+} on silica samples, we tried to optimize the $CaCO_3$ loading process.,

The silica particles were dispersed in the solution of $CaCl_2$ and NH_3 for 15 min by sonicating. Then particles were left for fixed durations (2 h, 24 h, 48 h) to sediment bottom and loaded amounts were calculated by conductivity measurements. Then $CaCO_3$ formation was completed by dispersing particles into Na_2CO_3 aqueous solution.

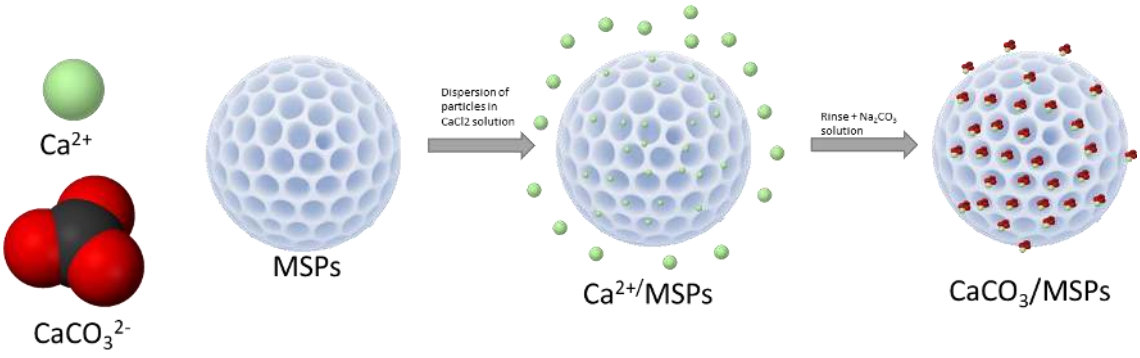

Figure 5.1 Schematic illustration of loading $CaCO_3$ on MSPs

5.3 Results And Discussions

5.3.1 Structural Properties Of The Particles Used To Obtain Micromotors

The particles to obtain self-propelled mesoporous silica micromotors were synthesized by TEOS/Pluronic F127/HCl system that is well investigated in the first chapter. Additionally, a commercially available sample (CA) that is used as column filling material for high-performance liquid chromatography was used to compare the locomotion ability of our silica particles. As it is represented in Fig 5.2., we obtained mainly spherical particles with the concentrations of the three components of the system and experimental conditions, summarized in Table 5.1. Although the main morphology of our silica particles was spherical, they were more fused (plus some monolith structures) compared to the commercially available silica particles. Also, the uniformity of particle sizes was lower than CA particles. The effect of the acid-catalyzed system was explained in the previous chapters in more detail. On the other hand, the effect of the HT process on the morphology of particles was obtained once more. Especially with the particles that were synthesized by a higher amount of surfactant (PD09: 0.09 g/mL and KS16: 0.03 g/mL Pluronic F127) and lower acidity (PD09: 2.56 M and KS16: 4.00 M HCl), the HT processes were more effective and formed monolith structures from fused spherical particles. However, CA particles were not even in contact with each other, and their colloidal stability was much higher than our particles. Additionally, largest and more uniform particle size were obtained on those particles as mean particle diameter size were equal to 5 ± 1.5 μm. Moreover, SEM images once more showed that our system can produce spherical particles with a diameter larger than a micron.

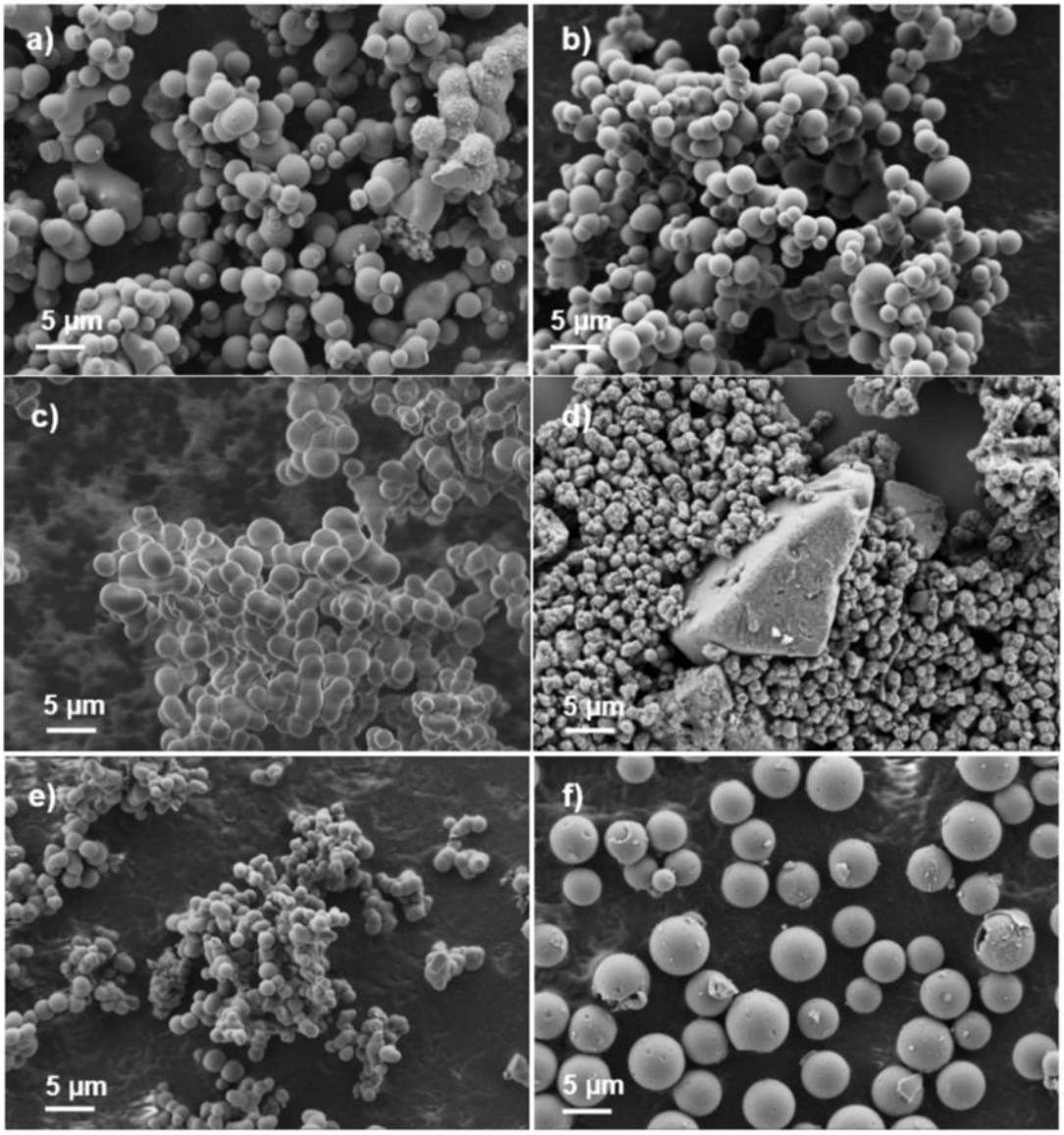

Figure 5.2 SEM images of the particles to be utilized as micromotors. a) KS16, b) HTKS16, c) PD09, d) HTPD09, e) KS17 and f) CA. The scale bars correspond to 5 micrometers for each image.

Investigation of the N_2 gas adsorption/desorption curves of the used particles in this study was represented in Fig 5.3. The types of isotherms obtained from the particles clearly showed that the synthesized particles had the pore sizes as a mixture of both micropores and mesopores (the border is 4 nm). Moreover, hydrothermally treated samples had domination of mesopores. The increase in the SSA of the particles even when the pore sizes were larger can be attributed to the more ordered pores obtained by the HT process. On the other hand, a larger hysteresis between adsorption and desorption N_2 gas was obtained from CA particles. Those larger pore sizes (7-9 nm) in the particles were the reason to obtain lower SSA on those particles. Also, larger particle size was influencing the SSA.

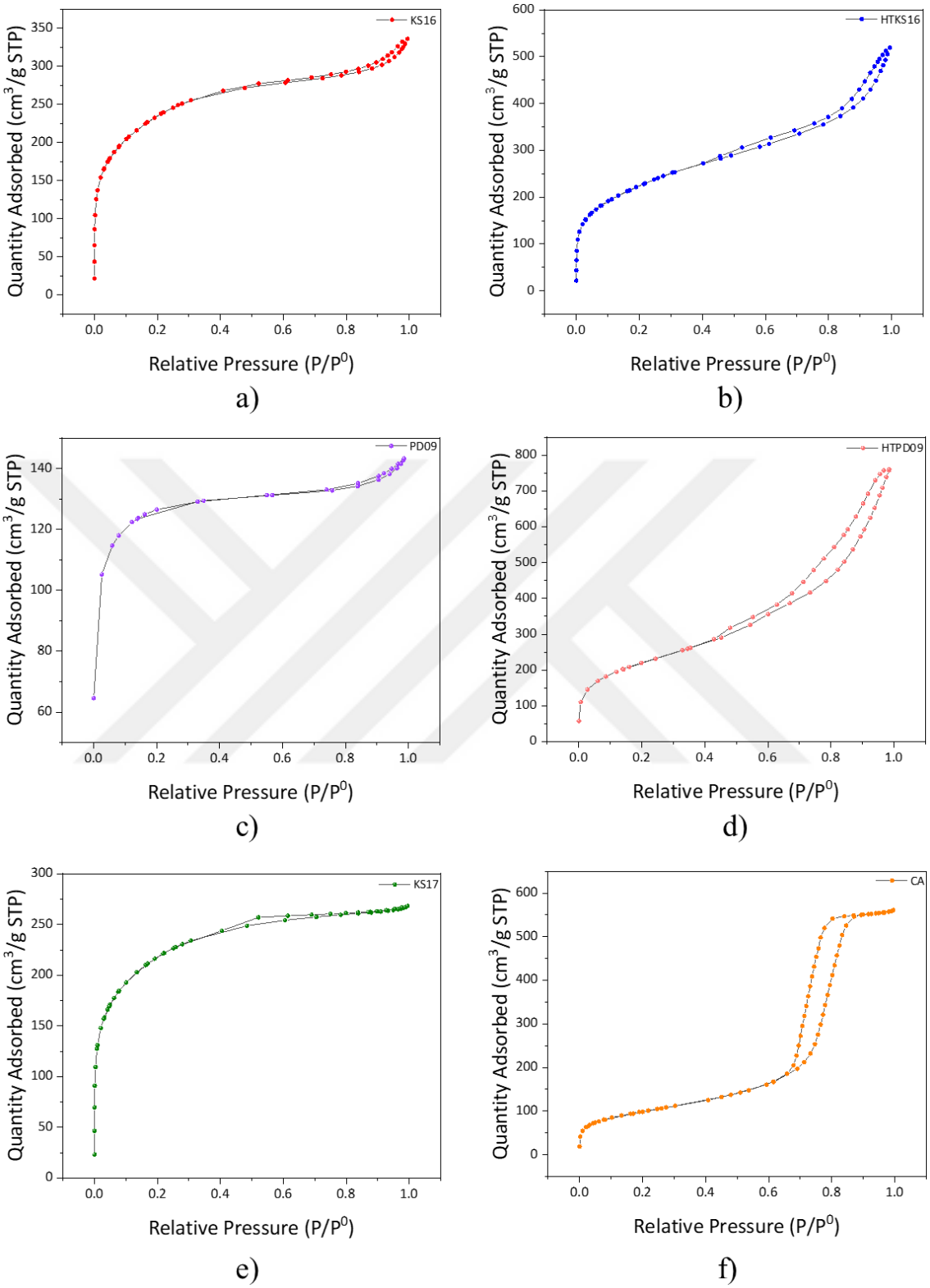

Figure 5.3 Adsorption isotherm plots of silica particles that were used for synthesizing self-propelled mesoporous silica Micromotors.

Specific surface area (BET) and pore size (BJH) distribution results were summarized in Table 5.2. with sample codes.

Table 5.2 Particle properties of mesoporous silica samples used to synthesize Micromotors

Sample No:	SSA (m2/g)	Pore Size (nm)	Particle Size (M)	Morphology
KS16	789	3-4	1.5-2.5	spherical
HTK16	698	4-5	1.5-2.5	spherical
KS17	719	3-4	1.4-2.0	spherical (fused)
PD09	448	<5	2.0-3.6	spherical (fused)
HTPD09	760	5 and 12	1.3 + 16-27	spherical (fused) + monolith
CA	326	7-9	4.0-6.5	spherical

5.3.2 Surface Charge Of The Samples

In this study, $CaCO_3$ loading on the porous silica samples was tried to be achieved by attracting Ca^{2+} ions to silica particles in aqueous systems. As it was described in the experimental procedure, electrostatic interaction between silica colloids and Ca^{2+} ions were used as the driving force for the loading process.

It is well-known from the literature that the surface charge of silica particles is below zero above the isoelectric point of silica particles [199]. Moreover, the magnitude of negative charge increases by increasing the pH of the solution in which silica particles are dispersed. To find the optimum pH to uptake Ca^{2+} ions by our silica particles, we investigated the surface charge values of the samples in a pH range between 2-12. Mesoporous silica particles (listed in Table 5.1 and 5.2) were dispersed in buffer solutions to determine the Zeta potentials. The list of buffer solutions to have certain pH is listed in Table 5.3. The buffer solutions were prepared to have similar ionic strength.

Table 5.3 List of the solution composition in the tabulated form used for the Zeta potential measurements of silica samples at given pH values.

pH	Composition of Buffer solution (in 100 mL)
1.0	25 ml 0.2 M KCl + 67 ml 0.2 M HCl
2.0	25 ml 0.2 M KCl + 6.5 ml 0.2 M HCl
3.0	50 ml 0.1 M potassium hydrogen phthalate + 22.3 ml of 0.1 M HCl.
4.0	50 ml 0.1 M potassium hydrogen phthalate + 0.1 ml of 0.1 M HCl.
5.0	50 ml 0.1 M potassium hydrogen phthalate + 22.6 ml of 0.1 M NaOH
6.0	50 ml 0.1 M KH_2PO_4 + 5.6 ml of 0.1 M NaOH
7.0	50 ml 0.1 M KH_2PO_4 + 29.1 ml of 0.1 M NaOH
8.0	50 ml 0.1 M KH_2PO_4 + 46.7 ml of 0.1 M NaOH
9.0	50 mL 0.025 M $Na_2B_4O_7.10H_2O$ (borax) + 4.6 ml of 0.1 M HCl.
10.0	50 mL 0.05 M $NaHCO_3$ + 10.7 ml of 0.1 M NaOH.
11.0	50 mL 0.05 M Na_2HPO_4 + 4.1 ml of 0.1 M NaOH.
12.0	25 mL 0.2 M KCl + 66 ml of 0.2 M NaOH.

Silica samples with 1.0 mg/mL concentration were dispersed in the buffer solutions given in Table 5.3. and waited for a 30 min to reach to the equilibrium of the double layer formation on the solid particles. It was clearly understood from the zeta potential results (Fig 5.4.) that electrostatic interaction between positively charged ions and MSPs would be enhanced significantly by increasing the pH of the medium to 10-12. The uptake of Ca^{2+} by MSPs was continued in NH_3 aqueous solutions to have higher pH values after these results.

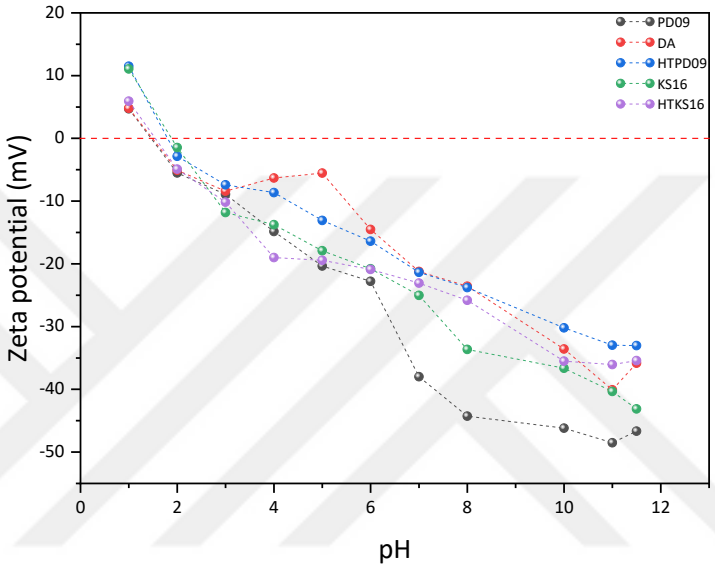

Figure 5.4 Zeta potential dependency of MSPs as the function of pH

5.3.3 Ca^{2+}loading of MSPs

Uptake of calcium ions on MSPs with electrostatic interaction was the first challenge to reach our goal that was loading the silica samples with $CaCO_3$. We tried different ways to optimize these processes. First, we used the ionization of $CaCl_2$ salt in water under its solubility limit. $CaCl_2$ in aqueous solutions produces a strong electrolyte by its ionization to Ca^{2+} and Cl^- ions. We knew that MSPs are negatively charged in neutral pH values, and they can adsorb Ca^{2+} ions when they repel Cl^- ions. The uptake experiments were completed by dispersing silica samples in 0.0125 M $CaCl_2$ aqueous solutions. After waiting overnight, the change in the solution concentration was measured by conductivity experiments to understand the uptake ratio. However, we needed a calibration curve to calculate the adsorbed concentration of $CaCl_2$ by silica samples. Figure 5.5. represents the conductivity against the concentration of $CaCl_2$ in an aqueous solution. The

conductivity of the solution was measured after each 100 µL addition of 0.0125 M $CaCl_2$ to 50 µL DI water.

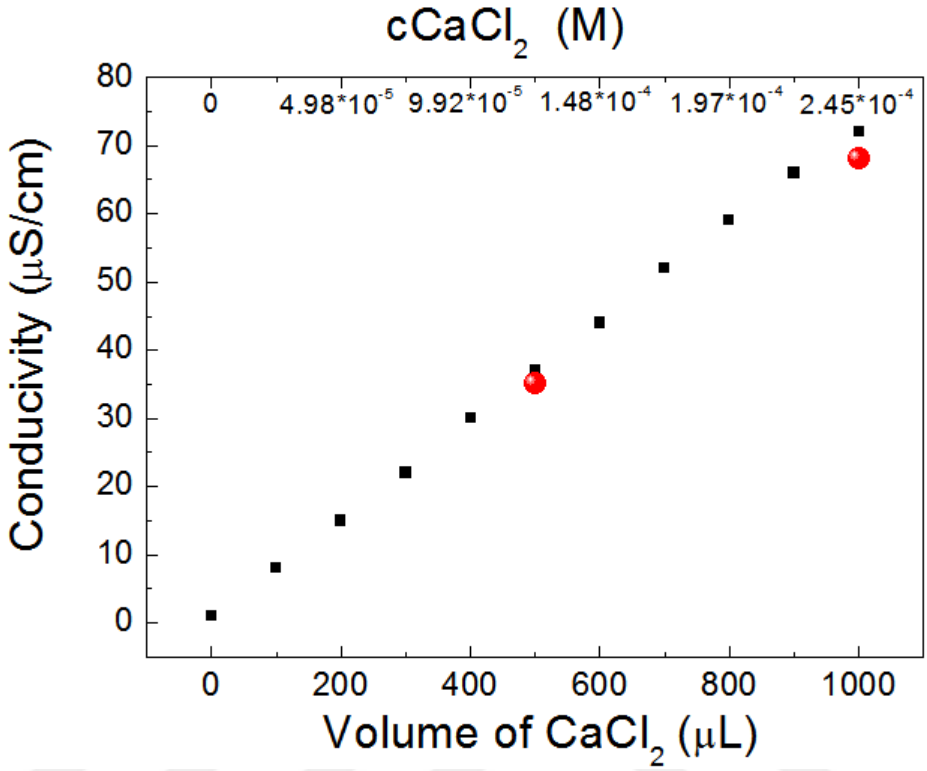

Figure 5.5 Change in the conductivity of CaCl2 solution as a function of concentration in deionized water. The volume was added to 50 mL deionized water and the conductivity of the solution was determined. Red points represent the conductivity values after dispersing silica particles in solutions for 2h and 24h

After having the linear fit of conductivity values by increasing the amount of $CaCl_2$ in the solution mixture, detecting any possible ion uptake by silica particles was made by dispersion of 0.05 g of silica samples in 2 mL solution. The solution mixture with silica particles was sonicated for 15 mins and left for 2 h, 24 h, or 48 h. Then, the top solution was taken and mixed with DI water to see the uptake of ions. Red points in the plot showed that a few amounts of Ca^{2+} ions that can be negligible were adsorbed by silica samples after 2 h and 24 h, respectively. It was concluded that this way is not sufficient to adsorb ions onto the sample surfaces. Therefore, we combined the results from zeta potential measurements and these experiments to have better adsorption of Ca^{2+} ions by MSPs. NH_3 weak base was used to increase the pH of the reaction mixture to have higher electrostatic interaction between silica surfaces and cations. However, it was needed to have a new calibration curve to estimate the adsorption efficiency of the ions by the samples. The same technique above was used to plot the calibration curve of $CaCl_2$

concentration in a 1.0 M NH_3 aqueous solution. Figure 5.6 represents the calibration curve of this mixture.

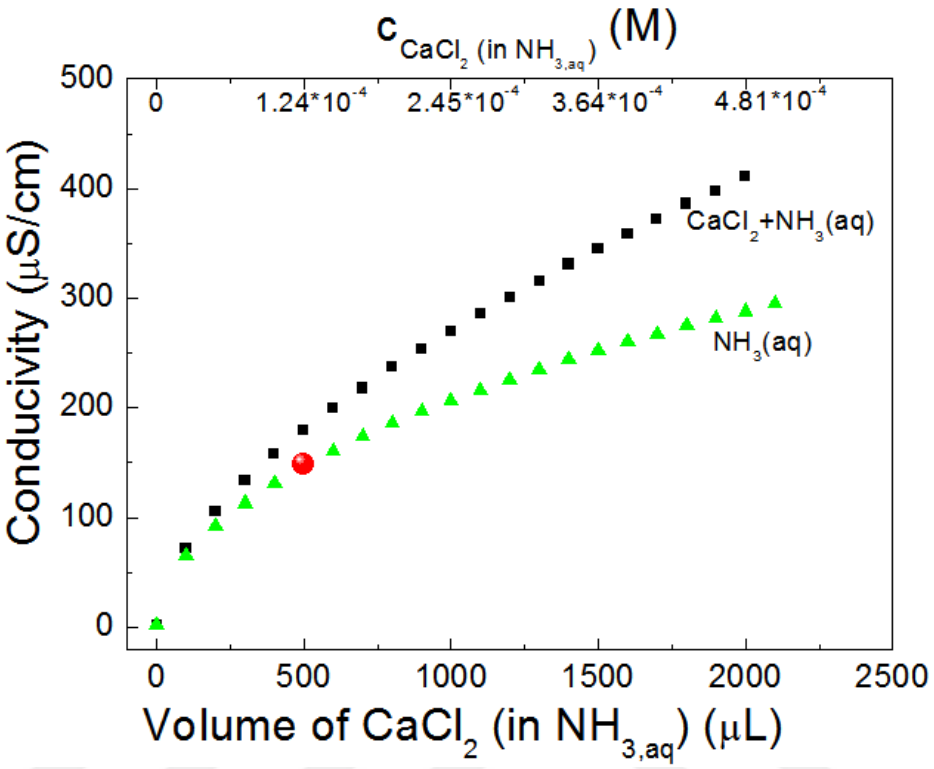

Figure 5.6 Change in the conductivity of $CaCl_2$ solution (0.0125 M) as a function of concentration in 1 M ammonia solution. The green triangles represent the conductivity values of 1 M ammonia solution without $CaCl_2$. The red point represents the conductivity values after dispersing silica particles in solutions

The second calibration curve showed a clear change of the conductivity values in the presence of NH_3. Conductivity values under the same concentration of $CaCl_2$ were higher around 10 times but the linearity of the curve slightly decreased. The conductivity of the weak base could be used as a baseline during the experiments. Keep in mind that adding these low amounts of additive conductive affects the values as a mixture, so the change can be calculated as the summation of ammonia conductivity, as the baseline, and $CaCl_2$ conductivity. That makes measuring the conductivity of the solutions an appropriate tool to estimate the adsorbed quantity of ions. As it can be followed by the red point in Fig. 5.6. the conductivity of the solution decreased to the baseline after dispersing the silica sample (KS16) into the reaction mixture. Since the conductivity measurement is not an ion-selective approach, it was hard to conclude that which ions were adsorbed by silica samples. However, visual observations of $CaCO_3$ formation were used to understand that Ca^{2+} ions were captured by the silica samples. When the $CaCl_2/NH_3$ mixture was reacted with Na_2CO_3 white precipitates of $CaCO_3$ were observed. On the other hand, the top

solution of $CaCl_2/NH_3$ and silica particles mixture did not show any precipitates after reacting with Na_2CO_3.

All types of mesoporous silica particles showed adsorption of Ca^{2+} ions within 2 h of contact time. After that, there was no change in the conductivity for the next 48 h. Figure 5.7 represents the conductivity values of the solutions which were exposed to different silica samples for 2 h. All of the measurements were completed with the same concentrations as 0.0125 M $CaCl_2$ and 1.0 M NH_3. Apparently, all of the particles decreased the conductivity to the baseline with negligible differences.

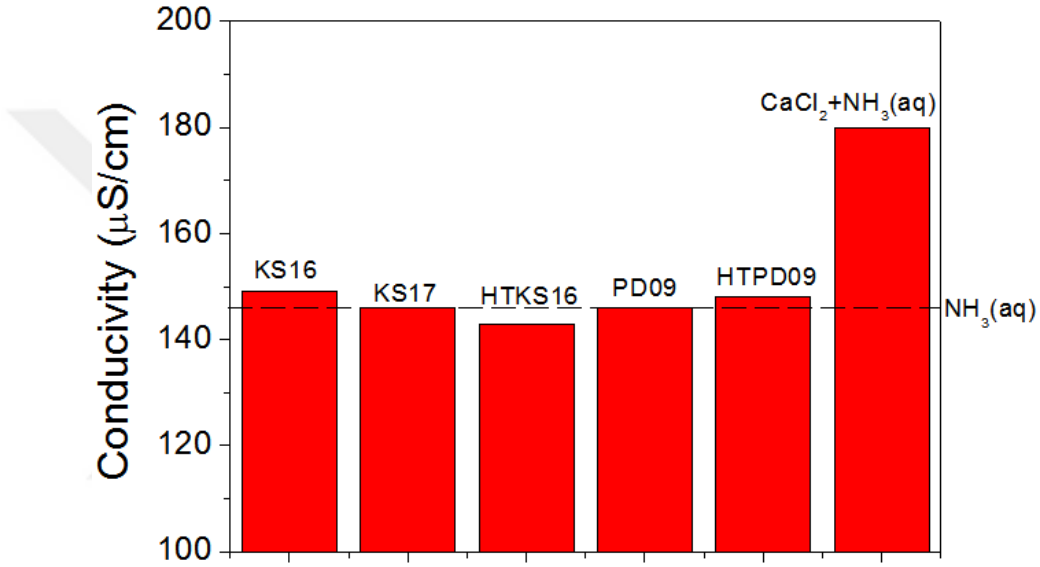

Figure 5.7 Conductivity change of the solutions composed of 1.0 M NH_3 plus 0.0125 M $CaCl_2$ after exposure of silica samples.

Since we observed that MSPs were able to capture all of the Ca^{2+} ions from a solution concentration of 0.0125 M $CaCl_2$, we increased the concentration to 0.07 M in a 1.0 M NH_3 aqueous solution. Additionally, the particle and ammonia concentration during the uptake of Ca^{2+} ions were also optimized in this method.

First of all, the calibration curves of all solutions that have various solution concentrations of $CaCl_2$ and NH_3. The concentration of ammonia varied in a range between 0.005 M and 1.0 M in DI water. Then 0.07 M $CaCl_2$ solutions were systematically added to those solutions to have calibration curves for determining the adsorbed quantity of ions. Figure 5.8 represents these curves by the change in the conductivity of the solutions.

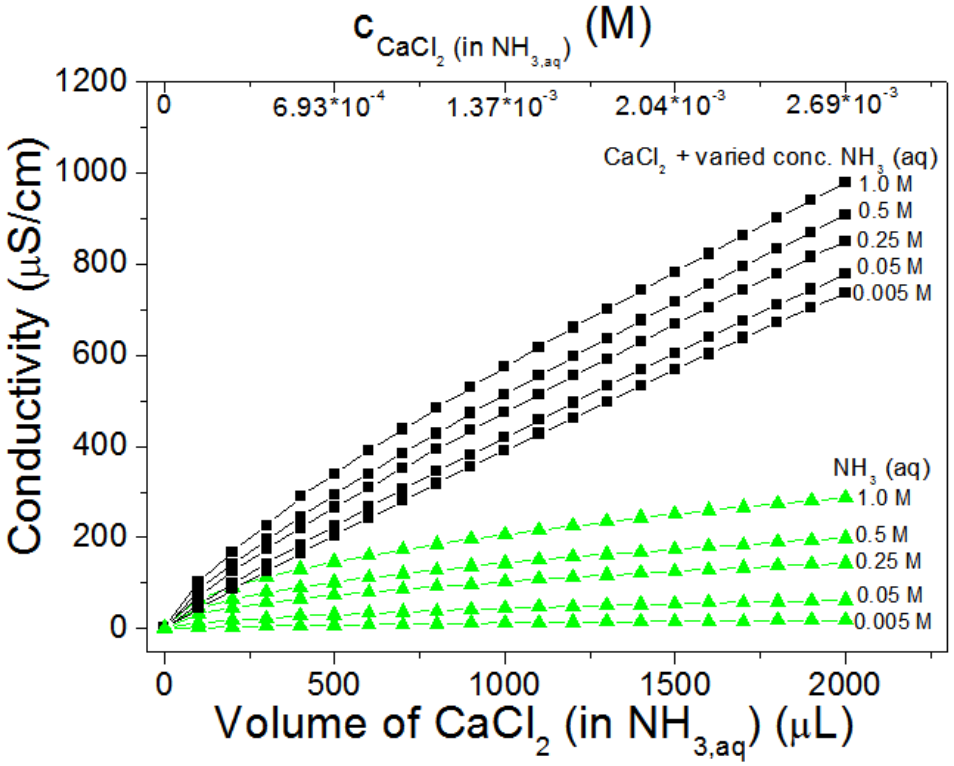

Figure 5.8 Change in the conductivity of $CaCl_2$ solution (0.07 M) as a function of concentration in 0.005 M -1.0 M ammonia solution. The green triangles represent the conductivity values of the ammonia solution without $CaCl_2$. The volume was added to 50 mL deionized water and the conductivity of the solution was determined.

Similar to the previous calibration curve plotted by 0.0125 M $CaCl_2$ and 1.0 M ammonia mixture, a slightly non-linear curve was obtained by those solution mixtures. Moreover, an increase in the conductivity values of the mixtures was obtained with the baseline shift by the increase in the amount of NH_3 concentration. Furthermore, three different concentrations of NH_3 as 0.005 M, 0.25 M, and 1.0 M were selected to see the effect of pH on the adsorption of Ca^{2+} ions by silica samples. The pH values of those solutions were measured as 10.00, 11.05, and 11.35, respectively. As they are represented in Fig. 5.9, the largest uptake was observed when the solution mixture had a 1.0 M NH_3 solution concentration. This can be attributed to the surface charge of silica particles which was increasing by increasing the pH. Larger negativity of the zeta potentials improved the uptake capacity of particles by enhancing the strength of electrostatic interaction. These results were obtained by dispersing 0.03 g of MSPs into 2 mL of solution mixtures for 48 h. The conductivity of the solution mixtures was measured by the same method described above.

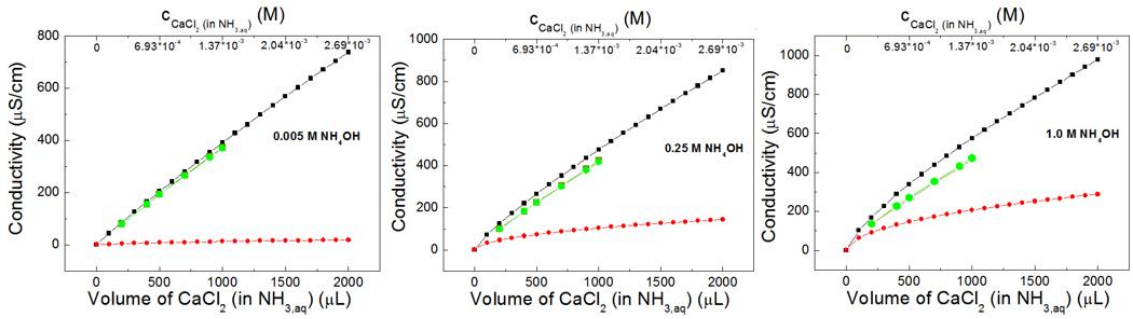

Figure 5.9 Effect of aqueous ammonia concentration on the Ca^{2+} uptake of silica particles. The solution was exposed to silica particles (HTKS16 and KS16) for 48 h and added to 50 mL water to measure the conductivity.

The optimum concentration of ammonia in the solution mixture was found as 1.0 M which resulted in the highest decrease in the conductivity. However, we could not increase the concentration of ammonia due to the instability of MSPs at very high pH and precipitation of calcium as hydroxide. The adsorption capacity of four different types of particles which were summarized in Table 5.1 was also investigated and compared to each other (Figure 5.10). It was found that PD09 and KS16 were the best samples for adsorption of Ca^{2+} ions in a 1.0 M ammonia solution. This can be attributed to their surface charges. Those silica samples had Zeta potential when pH was approximately 12.0 (-46.66 mV and 43.13 mV for PD09 and KS16, respectively).

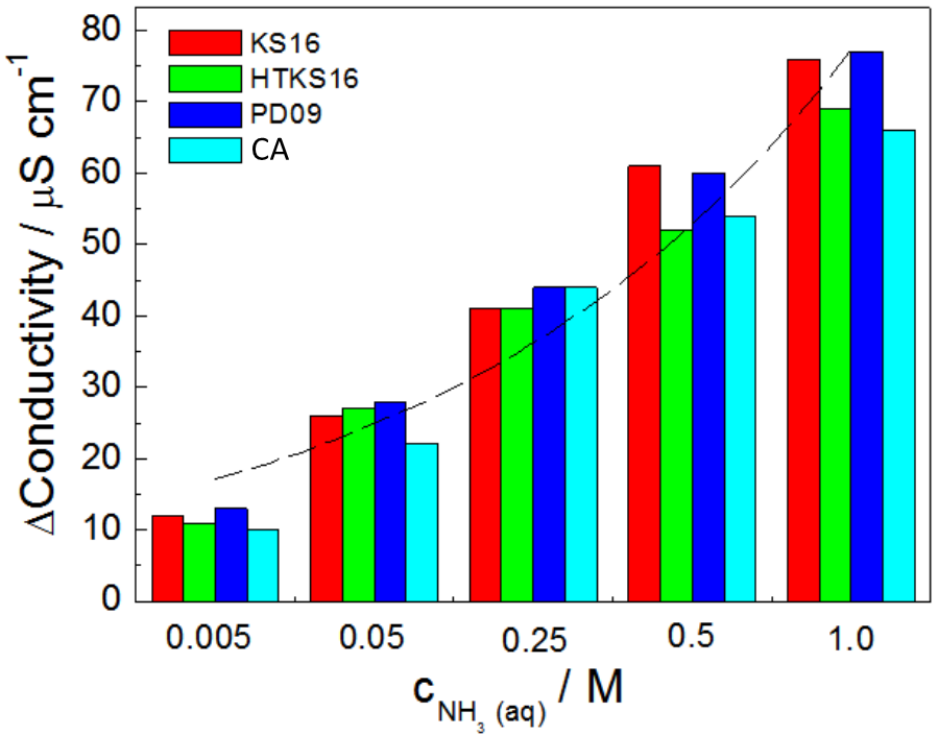

Figure 5.10 Conductivity change of $CaCl_2/NH_3$ aqueous solution due to the exposure of 0.03 g silica particles in 2 mL solution mixture.

After these optimization studies, determination of the optimum exposure time during the ion uptake process was also studied. Conductivity measurements after different exposure times were done with the same method above. After a certain time of the dispersion of the samples, top solutions were mixed with DI water and analyzed. Figure 5.11 represents the change in conductivity by increasing the contact time. It was found that the MSPs can have their maximum adsorption of Ca^{2+} ions within 2 h of exposure time. Therefore 2 h contact time was used for the further experiments.

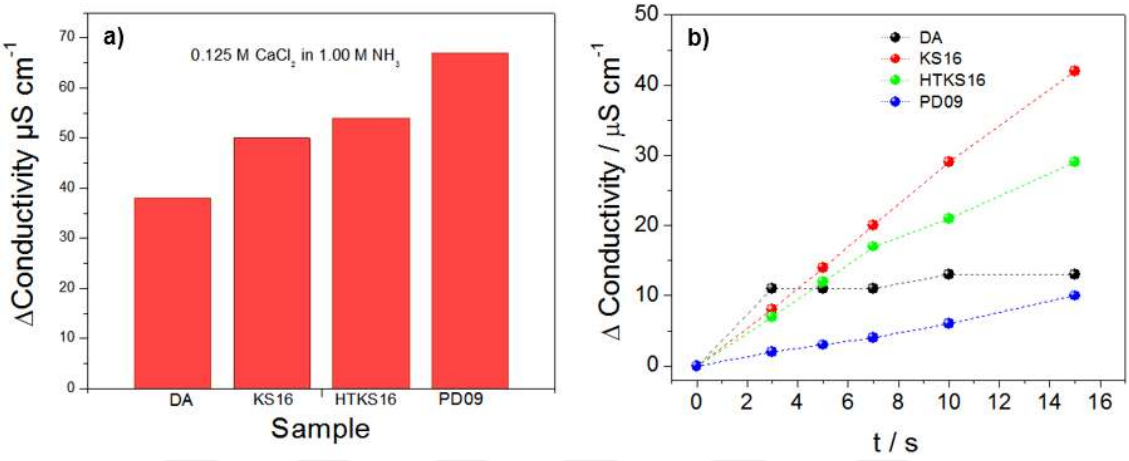

Figure 5.11 a) Uptake capacity of silica samples in 0.125 M $CaCl_2$ solution in 1.0 M ammonia and b) the release of the Ca^{2+} ions into deionized water as a function of time.

5.3.4 Synthesis Of $CaCO_3$/MSPs

The second challenge to have self-propelled mesoporous silica micromotors was forming the $CaCO_3$ on MSPs with in situ synthesis method. First of all, we tried to synthesize those particles with a method reported by Bahrom et al. in 2019 [200]. According to that method, the morphology of $CaCO_3$ particles can be controlled by the room temperature reaction between 0.3 M $CaCl_2$ and 0.3 M Na_2CO_3. After we synthesized spherical (10-20 nm diameter) $CaCO_3$ particles by this method, we investigated how those particles can form in confined space on porous silica particles. We started loading the samples with $CaCO_3$ from the beginning as capturing Ca^{2+} ions from 0.3 M $CaCl_2$/1.0 M NH_3 solution mixture. 0.03 g of silica particles dispersed in 2 mL solution mixture for 24 h. Then, the particles were centrifuged to remove the top solution and 2 mL of 0.3 Na_2CO_3 was exposed to those particles to load silica particles with $CaCO_3$. The mixtures were stirred at 650 rpm for 15 min then stayed at room temperature for 30 mins. The centrifuged particles were rinsed to remove the excess amount of NaCl which was the byproduct of the synthesis and Na_2CO_3 which was used in high excess. The resulted particles were

monitored by SEM images in Fig 5.12. The yellow marks on the images indicate the $CaCO_3$ formation. It was observed from the SEM images that some of the particles were formed shell-like structures on top of the surfaces of silica particles. The centrifuging and shaking with vortex steps of rinsing processes caused the release of the shell from particles. Those results were not obtained by CA silica samples. They were more spherical and closed-shaped $CaCO_3$ obtained. That can be attributed to the porous structure of those samples. Because of larger pores, these particles released calcium chloride back to the water faster than the others. These releasing profiles of those particles caused a problem as loading less amount of Ca^{2+} ions there for lower loading of calcium carbonate was observed. Rather than extra loading of $CaCO_3$ on top of the particle surfaces, it was limited by the pores of the particles.

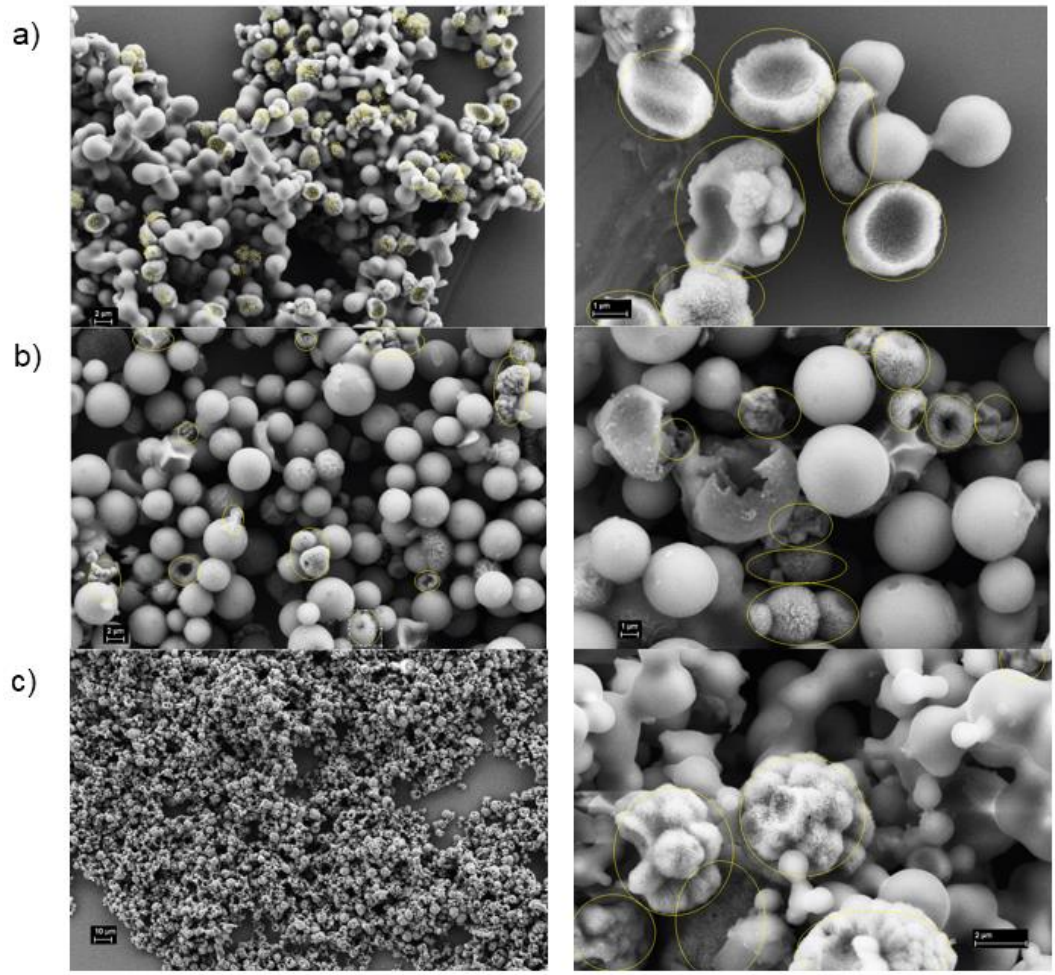

Figure 5.12 $CaCO_3$ loaded sample loaded at 0.3 M $CaCl_2$ solution (in 1 M NH_3 aqueous) - 0.3 M Na_2CO_3 solutions, a) corresponds to sample PD09, b) CA, and c) KS16.

The EDX results represented in Figure 5.13 also proved the formation of $CaCO_3$ on MSPs by giving strong peaks of Ca, C, and O signals. Interestingly, Cl signals were also

obtained by those particles in EDX analysis even after washing the particles 5 times with DI water. That can be concluded as that calcium carbonate shell prevented the release of excess amount of $CaCl_2$ during the rinsing of particles. Additionally, it also means that mesoporous silica particles adsorbed not only Ca^{2+} ions but also Cl^- ions from the solution mixture. These results are in line with the observations from conductivity measurements during the formation of Ca^{2+}/MSPs. The decrease of the conductivity to the conductivity values of baseline (NH_3 solution) can be explained by those results.

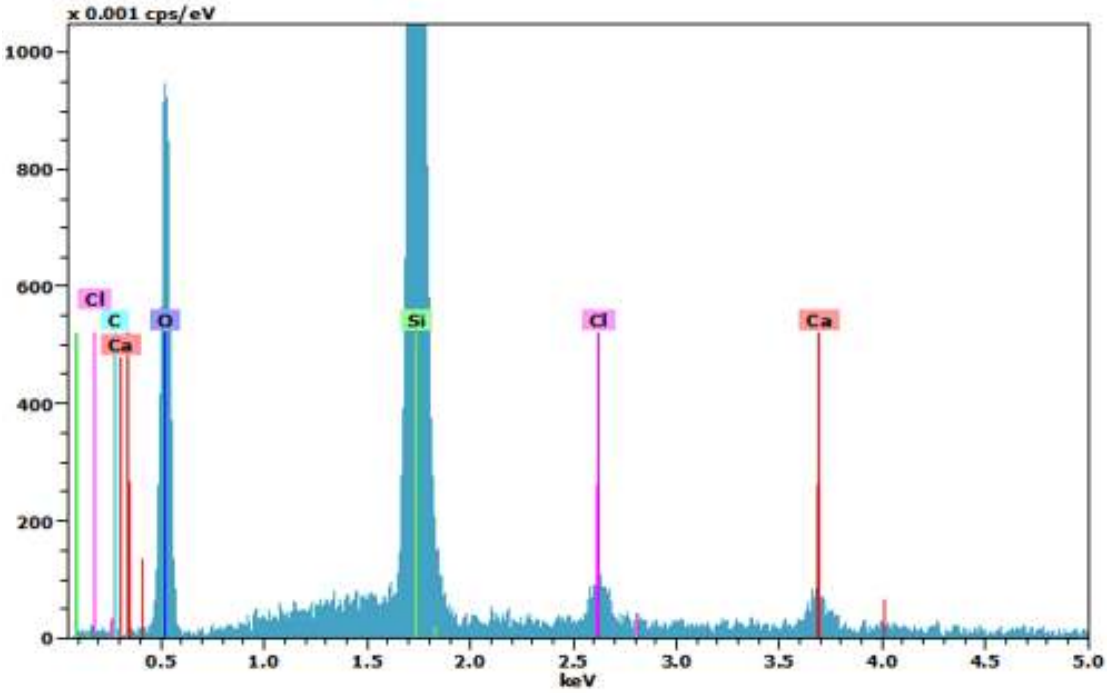

Figure 5.13 EDX analysis of $CaCO_3$ loaded PD09 sample. The loading concentrations were 0.3 M $CaCl_2$ (in 1 M ammonia aqueous solution) and 0.3 M Na_2CO_3.

The optimization studied to synthesize $CaCO_3$ loaded silica particles showed that the optimum conditions were 0.125 M $CaCl_2$ solution concentration in 0.25 M of NH_3 aqueous solution and 0.3 M Na_2CO_3 solution concentration. Higher concentrations of $CaCl_2$ and ammonia showed change in the morphology of the silica particles due to high amount $CaCO_3$ formation. Within the higher concentrations of $CaCl_2$ whether we had excess $CaCO_3$ particles that were impossible to remove or additional rinsing process which caused lower loading. The concentrations were used as described above to have highly reproducible $CaCO_3$ loading on MSPs.

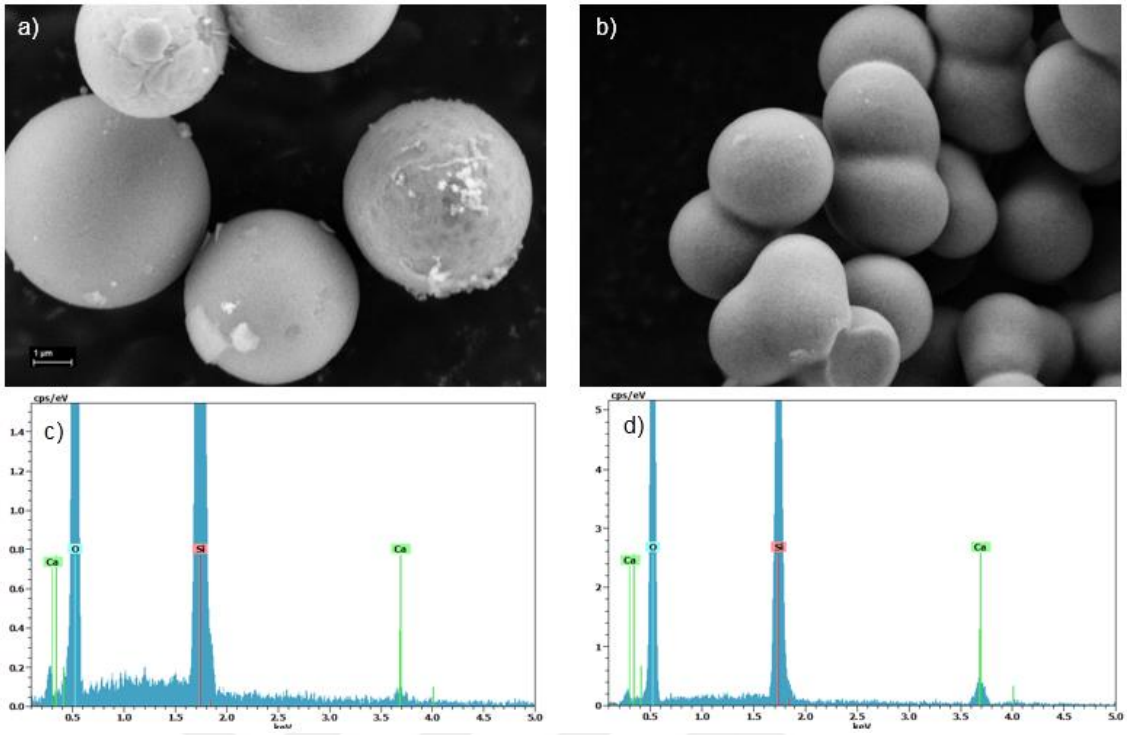

Figure 5.14 Sample a) CA and sample b) PD09 loaded in 0.125 M $CaCl_2$ - 0.25 M NH_3 solution which was reacted with 0.30 M Na_2CO_3 solution. The samples were rinsed 5 times with deionized water. The corresponding EDX results are shown for c) CA and d) PD09.

5.3.5 Investigation of CaCO3 loaded/MS micromotors motion

The self-propelled motion of $CaCO_3$ loaded MSPs was observed in acetic acid solution by a camera-attached optical microscope. As was expected, bare silica samples did not show any movement when loaded samples were moving randomly in the acidic solution. The reason for the particles was obviously the CO_2 bubbles that were formed from calcium carbonate. However, the motion was observed as random movements by loaded silica particles. $CaCO_3$ has 3 phases among Vaterite is the one able to achieve considerable motion during the decomposition in acidic medium. However, Calcite is more stable in aqueous medium readily forms from Vaterite giving limited lifetime of the micromotors. One way is to dry the samples and keep them in humidity free environment. Three different solvents have been employed to increase the drying time of the stabile $CaCO_3$ phase able to locomote silica particles. For drying the micromotors $CaCO_3$ loaded particles were dispersed in ethanol, methanol, or toluene to have faster evaporation of the solvent before losing the stability of loaded $CaCO_3$ structures. However, in these solution micromotors were unable to dry enough fast (within 6 h) and lost their ability to move. DMSO has been reported [200] to increase the time required for the phase transition of

the Vaterite phase. We were able to successfully stabilize micromotors up to 24 h with using DMSO as 1 to 12 ratios in water.

We compared the $CaCO_3$ loaded silica particles movement in acidic medium. The samples are listed in Table 5.1. were loaded by $CaCO_3$ under optimum conditions. The particles were dispersed in 0.125 M $CaCl_2$ solution concentration in 0.25 M NH_3 aqueous solution for 2h. Then centrifuged particles were dispersed in 0.3 M Na_2CO_3 solution for 10 min and stirred continuously at 600 rpm. Lastly, the particles were rinsed 5 times with DI water.

First, we tried to obtain locomotion in an acidic solution which was pH = 2.88. However, it was very hard to visualize particles' motion because bubble propulsion was completed within a minute. Then we increased the pH of the solution to 4 to have a slower formation of bubbles and monitored the motion. Since we prepared the acidic solution (pH = 4) with acetic acid (CH_3COOH) the mechanism of the motion was changed to self-diffusiophoresis because of the concentration gradient created by the decomposition of $CaCO_3$ [201]. It was possible to observe a small amount of bubble formation, but the main mechanism was attributed to self-diffusiophoresis. The locomotion of $CaCO_3$ loaded silica samples was represented in Figure 5.15. Movements of all particles were Brownian motion and bubble formations were observed all-around of the samples which was the proof of $CaCO_3$ loaded symmetric silica spheres. On the other hand, no motion and no bubble formation were obtained by bare silica particles.

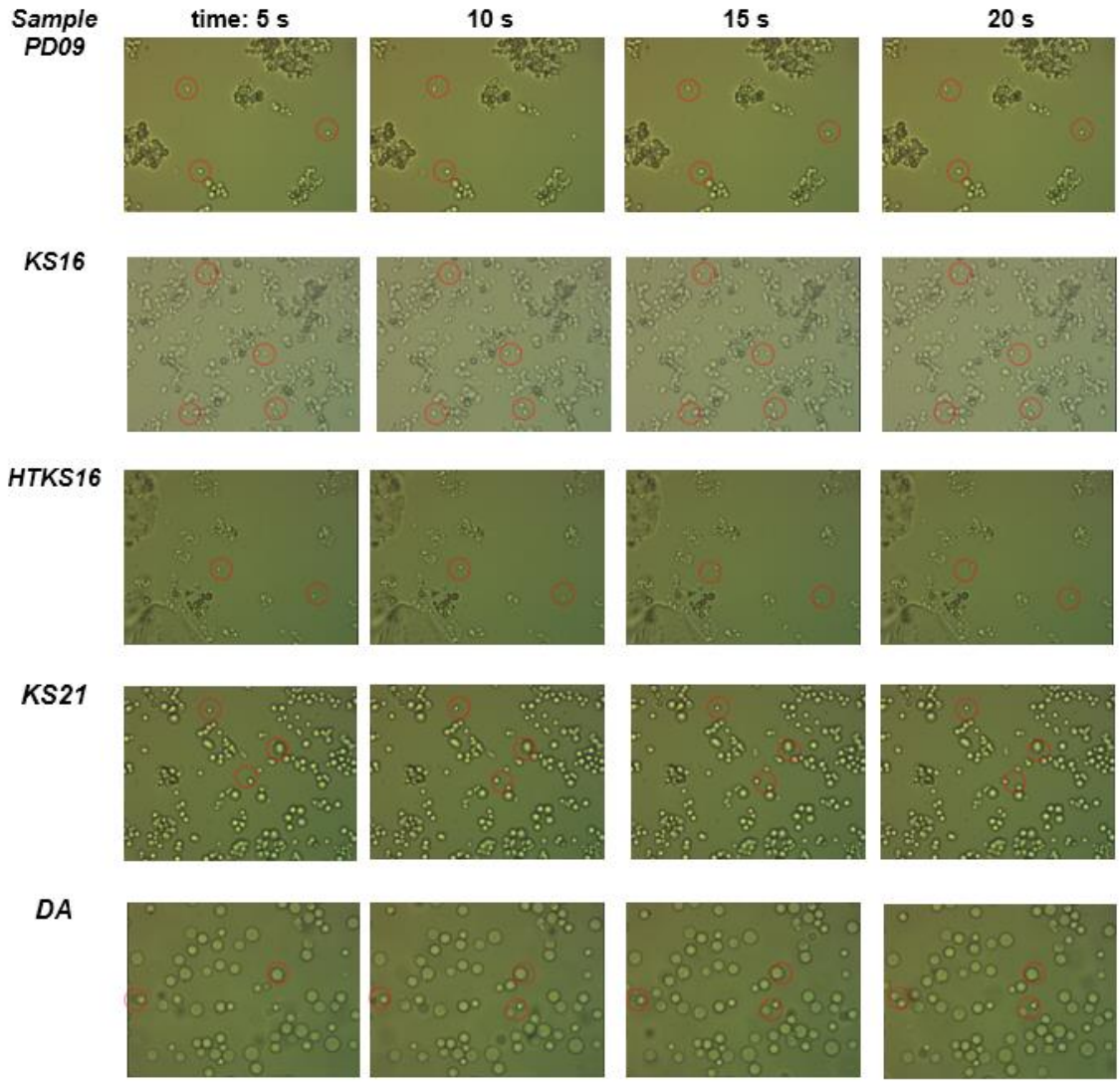

Figure 5.15 Locomotion of $CaCO_3$ loaded silica particles in pH=4 acetic acid solution.

When we compared the velocity of silica samples, it was observed that the fastest sample was KS16. The porous structure of KS16 was the mixture of micropores and its surface area was the highest (789 m^2/g) in this group of samples. In addition, KS16 had the smallest diameter in size of the particles. On the other hand, when we compare the velocity of larger particles (above 4 micrometer diameter), we observed that KS21 samples which contain mainly micropores were moving faster than CA mesoporous particles. The results showed that pore size plays a significant role in the velocity of self-propelled micromotors. Also, the surface area is critical because of enhancing the loading amount of the fuel.

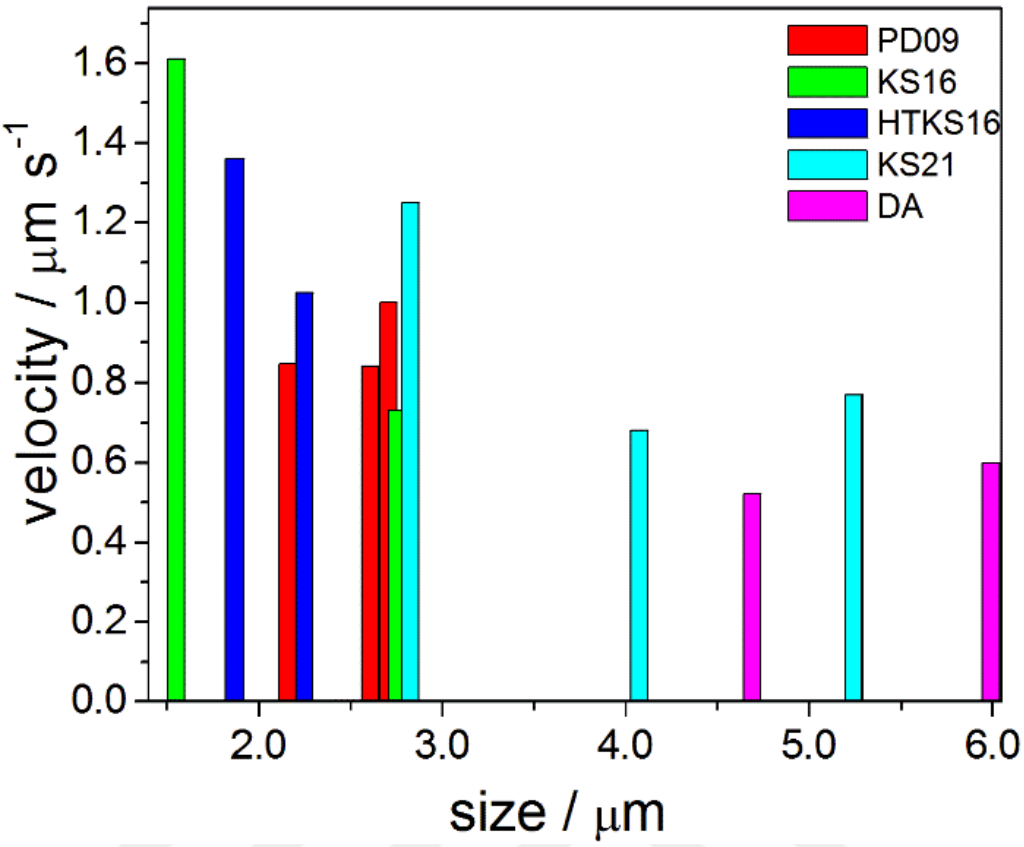

Figure 5.16 Particle movement velocity in pH=4 acetic acid solution. The silica particles were loaded with $CaCO_3$ under the optimized condition.

5.4 Conclusion

This part of the study aimed to design and synthesize self-propelled mesoporous silica micromotors. As a micromotor, the system is designed to be made of porous silica particles synthesized with a novel preparation route described in the previous chapters. It was estimated that the high surface area of the particles synthesized with the TEOS/Pluronic F127/HCl method would be critical to carry $CaCO_3$ which was supposed to be the fuel of micromotors. The self-propelling micromotors were produced, and successful random motions were observed after loading silica particles with $CaCO_3$ fuel by in situ synthesis reactions. Mesoporous silica samples with different particle properties such as surface area, pore size, pore ordering, and particle sizes were compared in terms of ability to adsorb Ca^{2+} ions, carry $CaCO_3$ particles and locomote in aqueous solutions. Optimization processes for producing $CaCO_3$ loaded silica particles were determined by systematic experiments. The optimum conditions were found as dispersing 0.03 g MSPS in 2 mL solution composed of 0.125 M $CaCl_2$ in 0.25 M NH_3 aqueous solutions, then dispersing them into 0.3 M Na_2CO_3 aqueous solutions at room temperature for in situ

formation of $CaCO_3$. Ammonia was selected as the weak base to enhance the electrostatic interaction between silica surfaces and cations. Because it was understood from Zeta potential measurements that the surface of MSPs was larger negative in basic solutions (pH=10=12). In addition, 2 h for Ca^{2+} and 15 min for $CaCO_3$ formation were decided as optimum times. The motion of particles loaded under these conditions showed random motion in acidic solution (pH=4) and KS16 (largest SSA, smallest particle size) was decided as the fastest particle. The mechanism of those particles was the combination of bubble propulsion and self-diffusiophoresis but the dominant one was the self-diffusiophoresis. The Brownian motion and characterization results (SEM, EDX, and Zeta potential measurements) proved that the loading silica particles with $CaCO_3$ by our technique was successfully completed.

Observations on the locomotion of those particles indicated that the particle properties were significantly effective on the self-propelled motion. Analyzing the movement of the samples and their speed showed that the highest velocity was 1.6 μm/s when the particle size was ~1.5 micrometer and surface area was 789 m^2/g (KS16). On the other hand, when the particle sizes were larger (above 4 μm) the silica spheres synthesized with the acid-catalyzed method were faster than commercially available traditional particles (CA). Those results indicated that the pore size is effective as well as high surface area on the locomotion ability of the particles. When the pore sizes were in the microporosity range (below 4 nm) the movement was faster than mesoporous (above 4nm) particles.

The locomotion ability of silica-based micromotors using $CaCO_3$ as fuel is promising for micromotor applications. Especially for in-body applications, these particles can serve as a good opportunity because any part of them is not toxic. These particles can be used in targeted drug delivery or monitoring biological presents. Further investigations will be continued to have directed motion of the particles by two faces Janus Particles.

Chapter 6:
CONCLUSION

The demand for advanced materials that have unique properties and enhanced performances has been increased with emerging applications like drug delivery, environmental pollution control, sensor, catalyst. Mesoporous silica particles which have properties such as good stability, high surface area and tunable morphology are promising candidates to satisfy these emerging requirements. The important challenge is finding optimum combinations of utilization processes of the particles to meet the needs of each application. On the other hand, synthesizing silica particles with ease and control over the particle properties in micron level is another difficulty. Mesoporous silica based advanced particles can be used in various applications ranging from environmental pollution control to in vitro applications, or electronics to catalytic applications. However, most of the time the cost of producing those particles does not worth to use them in such applications especially in pollution control. On the other hand, MSPs can improve the capacity of applications to have sustainable environment with their higher specific surface area, chemical stability, biocompatibility, easy surface functionalization and easy-to-tune morphologies. In this thesis work, several applications of mesoporous silica particles have been investigated and designed to be novel, efficient, cost-friendly and simple. Porous silica samples used as adsorbent, utilized as photocatalyst or Janus particles by loading them with metals or $CaCO_3$, respectively.

Mesoporous silica assemblies having different properties such as morphology, size, pore structure was produced by surfactant-templated sol-gel method. Pluronic F127 triblock copolymer was used as surfactant and mixed with tetra ethyl orthosilicate (TEOS), silica precursor, in highly acidic solutions at room temperature. The effect of reactants' concentrations on the particle properties were investigated particularly. Also combined effects of concentrations were also studied to discover the ternary phase diagram of the synthesis method, depending on the morphology. It was found that spherical, monolith and polyhedron shaped morphologies were the possible with TEOS/Pluronic F127/HCl system. Additionally, MSPs having high specific surface area of 400-800 m^2/g can be successfully synthesized at room temperature with the synthesis system without applying any additional process. The particle properties, especially the morphology can be tuned by adjusting the initial concentration of the reactant. The changes were successfully

controlled by concentration, ratios of the reactants and pH of the reaction mixture. Smaller size spherical particles were obtained by increasing the amount of silica precursor. Moreover, it was observed that after a certain level of TEOS concentrations, spherical secondary particles tend to form monolith by agglomeration. These formations enlarged the pore sizes and hysteresis between curves of N_2 adsorption/desorption results. On the other hand, higher specific surface areas were achieved without disturbing the shape of particles by applying hydrothermal treatment processes. More uniform and oriented pores and specific surface areas around 1000 m^2/g were successfully produced by hydrothermally treated samples.

In addition, controlling particle properties was also shown by changing the type of acid used as catalyst. Instead of HCl acid, HNO_3 and H_2SO_4 were used with same concentrations to see the effect of acid catalyst type. Although the shape of particles was not affected from the change, pore structure and particle sizes were influenced significantly. Similar to the previous results, spherical particles were obtained under very high concentrations of all acids. The particle sizes remained similar with HCl and HNO_3, but the diameter of H_2SO_4 particles were significantly smaller than others. Same results were obtained also for the pore sizes. H_2SO_4 catalyzed synthesis resulted in mesoporous structures, while the other acid catalyzed synthesis particles showed the mixture of micro and mesopores. Consequently, these particle properties affected the adsorption behavior of particles for removal of Rhodamine 6G dye from water. The adsorption capacity results of the samples under different conditions like pH, temperature and initial concentrations of particles and dye showed that H_2SO_4 catalyzed synthesis produced the best adsorbent. The uptake capacity of the samples in 10 minutes was 9.25 mg/g, 7.07 mg/g, and 4.28 mg/g for Si/H_2SO_4, Si/HCl, and Si/HNO_3, respectively. In addition, Si/H_2SO_4 particles showed the maximum adsorption capacity of 19.56 mg/g which is promising for wastewater treatment applications. Adsorption isotherms were modeled by linearized Langmuir and Freundlich isotherms. Results showed that the adsorption processes by Si/HCl and Si/HNO_3 were fitting to the Freundlich isotherm, and it fitted better to the Langmuir isotherm for Si/H_2SO_4 adsorbent. It means that adsorption by a larger pore sized adsorbent is monolayer formation of dye molecules on the surfaces. In addition, more negative values of Gibb's free energy was observed with Si/H_2SO_4 adsorbent by applying thermodynamical calculations according to Langmuir model. Gibbs Free Energy

value of the adsorption of the dye with Si/H_2SO_4 was -6.11 kJ mol^{-1} compared to 0.90 kJ mol^{-1} and -1.57 kJ mol^{-1} for Si/HCl and Si/HNO3 respectively. The adsorption capacities at a certain time (1 h) were better estimated by the pseudo-second-order kinetic model for all of the samples, in line with the results in literature data. Similar reaction rates from the particles were calculated but the higher saturation level obtained from Si/H_2SO_4 particles. The results of adsorption studies showed that Si/H_2SO_4 particles are promising for wastewater treatment of the textile industry. The adsorption behavior of the sample was significantly high without any coating and/or complex process. It was also realized that uptake performances of MSPs synthesized with our method are highly promising to be used in other applications such as drug delivery and host material for catalytic purposes.

For the catalytic activity, a comparative study was done on silica-based metal loaded catalyst composites. A simple method was used to utilize silica particles as host materials by metal loading on the structure for catalytic degradation of Methylene Blue (MB) textile dye. $FeCl_2$ and $CuCl_2$ salts were included to the synthesis process of mesoporous silica particles. Different concentrations of metal salts were dissolved in Pluronic/HCl aqueous solution before adding TEOS. The structural and chemical analysis of those particles proved the presence of metals in the structure of MSPs. The SEM images showed that loading metal ions onto silica structures does not have influence on the morphology of the particles. On the other hand, composite particles showed very high efficiency of MB degradation in the presence of H_2O_2. Hydroxyl radicals were successfully formed with Fenton and Fenton-like reactions by iron and copper loaded silica particles, respectively. Iron loaded particles showed better catalytic activity under dark and UV light exposed conditions. Faster and more efficient degradation of MB by Fe^{2+} loaded silica particles can be attributed to the oxidation state of iron ions. Fe^{2+} ions show catalytic activity by Fenton reaction, while Cu^{2+} ions show it by Fenton-like reaction. It is well-known that Fenton-like reactions are the slower reactions. Our comparative study also supported this idea. The degradation of MB was completed in approximately 20 mins by Fe^{2+} loaded MSPs, but Cu^{2+} loaded particles completed it over 60 mins. The photocatalytic activity of synthesized composites was also compared by exposing them to UV light. UV light improved the capacity of particles to remove dye from water due to the additional hydroxyl radicals formed by photo Fenton (PH-Fenton) and photo Fenton-like (PH-Fenton-like) reactions. Additionally, supportive effect of silica as host material by 20 %

degradation of MB was observed in this study. The results showed that Fe^{2+} loaded silica samples are better in catalytic degradation of MB. The comparison of the results showed that the efficiency of the reactions is ordered as PH-Fenton > PH-Fenton-like > Fenton > Fenton-like. These particles can be used in the future to improve the efficiency in environmental health protection from hazardous pollutions.

In the last part of this thesis work, self-propelled mesoporous silica particles using $CaCO_3$ as fuel for bubble propulsion were successfully synthesized, and locomotion of the particles were obtained. Optimum parameters such as concentrations, time and pH were determined for $CaCO_3$ loading onto MSPs by in situ reaction were determined. The amount of $CaCO_3$ particles in mesoporous silica structures was enhanced by including NH_3 in the reaction mixture. This enhancement in silica and calcium carbonate incorporation was attributed to larger negative zeta potential values (~50 mV) of the particles in basic solutions. Because the electrostatic interaction between cations and silica surfaces was the main driving force of attaching Ca^{2+} ions on particles. Then, CO_3 was attached by dispersing Ca^{2+} attached MSPs in aqueous solution of $NaCO_3$. The formation of $CaCO_3$ on MSPs were proven by EDX analysis. The locomotion of loaded particles in acidic solution were successfully monitored with camera attached optical microscope. In addition, the velocities of prepared samples were compared according to the particle properties such as pore size, surface area and particle size. It was observed that the velocity of the particles depended on the pore size as well as surface area and particle diameter. Microporous particles were able to move faster than mesoporous particles when their particle diameters were similar as 4-5 μm. The biocompatibility of these particles can give opportunity to be used in vivo applications such as targeted drug delivery.

BIBLIOGRAPHY

[1] S. H. Joo, J. Y. Park, C.-K. Tsung, Y. Yamada, P. Yang, and G. A. Somorjai, "Thermally stable Pt/mesoporous silica core--shell nanocatalysts for high-temperature reactions," *Nat. Mater.*, vol. 8, pp. 126–131, 2008, doi: 10.1038/NMAT2329.

[2] B. M. Al-Shehri, A. E. R. S. Khder, S. S. Ashour, and M. S. Hamdy, "A review: The utilization of mesoporous materials in wastewater treatment," *Mater. Res. Express*, vol. 6, no. 12, p. 122002, 2019, doi: 10.1088/2053-1591/ab52af.

[3] K. W. Gallis, A. G. Eklund, S. T. Jull, J. T. Araujo, J. G. Moore, and C. C. Landry, "The use of mesoporous silica in liquid chromatography," *Stud. Surf. Sci. Catal.*, vol. 129, no. 17, pp. 747–755, 2000, doi: 10.1016/s0167-2991(00)80279-7.

[4] B. H. Han, I. Manners, and M. A. Winnik, "Oxygen sensors based on mesoporous silica particles on layer-by-layer self-assembled films," *Chem. Mater.*, vol. 17, no. 12, pp. 3160–3171, 2005, doi: 10.1021/cm047770k.

[5] S. Kumar, M. M. Malik, and R. Purohit, "Synthesis Methods of Mesoporous Silica Materials," *Mater. Today Proc.*, vol. 4, no. 2, pp. 350–357, 2017, doi: 10.1016/j.matpr.2017.01.032.

[6] C. T. Kresge, M. E. Leonowicz, W. J. Roth, J. C. Vartuli, and J. S. Beck, "Ordered mesoporous molecular sieves synthesized by a liquid-crystal template mechanism," *Nature*, vol. 359, no. 6397, pp. 710–712, 1992, doi: 10.1038/359710a0.

[7] A. Ijaz, M. B. Yagci, C. W. Ow-Yang, A. L. Demirel, and A. Mikó, "Formation of mesoporous silica particles with hierarchical morphology," *Microporous Mesoporous Mater.*, vol. 303, p. 110240, Aug. 2020, doi: 10.1016/j.micromeso.2020.110240.

[8] A. Farrukh *et al.*, "Surface-functionalized silica gel adsorbents for efficient remediation of cationic dyes," *Pure Appl. Chem.*, vol. 86, no. 7, pp. 177–1188,

2014, doi: 10.1515/pac-2014-0105.

[9] A. Al-Kdasi, A. Idris, K. Saed, and C. T. Guan, "Treatment of textile wastewater by advanced oxidation processes– A review," *Glob. Nest J.*, vol. 6, no. 1, pp. 222–230, 2004.

[10] T. Robinson, G. McMullan, R. Marchant, and P. Nigam, "Remediation of dyes in textile effluent: a critical review on current treatment technologies with a proposed alternative.," *Bioresour. Technol.*, vol. 77, no. 3, pp. 247–255, May 2001, doi: 10.1016/s0960-8524(00)00080-8.

[11] E. Forgacs, T. Cserháti, and G. Oros, "Removal of synthetic dyes from wastewaters: A review," *Environ. Int.*, vol. 30, no. 7, pp. 953–971, 2004, doi: 10.1016/j.envint.2004.02.001.

[12] A. K. Verma, R. R. Dash, and P. Bhunia, "A review on chemical coagulation/flocculation technologies for removal of colour from textile wastewaters," *J. Environ. Manage.*, vol. 93, no. 1, pp. 154–168, 2012, doi: 10.1016/j.jenvman.2011.09.012.

[13] C. A. Martínez-Huitle and E. Brillas, "Decontamination of wastewaters containing synthetic organic dyes by electrochemical methods: A general review," *Appl. Catal. B Environ.*, vol. 87, no. 3–4, pp. 105–145, 2009, doi: 10.1016/j.apcatb.2008.09.017.

[14] V. K. Gupta and Suhas, "Application of low-cost adsorbents for dye removal - A review," *J. Environ. Manage.*, vol. 90, no. 8, pp. 2313–2342, 2009, doi: 10.1016/j.jenvman.2008.11.017.

[15] Y. Anjaneyulu, N. Sreedhara Chary, and D. Samuel Suman Raj, "Decolourization of industrial effluents - Available methods and emerging technologies - A review," *Rev. Environ. Sci. Biotechnol.*, vol. 4, no. 4, pp. 245–273, 2005, doi: 10.1007/s11157-005-1246-z.

[16] M. T. Yagub, T. K. Sen, S. Afroze, and H. M. Ang, "Dye and its removal from aqueous solution by adsorption: A review," *Adv. Colloid Interface Sci.*, vol. 209,

pp. 172–184, 2014, doi: 10.1016/j.cis.2014.04.002.

[17] C. Z. Liang, S. P. Sun, F. Y. Li, Y. K. Ong, and T. S. Chung, "Treatment of highly concentrated wastewater containing multiple synthetic dyes by a combined process of coagulation/flocculation and nanofiltration," *J. Memb. Sci.*, vol. 469, pp. 306–315, Nov. 2014, doi: 10.1016/j.memsci.2014.06.057.

[18] S. L. E. W. Jiangning, A. E. Mark, "Evaluation of Membrane Filtration and Ozonation," *J. Environ. Eng. ASCE*, no. March, pp. 272–277, 1996.

[19] Q. H. Hu, S. Z. Qiao, F. Haghseresht, M. A. Wilson, and G. Q. Lu, "Adsorption study for removal of basic red dye using bentonite," *Ind. Eng. Chem. Res.*, vol. 45, no. 2, pp. 733–738, 2006, doi: 10.1021/ie050889y.

[20] T. L. Silva *et al.*, "Mesoporous activated carbon from industrial laundry sewage sludge: Adsorption studies of reactive dye Remazol Brilliant Blue R," *Chem. Eng. J.*, vol. 303, pp. 467–476, 2016, doi: 10.1016/j.cej.2016.06.009.

[21] E. Lorenc-Grabowska and G. Gryglewicz, "Adsorption characteristics of Congo Red on coal-based mesoporous activated carbon," *Dye. Pigment.*, vol. 74, no. 1, pp. 34–40, 2007, doi: 10.1016/j.dyepig.2006.01.027.

[22] S. Nayab *et al.*, "Silica based inorganic-organic hybrid materials for the adsorptive removal of chromium," *RSC Adv.*, vol. 8, no. 42, pp. 23963–23972, 2018, doi: 10.1039/c8ra04209h.

[23] K. Rajeshwar *et al.*, "Heterogeneous photocatalytic treatment of organic dyes in air and aqueous media," *J. Photochem. Photobiol. C Photochem. Rev.*, vol. 9, no. 4, pp. 171–192, 2008, doi: 10.1016/j.jphotochemrev.2008.09.001.

[24] A. Demirbas, "Agricultural based activated carbons for the removal of dyes from aqueous solutions: A review," *J. Hazard. Mater.*, vol. 167, no. 1–3, pp. 1–9, 2009, doi: 10.1016/j.jhazmat.2008.12.114.

[25] D. K. Laing, R. J. Dudley, A. W. Hartshorne, J. M. Home, R. A. Rickard, and D. C. Bennett, "The extraction and classification of dyes from cotton and viscose fibres," *Forensic Sci. Int.*, vol. 50, no. 1, pp. 23–35, Jul. 1991, doi: 10.1016/0379-

0738(91)90129-7.

[26] M. A. M. Salleh, D. K. Mahmoud, W. A. W. A. Karim, and A. Idris, “Cationic and anionic dye adsorption by agricultural solid wastes: A comprehensive review,” *Desalination*, vol. 280, no. 1–3, pp. 1–13, 2011, doi: 10.1016/j.desal.2011.07.019.

[27] A. H. Karim *et al.*, “Amino modified mesostructured silica nanoparticles for efficient adsorption of methylene blue,” *J. Colloid Interface Sci.*, vol. 386, no. 1, pp. 307–314, 2012, doi: 10.1016/j.jcis.2012.07.043.

[28] C. H. Huang, K. P. Chang, H. De Ou, Y. C. Chiang, and C. F. Wang, “Adsorption of cationic dyes onto mesoporous silica,” *Microporous Mesoporous Mater.*, vol. 141, no. 1–3, pp. 102–109, 2011, doi: 10.1016/j.micromeso.2010.11.002.

[29] T. L. Chew, A. L. Ahmad, and S. Bhatia, “Ordered mesoporous silica (OMS) as an adsorbent and membrane for separation of carbon dioxide (CO2),” *Adv. Colloid Interface Sci.*, vol. 153, no. 1–2, pp. 43–57, 2010, doi: 10.1016/j.cis.2009.12.001.

[30] J. Liu, X. Feng, G. E. Fryxell, L. Q. Wang, A. Y. Kim, and M. Gong, “Hybrid mesoporous materials with functionalized monolayers,” *Adv. Mater.*, vol. 10, no. 2, pp. 161–165, 1998, doi: 10.1002/(SICI)1521-4095(199801)10:2<161::AID-ADMA161>3.0.CO;2-Q.

[31] A. Taguchi and F. Schüth, *Ordered mesoporous materials in catalysis*, vol. 77, no. 1. 2005.

[32] H. Yang and Q. Feng, “Direct synthesis of pore-expanded amino-functionalized mesoporous silicas with dimethyldecylamine and the effect of expander dosage on their characterization and decolorization of sulphonated azo dyes,” *Microporous Mesoporous Mater.*, vol. 135, no. 1–3, pp. 124–130, 2010, doi: 10.1016/j.micromeso.2010.06.019.

[33] W. Xu *et al.*, “Nanoporous CuS with excellent photocatalytic property,” *Sci.*

Rep., vol. 5, pp. 1–11, 2015, doi: 10.1038/srep18125.

[34] I. K. Konstantinou and T. A. Albanis, "TiO2-assisted photocatalytic degradation of azo dyes in aqueous solution: Kinetic and mechanistic investigations: A review," *Appl. Catal. B Environ.*, vol. 49, no. 1, pp. 1–14, 2004, doi: 10.1016/j.apcatb.2003.11.010.

[35] O. J. Hao, H. Kim, and P. C. Chiang, "Decolorization of wastewater," *Crit. Rev. Environ. Sci. Technol.*, vol. 30, no. 4, pp. 449–505, 2000, doi: 10.1080/10643380091184237.

[36] Y. M. Slokar and A. Majcen Le Marechal, "Methods of decoloration of textile wastewaters," *Dye. Pigment.*, vol. 37, no. 4, pp. 335–356, 1998, doi: 10.1016/S0143-7208(97)00075-2.

[37] M. Sleiman, D. Vildozo, C. Ferronato, and J. M. Chovelon, "Photocatalytic degradation of azo dye Metanil Yellow: Optimization and kinetic modeling using a chemometric approach," *Appl. Catal. B Environ.*, vol. 77, no. 1–2, pp. 1–11, 2007, doi: 10.1016/j.apcatb.2007.06.015.

[38] N. H. Ince and D. T. Gönenç, "Treatability of a textile azo dye by uv/h2o2," *Environ. Technol. (United Kingdom)*, vol. 18, no. 2, pp. 179–185, 1997, doi: 10.1080/09593330.1997.9618484.

[39] W. G. Kuo, "Decolorizing dye wastewater with Fenton's reagent," *Water Res.*, vol. 26, no. 7, pp. 881–886, 1992, doi: 10.1016/0043-1354(92)90192-7.

[40] M. N. Chong, B. Jin, C. W. K. Chow, and C. Saint, "Recent developments in photocatalytic water treatment technology: A review," *Water Res.*, vol. 44, no. 10, pp. 2997–3027, 2010, doi: 10.1016/j.watres.2010.02.039.

[41] Slamet, P. P. D. K. Wulan, D. Heltina, A. Fisli, and D. Philo, "Synthesis and Characterization of Magnetically Modified Composites (TiNT/CNT/Fe3O4)," *J. Phys. Conf. Ser.*, vol. 1091, no. 1, pp. 2640–2645, 2018, doi: 10.1088/1742-6596/1091/1/012024.

[42] A. B. Bourlinos, M. A. Karakassides, A. Simopoulos, and D. Petridis, "Synthesis

and Characterization of Magnetically Modified Clay Composites," *Chem. Mater.*, vol. 12, no. 9, pp. 2640–2645, Sep. 2000, doi: 10.1021/cm000137o.

[43] J. Liang, Z. Liang, R. Zou, and Y. Zhao, "Heterogeneous Catalysis in Zeolites, Mesoporous Silica, and Metal–Organic Frameworks," *Adv. Mater.*, vol. 29, no. 30, pp. 1–21, 2017, doi: 10.1002/adma.201701139.

[44] Y. Mei *et al.*, "Versatile approach for integrative and functionalized tubes by strain engineering of nanomembranes on polymers," *Adv. Mater.*, vol. 20, no. 21, pp. 4085–4090, 2008, doi: 10.1002/adma.200801589.

[45] A. A. Solovev, Y. Mei, E. B. Ureña, G. Huang, and O. G. Schmidt, "Catalytic microtubular jet engines self-propelled by accumulated gas bubbles," *Small*, vol. 5, no. 14, pp. 1688–1692, 2009, doi: 10.1002/smll.200900021.

[46] J. L. ANDERSON, "Transport Mechanisms of Biological Colloidsa," *Ann. N. Y. Acad. Sci.*, vol. 469, no. 1, pp. 166–177, May 1986, doi: https://doi.org/10.1111/j.1749-6632.1986.tb26495.x.

[47] J. L. Anderson, "Colloid Transport by Interfacial Forces," *Annu. Rev. Fluid Mech.*, vol. 21, no. 1, pp. 61–99, Jan. 1989, doi: 10.1146/annurev.fl.21.010189.000425.

[48] M. Kuron, P. Kreissl, and C. Holm, "Toward Understanding of Self-Electrophoretic Propulsion under Realistic Conditions: From Bulk Reactions to Confinement Effects," *Acc. Chem. Res.*, vol. 51, no. 12, pp. 2998–3005, 2018, doi: 10.1021/acs.accounts.8b00285.

[49] R. Larter and P. Ortoleva, "A theoretical basis for self-electrophoresis," *J. Theor. Biol.*, vol. 88, no. 4, pp. 599–630, 1981, doi: https://doi.org/10.1016/0022-5193(81)90241-1.

[50] R. He *et al.*, "Design and fabrication of highly ordered ion imprinted SBA-15 and MCM-41 mesoporous organosilicas for efficient removal of Ni2+ from different properties of wastewaters," *Microporous Mesoporous Mater.*, vol. 257, pp. 212–221, Feb. 2018, doi: 10.1016/j.micromeso.2017.08.007.

[51] J. Wang, S. Zheng, Y. Shao, J. Liu, Z. Xu, and D. Zhu, "Amino-functionalized Fe3O4@SiO2 core-shell magnetic nanomaterial as a novel adsorbent for aqueous heavy metals removal," *J. Colloid Interface Sci.*, vol. 349, no. 1, pp. 293–299, Sep. 2010, doi: 10.1016/j.jcis.2010.05.010.

[52] A. Benhamou, M. Baudu, Z. Derriche, and J. P. Basly, "Aqueous heavy metals removal on amine-functionalized Si-MCM-41 and Si-MCM-48," *J. Hazard. Mater.*, vol. 171, no. 1–3, pp. 1001–1008, Nov. 2009, doi: 10.1016/j.jhazmat.2009.06.106.

[53] M. Anbia, S. A. Hariri, and S. N. Ashrafizadeh, "Adsorptive removal of anionic dyes by modified nanoporous silica SBA-3," *Appl. Surf. Sci.*, vol. 256, no. 10, pp. 3228–3233, Mar. 2010, doi: 10.1016/j.apsusc.2009.12.010.

[54] C. K. Lee, S. S. Liu, L. C. Juang, C. C. Wang, K. S. Lin, and M. Du Lyu, "Application of MCM-41 for dyes removal from wastewater," *J. Hazard. Mater.*, vol. 147, no. 3, pp. 997–1005, Aug. 2007, doi: 10.1016/j.jhazmat.2007.01.130.

[55] S. Wang and H. Li, "Structure directed reversible adsorption of organic dye on mesoporous silica in aqueous solution," *Microporous Mesoporous Mater.*, vol. 97, no. 1–3, pp. 21–26, Dec. 2006, doi: 10.1016/j.micromeso.2006.08.005.

[56] F. Tang, L. Li, and D. Chen, "Mesoporous silica nanoparticles: Synthesis, biocompatibility and drug delivery," *Adv. Mater.*, vol. 24, no. 12, pp. 1504–1534, 2012, doi: 10.1002/adma.201104763.

[57] C. Bharti, N. Gulati, U. Nagaich, and A. Pal, "Mesoporous silica nanoparticles in target drug delivery system: A review," *Int. J. Pharm. Investig.*, vol. 5, no. 3, p. 124, 2015, doi: 10.4103/2230-973x.160844.

[58] E. Stöber, W.; Fink, A.; Bohn, "Controlled Growth of Monodisperse Silica Spheres in the Micron Size Range," *J. Colloid Interface Sci.*, vol. 26, no. 1, pp. 62–69, 1968, doi: 10.1589/jpts.29.112.

[59] Q. Huo *et al.*, "Organization of Organic Molecules with Inorganic Molecular Species into Nanocomposite Biphase Arrays," *Chem. Mater.*, vol. 6, no. 8, pp.

1176–1191, 1994, doi: 10.1021/cm00044a016.

[60] L. P. Singh *et al.*, "Sol-Gel processing of silica nanoparticles and their applications," *Adv. Colloid Interface Sci.*, vol. 214, pp. 17–37, 2014, doi: 10.1016/j.cis.2014.10.007.

[61] A. Pisal and A. Rao, "Comparative studies on the physical properties of TEOS, TMOS and Na2SiO3 based silica aerogels by ambient pressure drying method," *J. Porous Mater.*, vol. 23, Dec. 2016, doi: 10.1007/s10934-016-0215-y.

[62] R. K. Nagarale, W. Shin, and P. K. Singh, "Progress in ionic organic-inorganic composite membranes for fuel cell applications," *Polym. Chem.*, vol. 1, pp. 388–408, 2010, doi: 10.1039/b9py00235a.

[63] U. Schubert, "Part One Sol – Gel Chemistry and Methods," in *The Sol-Gel Handbook: Synthesis, Characterization and Applications*, 2015, pp. 1–28.

[64] R. I. Nooney, D. Thirunavukkarasu, C. Yimei, R. Josephs, and A. E. Ostafin, "Synthesis of nanoscale mesoporous silica spheres with controlled particle size," *Chem. Mater.*, vol. 14, no. 11, pp. 4721–4728, 2002, doi: 10.1021/cm0204371.

[65] A. Corma, "From microporous to mesoporous molecular sieve materials and their use in catalysis," *Chem. Rev.*, vol. 97, no. 6, pp. 2373–2419, 1997, doi: 10.1021/cr960406n.

[66] X. S. Zhao, G. Q. Lu, and G. J. Millar, "Advances in mesoporous molecular sieve MCM-41," *Ind. Eng. Chem. Res.*, vol. 35, no. 7, pp. 2075–2090, 1996, doi: 10.1021/ie950702a.

[67] P. Behrens, "Mesoporous Inorganic Solids," *Adv. Mater.*, vol. 5, no. 2, pp. 127–132, 1993.

[68] S. Mann *et al.*, "Sol-Gel Synthesis of Organized Matter," *Chemistry of Materials*, vol. 9, no. 11. pp. 2300–2310, 1997, doi: 10.1021/cm970274u.

[69] K. Sinkó, "Influence of Chemical Conditions on the Nanoporous Structure of Silicate Aerogels," *Materials (Basel).*, vol. 3, pp. 704–740, 2010, doi:

10.3390/ma3010704.

[70] L. P. Singh, S. K. Bhattacharyya, G. Mishra, and S. Ahalawat, “Functional role of cationic surfactant to control the nano size of silica powder,” *Appl. Nanosci.*, vol. 1, no. 3, pp. 117–122, 2011, doi: 10.1007/s13204-011-0016-1.

[71] V. Boonamnuayvitaya, C. Tayamanon, S. Sae-Ung, and W. Tanthapanichakoon, “Synthesis and characterization of porous media produced by a sol-gel method,” *Chem. Eng. Sci.*, vol. 61, no. 5, pp. 1686–1691, Mar. 2006, doi: 10.1016/j.ces.2005.10.002.

[72] J. Zhang, M. Liu, A. Zhang, K. Lin, C. Song, and X. Guo, “Facile synthesis of mesoporous silica nanoparticles with controlled morphologies using water-acetone media,” *Solid State Sci.*, vol. 12, no. 2, pp. 267–273, Feb. 2010, doi: 10.1016/j.solidstatesciences.2009.11.005.

[73] D. Zhao *et al.*, “Triblock Copolymer Syntheses of Mesoporous Silica with Periodic 50 to 300 Angstrom Pores,” *Science (80-.).*, vol. 279, no. 5350, pp. 548 LP – 552, Jan. 1998, doi: 10.1126/science.279.5350.548.

[74] P. T. Tanev and T. J. Pinnavaia, “A Neutral Templating Route to Mesoporous Molecular Sieves,” *Science (80-.).*, vol. 267, no. 5199, pp. 865 LP – 867, Feb. 1995, doi: 10.1126/science.267.5199.865.

[75] S. A. Bagshaw, E. Prouzet, and T. J. Pinnavaia, “Templating of Mesoporous Molecular Sieves by Nonionic Polyethylene Oxide Surfactants,” *Science (80-.).*, vol. 269, no. 5228, pp. 1242 LP – 1244, Sep. 1995, doi: 10.1126/science.269.5228.1242.

[76] G. S. Attard, J. C. Glyde, and C. G. Göltner, “Liquid-crystalline phases as templates for the synthesis of mesoporous silica,” *Nature*, vol. 378, no. 6555, pp. 366–368, 1995, doi: 10.1038/378366a0.

[77] M. Templin *et al.*, “Organically Modified Aluminosilicate Mesostructures from Block Copolymer Phases,” *Science (80-.).*, vol. 278, no. 5344, pp. 1795 LP – 1798, Dec. 1997, doi: 10.1126/science.278.5344.1795.

[78] Y. Wan, Y. Shi, and D. Zhao, "Designed synthesis of mesoporous solids via nonionic-surfactant-templating approach," *Chem. Commun.*, no. 9, pp. 897–926, 2007, doi: 10.1039/b610570j.

[79] P. Alexandridis, U. Olsson, and B. Lindman, "A record nine different phases (four cubic, two hexagonal, and one lamellar lyotropic liquid crystalline and two micellar solutions) in a ternary isothermal system of an amphiphilic block copolymer and selective solvents (water and oil)," *Langmuir*, vol. 14, no. 10, pp. 2627–2638, 1998, doi: 10.1021/la971117c.

[80] J. Fan *et al.*, "Cubic Mesoporous Silica with Large Controllable Entrance Sizes and Advanced Adsorption Properties," *Angew. Chemie*, vol. 115, pp. 3254–3258, Jul. 2003, doi: 10.1002/ange.200351027.

[81] D. Chen *et al.*, "Anionic surfactant induced mesophase transformation to synthesize highly ordered large-pore mesoporous silica structures," *J. Mater. Chem.*, vol. 16, no. 16, pp. 1511–1519, 2006, doi: 10.1039/b517975k.

[82] F. Kleitz *et al.*, "Large Cage Face-Centered-Cubic Fm3m Mesoporous Silica: Synthesis and Structure," *J. Phys. Chem. B*, vol. 107, no. 51, pp. 14296–14300, 2003, doi: 10.1021/jp036136b.

[83] L. Wang *et al.*, "Synthesis and characterization of small pore thick-walled SBA-16 templated by oligomeric surfactant with ultra-long hydrophilic chains," *Microporous Mesoporous Mater.*, vol. 67, pp. 135–141, Feb. 2004, doi: 10.1016/j.micromeso.2003.10.015.

[84] C. Yu, B. Tian, J. Fan, G. D. Stucky, and D. Zhao, "Nonionic block copolymer synthesis of large-pore cubic mesoporous single crystals by use of inorganic salts," *J. Am. Chem. Soc.*, vol. 124, no. 17, pp. 4556–4557, 2002, doi: 10.1021/ja025548f.

[85] M. A. Ballem, J. M. Córdoba, and M. Odén, "Influence of synthesis temperature on morphology of SBA-16 mesoporous materials with a three-dimensional pore system," *Microporous Mesoporous Mater.*, vol. 129, no. 1–2, pp. 106–111, 2010, doi: 10.1016/j.micromeso.2009.09.004.

[86] Z. Cao *et al.*, "Synthesis of mesoporous materials SBA-16 with different morphologies and their application in dibenzothiophene hydrodesulfurization," *Chem. Eng. Sci.*, vol. 155, pp. 141–152, Nov. 2016, doi: 10.1016/j.ces.2016.08.001.

[87] C. Yu, J. Fan, B. Tian, and D. Zhao, "Morphology Development of Mesoporous Materials: A Colloidal Phase Separation Mechanism," *Chem. Mater.*, vol. 16, no. 5, pp. 889–898, 2004, doi: 10.1021/cm035011g.

[88] H. I. Lee, J. H. Kim, G. D. Stucky, Y. Shi, C. Pak, and J. M. Kim, "Morphology-selective synthesis of mesoporous SBA-15 particles over micrometer, submicrometer and nanometer scales," *J. Mater. Chem.*, vol. 20, no. 39, pp. 8483–8487, 2010, doi: 10.1039/c0jm00820f.

[89] K. Kosuge, N. Kikukawa, and M. Takemori, "One-step preparation of porous silica spheres from sodium silicate using triblock copolymer templating," *Chem. Mater.*, vol. 16, no. 21, pp. 4181–4186, 2004, doi: 10.1021/cm0400177.

[90] L. M. Yang, Y. J. Wang, Y. W. Sun, G. S. Luo, and Y. Y. Dai, "Synthesis of micrometer-sized hard silica spheres with uniform mesopore size and textural pores," *J. Colloid Interface Sci.*, vol. 299, no. 2, pp. 823–830, Jul. 2006, doi: 10.1016/j.jcis.2006.02.043.

[91] C. Y. Mou and H. P. Lin, "Control of morphology in synthesizing mesoporous silica," *Pure Appl. Chem.*, vol. 72, no. 1–2, pp. 137–146, 2000, doi: 10.1351/pac200072010137.

[92] C. Boissière, A. Van Der Lee, A. El Mansouri, A. Larbot, and E. Prouzet, "A double step synthesis of mesoporous micrometric spherical MSU-X silica particles," *Chem. Commun.*, vol. 9, no. 20, pp. 2047–2048, 1999, doi: 10.1039/a906509a.

[93] M. Mesa, L. Sierra, B. López, A. Ramirez, and J. L. Guth, "Preparation of micron-sized spherical particles of mesoporous silica from a triblock copolymer surfactant, usable as a stationary phase for liquid chromatography," *Solid State Sci.*, vol. 5, no. 9, pp. 1303–1308, Sep. 2003, doi: 10.1016/S1293-

2558(03)00185-7.

[94] K. Kosuge, T. Sato, N. Kikukawa, and M. Takemori, “Morphological Control of Rod- and Fiberlike SBA-15 Type Mesoporous Silica Using Water-Soluble Sodium Silicate,” *Chem. Mater.*, vol. 16, no. 5, pp. 899–905, 2004, doi: 10.1021/cm030622u.

[95] D. Baute and D. Goldfarb, “Interaction of nitrates with pluronic micelles and their role in the phase formation of mesoporous materials,” *J. Phys. Chem. C*, vol. 111, no. 29, pp. 10931–10940, 2007, doi: 10.1021/jp070886u.

[96] K. S. W. Sing, “Reporting physisorption data for gas/solid systems with special reference to the determination of surface area and porosity (Recommendations 1984),” *Pure Appl. Chem.*, vol. 57, no. 4, pp. 603–619, 1985, doi: doi:10.1351/pac198557040603.

[97] M. Thommes *et al.*, “Physisorption of gases, with special reference to the evaluation of surface area and pore size distribution (IUPAC Technical Report),” 2015. doi: 10.1515/pac-2014-1117.

[98] S. Lowell, J. E. Shields, M. A. Thomas, and M. Thommes, *Characterization of porous solids and powders: surface area, pore size and density*, vol. 16. Springer Science & Business Media, 2012.

[99] G. Bellussi, C. Perego, A. Carati, S. Peratello, E. P. Massara, and G. Perego, “Amorphous mesoporous silica-alumina with controlled pore size as acid catalysts,” *Stud. Surf. Sci. Catal.*, vol. 84, no. C, pp. 85–92, 1994, doi: 10.1016/S0167-2991(08)64100-2.

[100] L. Cao and M. Kruk, “Facile method to synthesize platelet SBA-15 silica with highly ordered large mesopores,” *J. Colloid Interface Sci.*, vol. 361, no. 2, pp. 472–476, 2011, doi: 10.1016/j.jcis.2011.05.076.

[101] A. Sayari, B.-H. Han, and Y. Yang, “Simple synthesis route to monodispersed SBA-15 silica rods,” *J. Am. Chem. Soc.*, vol. 126, no. 44, p. 14348—14349, Nov. 2004, doi: 10.1021/ja0478734.

[102] J.-Z. Liu, T.-L. Wang, and L.-N. Ji, "Enhanced dye decolorization efficiency by citraconic anhydride-modified horseradish peroxidase," *J. Mol. Catal. B Enzym.*, vol. 41, pp. 81–86, 2006, doi: 10.1016/j.molcatb.2006.04.011.

[103] H. S. Rai, M. S. Bhattacharyya, J. Singh, T. K. Bansal, P. Vats, and U. C. Banerjee, "Removal of dyes from the effluent of textile and dyestuff manufacturing industry: A review of emerging techniques with reference to biological treatment," *Crit. Rev. Environ. Sci. Technol.*, vol. 35, no. 3, pp. 219–238, 2005, doi: 10.1080/10643380590917932.

[104] K. Hunger and W. Herbst, *Industrial dyes: chemistry, properties, applications*. John Wiley & Sons, 2007.

[105] T. L. Vigo, *Textile processing and properties: Preparation, dyeing, finishing and performance*. Elsevier, 2013.

[106] T. Tsoncheva, J. Rosenholm, M. Linden, L. Ivanova, and C. Minchev, "Iron and copper oxide modified SBA-15 materials as catalysts in methanol decomposition: Effect of copolymer template removal," *Appl. Catal. A Gen.*, vol. 318, pp. 234–243, 2007, doi: 10.1016/j.apcata.2006.11.008.

[107] H. H. Tseng, W. W. Lee, M. C. Wei, B. S. Huang, M. C. Hsieh, and P. Y. Cheng, "Synthesis of TiO 2/SBA-15 photocatalyst for the azo dye decolorization through the polyol method," *Chem. Eng. J.*, vol. 210, pp. 529–538, 2012, doi: 10.1016/j.cej.2012.09.036.

[108] Z. Salahshoor and A. Shahbazi, "Review of the use of mesoporous silicas for removing dye from textile wastewater," *Eur. J. Environ. Sci.*, vol. 4, no. 2, pp. 116–130, 2014, doi: 10.14712/23361964.2014.7.

[109] S. Wang and H. Li, "Structure directed reversible adsorption of organic dye on mesoporous silica in aqueous solution," *Microporous Mesoporous Mater.*, vol. 97, no. 1–3, pp. 21–26, 2006, doi: 10.1016/j.micromeso.2006.08.005.

[110] K. F. Lam, K. Y. Ho, K. L. Yeung, and G. McKay, "Selective adsorbents from chemically modified ordered mesoporous silica," *Stud. Surf. Sci. Catal.*, vol. 154

C, no. 26, pp. 2981–2986, 2004, doi: 10.1016/s0167-2991(04)80581-0.

[111] M. Anbia and S. Salehi, "Removal of acid dyes from aqueous media by adsorption onto amino-functionalized nanoporous silica SBA-3," *Dye. Pigment.*, vol. 94, no. 1, pp. 1–9, 2012, doi: 10.1016/j.dyepig.2011.10.016.

[112] N. M. Mahmoodi, S. Khorramfar, and F. Najafi, "Amine-functionalized silica nanoparticle: Preparation, characterization and anionic dye removal ability," *Desalination*, vol. 279, no. 1–3, pp. 61–68, 2011, doi: 10.1016/j.desal.2011.05.059.

[113] G. Crini and P. M. Badot, "Application of chitosan, a natural aminopolysaccharide, for dye removal from aqueous solutions by adsorption processes using batch studies: A review of recent literature," *Prog. Polym. Sci.*, vol. 33, no. 4, pp. 399–447, 2008, doi: 10.1016/j.progpolymsci.2007.11.001.

[114] P. Monash and G. Pugazhenthi, "Adsorption of crystal violet dye from aqueous solution using mesoporous materials synthesized at room temperature," *Adsorption*, vol. 15, no. 4, pp. 390–405, 2009, doi: 10.1007/s10450-009-9156-y.

[115] J. B. Joo, J. Park, and J. Yi, "Preparation of polyelectrolyte-functionalized mesoporous silicas for the selective adsorption of anionic dye in an aqueous solution," *J. Hazard. Mater.*, vol. 168, no. 1, pp. 102–107, 2009, doi: 10.1016/j.jhazmat.2009.02.015.

[116] G. McKay and V. J. P. Poots, "Kinetics and diffusion processes in colour removal from effluent using wood as an adsorbent," *J. Chem. Technol. Biotechnol.*, vol. 30, no. 6, pp. 279–292, 1980, doi: 10.1002/jctb.503300134.

[117] P. Peter Atkins and J. De Paula, *Atkins' physical chemistry*. OUP Oxford, 2014.

[118] T. Calvete, E. C. Lima, N. F. Cardoso, S. L. P. Dias, and F. A. Pavan, "Application of carbon adsorbents prepared from the Brazilian pine-fruit-shell for the removal of Procion Red MX 3B from aqueous solution-Kinetic, equilibrium, and thermodynamic studies," *Chem. Eng. J.*, vol. 155, no. 3, pp. 627–636, 2009, doi: 10.1016/j.cej.2009.08.019.

[119] Y. Feng *et al.*, "Methylene blue adsorption onto swede rape straw (Brassica napus L.) modified by tartaric acid: Equilibrium, kinetic and adsorption mechanisms," *Bioresour. Technol.*, vol. 125, pp. 138–144, 2012, doi: 10.1016/j.biortech.2012.08.128.

[120] F. Deniz and S. Karaman, "Removal of an azo-metal complex textile dye from colored aqueous solutions using an agro-residue," *Microchem. J.*, vol. 99, no. 2, pp. 296–302, 2011, doi: 10.1016/j.microc.2011.05.021.

[121] H. Parab, M. Sudersanan, N. Shenoy, T. Pathare, and B. Vaze, "Use of agro-industrial wastes for removal of basic dyes from aqueous solutions," *Clean - Soil, Air, Water*, vol. 37, no. 12, pp. 963–969, 2009, doi: 10.1002/clen.200900158.

[122] Q. Qin, J. Ma, and K. Liu, "Adsorption of anionic dyes on ammonium-functionalized MCM-41," *J. Hazard. Mater.*, vol. 162, no. 1, pp. 133–139, 2009, doi: 10.1016/j.jhazmat.2008.05.016.

[123] K. Parida, K. G. Mishra, and S. K. Dash, "Adsorption of copper(II) on NH 2-MCM-41 and its application for epoxidation of styrene," *Ind. Eng. Chem. Res.*, vol. 51, no. 5, pp. 2235–2246, 2012, doi: 10.1021/ie200109h.

[124] M. Y. Nassar, E. I. Ali, and E. S. Zakaria, "Tunable auto-combustion preparation of TiO2 nanostructures as efficient adsorbents for the removal of an anionic textile dye," *RSC Adv.*, vol. 7, no. 13, pp. 8034–8050, 2017, doi: 10.1039/c6ra27924d.

[125] D. Zhang, H. E. Hegab, Y. Lvov, L. Dale Snow, and J. Palmer, "Immobilization of cellulase on a silica gel substrate modified using a 3-APTES self-assembled monolayer," *Springerplus*, vol. 5, no. 1, 2016, doi: 10.1186/s40064-016-1682-y.

[126] L. Zhou, C. Gao, and W. Xu, "Magnetic dendritic materials for highly efficient adsorption of dyes and drugs," *ACS Appl. Mater. Interfaces*, vol. 2, no. 5, pp. 1483–1491, 2010, doi: 10.1021/am100114f.

[127] U. G. Akpan and B. H. Hameed, "Parameters affecting the photocatalytic degradation of dyes using TiO2-based photocatalysts: A review," *J. Hazard.*

Mater., vol. 170, no. 2–3, pp. 520–529, 2009, doi: 10.1016/j.jhazmat.2009.05.039.

[128] X. Lang, X. Chen, and J. Zhao, "Heterogeneous visible light photocatalysis for selective organic transformations," *Chem. Soc. Rev.*, vol. 43, no. 1, pp. 473–486, 2014, doi: 10.1039/c3cs60188a.

[129] M. P. Reddy, A. Venugopal, and M. Subrahmanyam, "Hydroxyapatite photocatalytic degradation of calmagite (an azo dye) in aqueous suspension," *Appl. Catal. B Environ.*, vol. 69, no. 3–4, pp. 164–170, 2007, doi: 10.1016/j.apcatb.2006.07.003.

[130] S. Chakrabarti and B. K. Dutta, "Photocatalytic degradation of model textile dyes in wastewater using ZnO as semiconductor catalyst," *J. Hazard. Mater.*, vol. 112, no. 3, pp. 269–278, 2004, doi: 10.1016/j.jhazmat.2004.05.013.

[131] I. Arslan and I. A. Balcioglu, "Advanced oxidation of raw and biotreated textile industry wastewater with O3, H2O2/UV-C and their sequential application," *J. Chem. Technol. Biotechnol.*, vol. 76, no. 1, pp. 53–60, 2001, doi: 10.1002/1097-4660(200101)76:1<53::AID-JCTB346>3.0.CO;2-T.

[132] A. Fujishima and K. Honda, "Electrochemical photolysis of water at a semiconductor electrode.," *Nature*, vol. 238, no. 5358, pp. 37–38, Jul. 1972, doi: 10.1038/238037a0.

[133] Z. Yi *et al.*, "An orthophosphate semiconductor with photooxidation properties under visible-light irradiation," *Nat. Mater.*, vol. 9, no. 7, pp. 559–564, 2010, doi: 10.1038/nmat2780.

[134] X. Wang *et al.*, "A metal-free polymeric photocatalyst for hydrogen production from water under visible light," *Nat. Mater.*, vol. 8, no. 1, pp. 76–80, 2009, doi: 10.1038/nmat2317.

[135] N. Pal and A. Bhaumik, "Mesoporous materials: Versatile supports in heterogeneous catalysis for liquid phase catalytic transformations," *RSC Adv.*, vol. 5, no. 31, pp. 24363–24391, 2015, doi: 10.1039/c4ra13077d.

[136] P. S. Shinde *et al.*, "A brief overview of recent progress in porous silica as catalyst supports," *J. Compos. Sci.*, vol. 5, no. 3, pp. 1–17, 2021, doi: 10.3390/jcs5030075.

[137] Y. Kuwahara, K. Maki, Y. Matsumura, T. Kamegawa, K. Mori, and H. Yamashita, "Hydrophobic modification of a mesoporous silica surface using a fluorine-containing silylation agent and its application as an advantageous host material for the tio2 photocatalyst," *J. Phys. Chem. C*, vol. 113, no. 4, pp. 1552–1559, 2009, doi: 10.1021/jp809191v.

[138] C. Kang, J. Huang, W. He, and F. Zhang, "Periodic mesoporous silica-immobilized palladium(II) complex as an effective and reusable catalyst for water-medium carbon-carbon coupling reactions," *J. Organomet. Chem.*, vol. 695, no. 1, pp. 120–127, 2010, doi: 10.1016/j.jorganchem.2009.09.036.

[139] N. H. Le *et al.*, "Photo-induced generation of size controlled Au nanoparticles on pure siliceous ordered mesoporous silica for catalytic applications," *Microporous Mesoporous Mater.*, vol. 295, no. December 2019, 2020, doi: 10.1016/j.micromeso.2019.109952.

[140] E. Kockrick *et al.*, "Platinum induced crosslinking of polycarbosilanes for the formation of highly porous CeO2/silicon oxycarbide catalysts," *J. Mater. Chem.*, vol. 19, no. 11, pp. 1543–1553, 2009, doi: 10.1039/b813669f.

[141] X. Chu, C. Wang, L. Guo, Y. Chi, X. Gao, and X. Yang, "Mesoporous Silica Supported Au Nanoparticles with Controlled Size as Efficient Heterogeneous Catalyst for Aerobic Oxidation of Alcohols," *J. Chem.*, vol. 2015, 2015, doi: 10.1155/2015/737921.

[142] J. González, J. A. Wang, L. F. Chen, M. E. Manríquez, and J. M. Dominguez, "Structural Defects, Lewis Acidity, and Catalysis Properties of Mesostructured WO3/SBA-15 Nanocatalysts," *J. Phys. Chem. C*, vol. 121, no. 43, pp. 23988–23999, 2017, doi: 10.1021/acs.jpcc.7b06373.

[143] M. Zheng, Y. Ding, X. Cao, T. Tian, and J. Lin, "Homogeneous and heterogeneous photocatalytic water oxidation by polyoxometalates containing the

most earth-abundant transition metal, iron," *Appl. Catal. B Environ.*, vol. 237, no. July, pp. 1091–1100, 2018, doi: 10.1016/j.apcatb.2018.07.014.

[144] I. Barroso-Martín, E. Moretti, A. Talon, L. Storaro, E. Rodríguez-Castellón, and A. Infantes-Molina, "Au and AuCu nanoparticles supported on SBA-15 ordered mesoporous titania-silica as catalysts for methylene blue photodegradation," *Materials (Basel).*, vol. 11, no. 6, pp. 1–17, 2018, doi: 10.3390/ma11060890.

[145] F. Chang, M. Jiao, Q. Xu, B. Deng, and X. Hu, "Facile fabrication of mesoporous Fe-Ti-SBA15 silica with enhanced visible-light-driven simultaneous photocatalytic degradation and reduction reactions," *Appl. Surf. Sci.*, vol. 435, pp. 708–717, 2018, doi: 10.1016/j.apsusc.2017.11.168.

[146] S. J. Canhaci, R. F. Perez, L. E. P. Borges, and M. A. Fraga, "Direct conversion of xylose to furfuryl alcohol on single organic–inorganic hybrid mesoporous silica-supported catalysts," *Appl. Catal. B Environ.*, vol. 207, pp. 279–285, 2017, doi: 10.1016/j.apcatb.2017.01.085.

[147] K. S. Sánchez-Zambrano *et al.*, "CO2 capture with mesoporous silicas modified with amines by double functionalization: Assessment of adsorption/desorption cycles," *Materials (Basel).*, vol. 11, no. 6, 2018, doi: 10.3390/ma11060887.

[148] Y. Kuwahara *et al.*, "Dramatic enhancement of CO 2 uptake by poly(ethyleneimine) using zirconosilicate supports," *J. Am. Chem. Soc.*, vol. 134, no. 26, pp. 10757–10760, 2012, doi: 10.1021/ja303136e.

[149] Y. Kuwahara *et al.*, "Enhanced CO2 adsorption over polymeric amines supported on heteroatom-incorporated SBA-15 silica: Impact of heteroatom type and loading on sorbent structure and adsorption performance," *Chem. - A Eur. J.*, vol. 18, no. 52, pp. 16649–16664, 2012, doi: 10.1002/chem.201203144.

[150] D. Großmann, K. Klementiev, I. Sinev, and W. Grünert, "Surface Alloy or Metal–Cation Interaction-The State of Zn Promoting the Active Cu Sites in Methanol Synthesis Catalysts," *ChemCatChem*, vol. 9, no. 2, pp. 365–372, 2017, doi: 10.1002/cctc.201601102.

[151] I. Nitoi, T. Oncescu, and P. Oancea, “Mechanism and kinetic study for the degradation of lindane by photo-Fenton process,” *J. Ind. Eng. Chem.*, vol. 19, no. 1, pp. 305–309, 2013, doi: 10.1016/j.jiec.2012.08.016.

[152] J. Wang and D. Liao, “Optimal partial regularity for nonlinear sub-elliptic systems related to hörmander’s vector fields,” *Kyushu J. Math.*, vol. 65, no. 2, pp. 251–277, 2011, doi: 10.2206/kyushujm.65.251.

[153] M. Klavarioti, D. Mantzavinos, and D. Kassinos, “Removal of residual pharmaceuticals from aqueous systems by advanced oxidation processes,” *Environ. Int.*, vol. 35, no. 2, pp. 402–417, 2009, doi: https://doi.org/10.1016/j.envint.2008.07.009.

[154] C. Comninellis, A. Kapalka, S. Malato, S. A. Parsons, I. Poulios, and D. Mantzavinos, “Advanced oxidation processes for water treatment: advances and trends for R&D,” *J. Chem. Technol. Biotechnol.*, vol. 83, no. 6, pp. 769–776, Jun. 2008, doi: https://doi.org/10.1002/jctb.1873.

[155] D. A. Nichela, A. M. Berkovic, M. R. Costante, M. P. Juliarena, and F. S. García Einschlag, “Nitrobenzene degradation in Fenton-like systems using Cu(II) as catalyst. Comparison between Cu(II)- and Fe(III)-based systems,” *Chem. Eng. J.*, vol. 228, pp. 1148–1157, 2013, doi: 10.1016/j.cej.2013.05.002.

[156] W. H. Glaze, J.-W. Kang, and D. H. Chapin, “The Chemistry of Water Treatment Processes Involving Ozone, Hydrogen Peroxide and Ultraviolet Radiation,” *Ozone Sci. Eng.*, vol. 9, no. 4, pp. 335–352, Sep. 1987, doi: 10.1080/01919518708552148.

[157] P. R. Gogate and A. B. Pandit, “A review of imperative technologies for wastewater treatment I: Oxidation technologies at ambient conditions,” *Adv. Environ. Res.*, vol. 8, no. 3–4, pp. 501–551, 2004, doi: 10.1016/S1093-0191(03)00032-7.

[158] M. Bobu, A. Yediler, I. Siminiceanu, and S. Schulte-Hostede, “Degradation studies of ciprofloxacin on a pillared iron catalyst,” *Appl. Catal. B Environ.*, vol. 83, no. 1–2, pp. 15–23, 2008, doi: 10.1016/j.apcatb.2008.01.029.

[159] H. Zhou, "Demonstration of an intermittent circulating fluidized bed coal gasification process for industrial application," *Fuel Energy Abstr.*, vol. 43, no. 4, p. 247, 2002, doi: https://doi.org/10.1016/S0140-6701(02)86172-0.

[160] A. Babuponnusami and K. Muthukumar, "Advanced oxidation of phenol: A comparison between Fenton, electro-Fenton, sono-electro-Fenton and photo-electro-Fenton processes," *Chem. Eng. J.*, vol. 183, pp. 1–9, 2012, doi: 10.1016/j.cej.2011.12.010.

[161] F. Ji, C. Li, J. Zhang, and L. Deng, "Heterogeneous photo-Fenton decolorization of methylene blue over LiFe(WO4)2 catalyst," *J. Hazard. Mater.*, vol. 186, no. 2–3, pp. 1979–1984, 2011, doi: 10.1016/j.jhazmat.2010.12.089.

[162] O. R. S. da Rocha, R. F. Dantas, M. M. M. B. Duarte, M. M. L. Duarte, and V. L. da Silva, "Oil sludge treatment by photocatalysis applying black and white light," *Chem. Eng. J.*, vol. 157, no. 1, pp. 80–85, 2010, doi: 10.1016/j.cej.2009.10.050.

[163] M. Tokumura, H. Katoh, T. Katoh, H. T. Znad, and Y. Kawase, "Solubilization of excess sludge in activated sludge process using the solar photo-Fenton reaction," *J. Hazard. Mater.*, vol. 162, no. 2–3, pp. 1390–1396, 2009, doi: 10.1016/j.jhazmat.2008.06.026.

[164] M. Tokumura, R. Morito, and Y. Kawase, "Photo-Fenton process for simultaneous colored wastewater treatment and electricity and hydrogen production," *Chem. Eng. J.*, vol. 221, pp. 81–89, 2013, doi: 10.1016/j.cej.2013.01.075.

[165] E. Ortega-Gómez, B. Esteban García, M. M. Ballesteros Martín, P. Fernández Ibáñez, and J. A. Sánchez Pérez, "Inactivation of Enterococcus faecalis in simulated wastewater treatment plant effluent by solar photo-Fenton at initial neutral pH," *Catal. Today*, vol. 209, pp. 195–200, 2013, doi: 10.1016/j.cattod.2013.03.001.

[166] T. T. H. Pham, S. K. Brar, R. D. Tyagi, and R. Y. Surampalli, "Optimization of Fenton oxidation pre-treatment for B. thuringiensis - Based production of value added products from wastewater sludge," *J. Environ. Manage.*, vol. 91, no. 8, pp.

1657–1664, 2010, doi: 10.1016/j.jenvman.2010.03.007.

[167] H. J. H. Fenton, “LXXIII.—Oxidation of tartaric acid in presence of iron,” *J. Chem. Soc. Trans.*, vol. 65, no. 0, pp. 899–910, 1894, doi: 10.1039/CT8946500899.

[168] P. Miró, A. Arques, A. M. Amat, M. L. Marin, and M. A. Miranda, “A mechanistic study on the oxidative photodegradation of 2,6-dichlorodiphenylamine-derived drugs: Photo-Fenton versus photocatalysis with a triphenylpyrylium salt,” *Appl. Catal. B Environ.*, vol. 140–141, pp. 412–418, 2013, doi: 10.1016/j.apcatb.2013.04.042.

[169] J. Jiang, J. F. Bank, and C. P. Scholes, “Subsecond Time-Resolved Spin Trapping Followed by Stopped-Flow EPR of Fenton Reaction Products,” *J. Am. Chem. Soc.*, vol. 115, no. 11, pp. 4742–4746, 1993, doi: 10.1021/ja00064a038.

[170] S.A. Abo Farha, “Comparative Study of Oxidation of Some Azo Dyes by Different Advanced Oxidation Processes : Fenton , Fenton-Like , Photo-Fenton and Photo-Fenton-Like,” *J. Am. Sci.*, vol. 6, no. 10, pp. 128–142, 2010.

[171] S. Rahim Pouran, A. R. Abdul Aziz, and W. M. A. Wan Daud, “Review on the main advances in photo-Fenton oxidation system for recalcitrant wastewaters,” *J. Ind. Eng. Chem.*, vol. 21, pp. 53–69, 2015, doi: 10.1016/j.jiec.2014.05.005.

[172] M. C. Ortega-Liébana, E. Sánchez-López, J. Hidalgo-Carrillo, A. Marinas, J. M. Marinas, and F. J. Urbano, “A comparative study of photocatalytic degradation of 3-chloropyridine under UV and solar light by homogeneous (photo-Fenton) and heterogeneous (TiO 2) photocatalysis,” *Appl. Catal. B Environ.*, vol. 127, pp. 316–322, 2012, doi: 10.1016/j.apcatb.2012.08.036.

[173] D. Hermosilla, M. Cortijo, and C. P. Huang, “Optimizing the treatment of landfill leachate by conventional Fenton and photo-Fenton processes,” *Sci. Total Environ.*, vol. 407, no. 11, pp. 3473–3481, 2009, doi: 10.1016/j.scitotenv.2009.02.009.

[174] P. Karaolia *et al.*, “Reduction of clarithromycin and sulfamethoxazole-resistant

Enterococcus by pilot-scale solar-driven Fenton oxidation," *Sci. Total Environ.*, vol. 468–469, pp. 19–27, 2014, doi: 10.1016/j.scitotenv.2013.08.027.

[175] I. García-Fernández, M. I. Polo-López, I. Oller, and P. Fernández-Ibáñez, "Bacteria and fungi inactivation using Fe 3+/sunlight, H 2O 2/sunlight and near neutral photo-Fenton: A comparative study," *Appl. Catal. B Environ.*, vol. 121–122, pp. 20–29, 2012, doi: 10.1016/j.apcatb.2012.03.012.

[176] M. I. Polo-López *et al.*, "Mild solar photo-Fenton: An effective tool for the removal of Fusarium from simulated municipal effluents," *Appl. Catal. B Environ.*, vol. 111–112, pp. 545–554, 2012, doi: 10.1016/j.apcatb.2011.11.006.

[177] N. Soltani *et al.*, "Visible light-induced degradation of methylene blue in the presence of photocatalytic ZnS and CdS nanoparticles," *Int. J. Mol. Sci.*, vol. 13, no. 10, pp. 12242–12258, 2012, doi: 10.3390/ijms131012242.

[178] H. Cao, X. Qian, C. Wang, X. Ma, J. Yin, and Z. Zhu, "High symmetric 18-facet polyhedron nanocrystals of Cu7S4 with a hollow nanocage.," *J. Am. Chem. Soc.*, vol. 127, no. 46, pp. 16024–16025, Nov. 2005, doi: 10.1021/ja055265y.

[179] S. Das, S. Kumar, S. Garai, R. Pochamoni, S. Paul, and S. Roy, "Softoxometalate [{K6.5Cu(OH)8.5(H2O)7.5}0.5@{K3PW12O40}]n (n = 1348-2024) as an Efficient Inorganic Material for CO2 Reduction with Concomitant Water Oxidation," *ACS Appl. Mater. Interfaces*, vol. 9, no. 40, pp. 35086–35094, 2017, doi: 10.1021/acsami.7b13507.

[180] L. Liu *et al.*, "How to make a fast, efficient bubble-driven micromotor: A mechanical view," *Micromachines*, vol. 8, no. 9, 2017, doi: 10.3390/mi8090267.

[181] P. G. de Gennes, "Soft Matter," *Science (80-.).*, vol. 256, no. 5056, pp. 495 LP – 497, Apr. 1992, doi: 10.1126/science.256.5056.495.

[182] P. Johal and C. Srishti, "Electronic paper technology," *Int. J. Adv. Res. Sci. Eng.*, vol. 2, no. 9, pp. 106–110, 2013.

[183] J. Zhang, J. Yan, and S. Granick, "Directed Self-Assembly Pathways of Active Colloidal Clusters," *Angew. Chemie - Int. Ed.*, vol. 55, no. 17, pp. 5166–5169,

2016, doi: 10.1002/anie.201509978.

[184] Y. Gao and Y. Yu, “How half-coated janus particles enter cells,” *J. Am. Chem. Soc.*, vol. 135, no. 51, pp. 19091–19094, 2013, doi: 10.1021/ja410687z.

[185] J. Zhang, B. A. Grzybowski, and S. Granick, “Janus Particle Synthesis, Assembly, and Application,” *Langmuir*, vol. 33, no. 28, pp. 6964–6977, 2017, doi: 10.1021/acs.langmuir.7b01123.

[186] R. F. Ismagilov, A. Schwartz, N. Bowden, and G. M. Whitesides, “Autonomous movement and self-assembly,” *Angew. Chemie - Int. Ed.*, vol. 41, no. 4, pp. 652–654, 2002, doi: 10.1002/1521-3773(20020215)41:4<652::AID-ANIE652>3.0.CO;2-U.

[187] S. Lee *et al.*, “Monofacet-Selective Cavitation within Solid-State Silica-Nanoconfinement toward Janus Iron Oxide Nanocube,” *J. Am. Chem. Soc.*, vol. 140, no. 45, pp. 15176–15180, 2018, doi: 10.1021/jacs.8b09869.

[188] Y. Wang, C. C. Mayorga-Martinez, J. G. S. Moo, and M. Pumera, “Structure-Function Dependence on Template-Based Micromotors,” *ACS Appl. Energy Mater.*, vol. 1, no. 7, pp. 3443–3448, 2018, doi: 10.1021/acsaem.8b00605.

[189] M. J. Tang *et al.*, “Controllable Microfluidic Fabrication of Magnetic Hybrid Microswimmers with Hollow Helical Structures,” *Ind. Eng. Chem. Res.*, vol. 57, no. 29, pp. 9430–9438, 2018, doi: 10.1021/acs.iecr.8b01755.

[190] J. Katuri, D. Caballero, R. Voituriez, J. Samitier, and S. Sanchez, “Directed Flow of Micromotors through Alignment Interactions with Micropatterned Ratchets,” *ACS Nano*, vol. 12, no. 7, pp. 7282–7291, 2018, doi: 10.1021/acsnano.8b03494.

[191] C. Liang *et al.*, “Bilayer Tubular Micromotors for Simultaneous Environmental Monitoring and Remediation,” *ACS Appl. Mater. Interfaces*, vol. 10, no. 41, pp. 35099–35107, 2018, doi: 10.1021/acsami.8b10921.

[192] J. Parmar, D. Vilela, K. Villa, J. Wang, and S. Sánchez, “Micro- and Nanomotors as Active Environmental Microcleaners and Sensors,” *J. Am. Chem. Soc.*, vol. 140, no. 30, pp. 9317–9331, 2018, doi: 10.1021/jacs.8b05762.

[193] N. Sugai, Y. Nakai, Y. Morita, and T. Komatsu, “Transparent protein microtubule motors with controllable velocity and biodegradability,” *ACS Appl. Nano Mater.*, vol. 1, no. 7, pp. 3080–3085, 2018, doi: 10.1021/acsanm.8b00791.

[194] W. Gao, S. Sattayasamitsathit, and J. Wang, “Catalytically propelled micro-/nanomotors: How fast can they move?,” *Chem. Rec.*, vol. 12, no. 1, pp. 224–231, 2012, doi: 10.1002/tcr.201100031.

[195] W. Huang, M. Manjare, and Y. Zhao, “Catalytic nanoshell micromotors,” *J. Phys. Chem. C*, vol. 117, no. 41, pp. 21590–21596, 2013, doi: 10.1021/jp4080288.

[196] W. Gao, A. Pei, and J. Wang, “Water-Driven Micromotors,” no. 9, pp. 8432–8438, 2012.

[197] X. Ma, H. Feng, C. Liang, X. Liu, F. Zeng, and Y. Wang, “Mesoporous silica as micro/nano-carrier: From passive to active cargo delivery, a mini review,” *J. Mater. Sci. Technol.*, vol. 33, no. 10, pp. 1067–1074, 2017, doi: 10.1016/j.jmst.2017.06.007.

[198] M. Guix, A. K. Meyer, B. Koch, and O. G. Schmidt, “Carbonate-based Janus micromotors moving in ultra-light acidic environment generated by HeLa cells in situ,” *Sci. Rep.*, vol. 6, no. February, pp. 1–7, 2016, doi: 10.1038/srep21701.

[199] P. Xu, H. Wang, R. Tong, Q. Du, and W. Zhong, “Preparation and morphology of SiO2/PMMA nanohybrids by microemulsion polymerization,” *Colloid Polym. Sci.*, vol. 284, no. 7, pp. 755–762, 2006, doi: 10.1007/s00396-005-1428-9.

[200] H. Bahrom *et al.*, “Controllable Synthesis of Calcium Carbonate with Different Geometry: Comprehensive Analysis of Particle Formation, Cellular Uptake, and Biocompatibility,” *ACS Sustain. Chem. Eng.*, vol. 7, no. 23, pp. 19142–19156, 2019, doi: 10.1021/acssuschemeng.9b05128.

[201] J. J. McDermott *et al.*, “Self-generated diffusioosmotic flows from calcium carbonate micropumps,” *Langmuir*, vol. 28, no. 44, pp. 15491–15497, 2012, doi: 10.1021/la303410w.